Award Number: 05HQGR0032

VALIDATION AND UPDATE OF HYBRID EMPIRICAL GROUND MOTION (ATTENUATION) RELATIONS FOR THE CEUS

Kenneth W. Campbell

ABS Consulting, Inc. (EQECAT)

1030 NW 161st Place
Beaverton, OR 97006

Phone: (503) 533-4359
Fax: (503) 533-4360

E-mail: KCampbell@eqecat.com

Final Technical Report
September 30, 2007

Research supported by the U.S. Geological Survey (USGS), Department of the Interior, under award number 05HQGR0032. The views and conclusions contained in this document are those of the author and should not be interpreted as necessarily representing the official polices, either expressed or implied, of the U.S. Government.

Award Number: 05HQGR0032

VALIDATION AND UPDATE OF HYBRID EMPIRICAL GROUND MOTION (ATTENUATION) RELATIONS FOR THE CEUS

Kenneth W. Campbell
ABS Consulting, Inc. (EQECAT)
1030 NW 161st Place, Beaverton, OR 97006
Phone: (503) 533-4350
Fax: (503) 533-4360
E-mail: KCampbell@eqecat.com

Abstract

Ground motion models are the most common means of calculating peak ground motion parameters and response spectra in engineering practice. Where strong motion recordings are abundant, these models are empirically derived. Where the number of recordings is limited, they are developed typically from seismological models and constrained using weak motion data. The use of seismological models to estimate ground motions in such regions has become the paradigm, but there is a large degree of uncertainty in extrapolating weak motion recordings to strong motion levels using only seismological models. As an alternative, Campbell (2003a, 2004) proposed a hybrid empirical method (HEM) that uses the ratio of stochastically simulated ground motions to adjust an empirical ground motion model (EGMM) in one region to use in another region with different seismological and tectonic conditions. By using empirical models, the HEM takes advantage of the vast amount of observational data and expertise that has been used to develop such models in high-seismicity regions around the world, including Western North America (WNA). In this study, I used the formal mathematical framework described in Campbell (2003a, 2004) to derive a new hybrid empirical ground motion model (HGMM) for peak ground acceleration and 5% damped linear elastic response spectra for periods ranging from 0.01–10 sec in Eastern North America (ENA) and the Central and Eastern United States (CEUS). Ground motions in WNA were estimated from a recent EGMM developed by Campbell and Bozorgnia (2007a, 2008) for the PEER Next Generation Attenuation (NGA) project. In the application of the HEM to ENA, differences in stress drop, source properties, crustal damping, regional crustal structure, and generic site conditions (amplification and damping) between the two regions were taken into account. Two alternative hypotheses are proposed regarding the appropriate near-source geometric attenuation in WNA. The resulting HGMM is considered to be most appropriate for estimating strong ground motions for earthquakes with moment magnitudes ranging from 4.0 to 8.0 and for sites with NEHRP B-C site conditions ($V_{S30} = 760$ m/sec) located within 100 km of the fault. Additional guidance is provided for extending the model to include the effects of fault mechanism, hanging-wall geometry, shallow site response, basin response, and intermediate-to-far field geometric and anelastic attenuation.

Introduction

Ground motion models, also known as attenuation relations or ground motion prediction equations, are traditionally used to estimate peak ground motion parameters and response spectra for site-specific and regional engineering and seismic hazard studies. The ground motion model is a relatively simple mathematical formulation that relates a given ground motion parameter to various explanatory variables, such as earthquake magnitude, source-to-site distance, fault mechanism, and local site conditions (e.g., Campbell, 2000c, 2003b, 2003c; Douglas, 2003, 2006; Bozorgnia and Campbell, 2004). The most common ground motion parameters estimated by these ground motion models are peak ground acceleration (PGA), peak ground velocity (PGV), and 5% damped pseudo-absolute response spectral acceleration (PSA). In active tectonic areas such as Western North America (WNA), southern Europe and the Middle East, and Japan, where seismicity is high and strong motion seismometry is well established, these ground motion models are empirically developed from strong motion data. However, in many regions of the world, including Eastern North America (ENA), there are not enough strong motion recordings to develop a reliable empirical ground motion model (EGMM). In these regions, ground motion models are usually developed using theoretical or semi-empirical methods.

Campbell (1985) provides a review of some of the earliest theoretical and semi-empirical methods that were used to develop ground motion models for ENA. One such method, promoted mostly by seismologists and referred to as the theoretical method, utilizes simple seismological theory and observations to define and calibrate a ground motion model. One of the most widely used theoretical model was developed by Nuttli and Herrmann (1984), who used theoretical constraints to define the magnitude and attenuation scaling characteristics of the model and calibrated it with limited seismological observations from the Mississippi Valley. Another such method, promoted mostly by engineers and called the intensity method, predicts quantitative ground motion parameters from qualitative measures of ground shaking, such as Modified Mercalli Intensity (MMI) or Medvedev-Spooner-Karnik (MSK) intensity. In the intensity method, seismic intensity is estimated from an intensity attenuation relationship and the ground motion parameter of interest is estimated from a relationship between ground motion amplitude and intensity (Campbell, 1986). These latter relationships have continued to be of interest even up through the present (e.g., Trifunac and Lee, 1989, 1992; Wald *et al*., 1999; Atkinson and Sonley, 2000; Ebel and Wald, 2003; Kaka and Atkinson, 2004), except that now they are used primarily to estimate seismic intensity from observed or predicted ground motion parameters.

Around the same time that Nuttli and Herrmann (1984) were developing their theoretical ground motion model, seismologists and engineers were devising an alternative stochastic method that utilizes more sophisticated seismological models to describe how ground motion scales with earthquake source size and source-to-site distance (McGuire and Hanks, 1980; Hanks and McGuire, 1981; Boore, 1983). This method provides a framework for estimating ground motion from the fundamental laws of seismology by characterizing a ground motion time series as band-limited white noise from which one or more ground motion parameters can be estimated

in the time domain using simulated time series or in the frequency domain using random process or vibration theory. Because of its success and simplicity, the stochastic method is now widely used to predict strong ground motions in many regions of the world where the number of strong motion recordings is limited (Boore, 2003). One such region is ENA (e.g., Atkinson and Boore, 1995, 1997, 2006; Frankel *et al*., 1996; Toro *et al*., 1997; Hwang and Huo, 1997; Beresnev and Atkinson, 1999). With the improvement of computers, it has become possible to use even more sophisticated numerical modeling techniques to simulate strong ground motion using empirical or theoretical source functions and 2-D and 3-D wave propagation theory, usually calibrated from strong motion recordings (e.g., Bolt, 1987; Somerville, 1993; Anderson, 2003). I refer to this technique as the numerical method in order to distinguish it from the earlier more simplified theoretical method. I am aware of only one ENA ground motion model that has been developed using the numerical method (Somerville *et al*., 2001).

The stochastic method is simple yet powerful, but ground motion models that have been developed using the point-source version of this method lack many of the important characteristics that are inherently incorporated in an EGMM. One of the more important of these characteristics is the near-source effect. This shortcoming has led to the development of the stochastic finite-source method (Beresnev and Atkinson, 1998; Motazedian and Atkinson, 2005). However, the reliance on any one method, no matter how popular that method might be or how many different investigators might apply it, will lead to an underestimation of epistemic uncertainty (uncertainty in scientific knowledge). A complete characterization of uncertainty is an important aspect of seismic hazard analysis (e.g., Reiter, 1990; Budnitz *et al*., 1997; Thenhaus and Campbell, 2003; McGuire, 2004). A true representation of epistemic uncertainty can only be achieved through the use of multiple models and methods.

The reliance of the vast majority of existing ENA ground motion models on the stochastic method led me to propose an alternative method that did not depend so strongly on the underlying seismological models (Campbell, 2003a, 2004). This hybrid empirical method (HEM) uses seismologically derived regional adjustment factors to estimate ground motion parameters in a region where the number of strong motion recordings is limited, which I call the target region, from ground motion estimates in a region where at least one reliable EGMM is available, which I call the host region. The adjustment factors are developed from the *ratio* of ground motion estimates calculated from stochastic simulations in each region and, as a result, rely only indirectly on the particular method that is used to derive them. Since the adjustment factors account for *differences* in the source, path, and site characteristics in the host and target regions, it is not necessary that the absolute value of the ground motion parameter be known with certainty.

In this paper, I review the mathematical basis for the HEM presented in Campbell (2003a, 2004) and use it to develop a new hybrid empirical ground motion model (HGMM) for ENA. The new HGMM incorporates a revised ENA seismological model (Atkinson, 2004; Atkinson and Boore, 2006) and a revised EGMM developed from WNA and other worldwide

strong motion recordings (Campbell and Bozorgnia, 2007a, 2008). This revised HGMM is shown to provide ground motion estimates at small magnitudes that are similar to those predicted from single-corner point-source and finite-source stochastic models, both of which use the same ENA seismological model as that used in this study. However, because of its reliance on a well-constrained EGMM, the revised HGMM provides an alternative means of predicting strong ground motion at large magnitudes and close distances as compared to models that are derived using the stochastic and numerical methods.

Review of Existing Ground Motion Models

A number of ground motion models are presently available for use in ENA. Ignoring those models that were developed using the intensity method, which are no longer considered to be credible, the remaining models have been developed using the stochastic, numerical, and hybrid empirical methods. The modern era of ground motion modeling in ENA began in the early 1990s with the development of a stochastic ground motion model (SGMM) by EPRI (1993). This model would later become publicly available (Toro *et al.*, 1997) in a landmark issue of *Seismological Research Letters*, which presented in one document all of the ground motion models that were currently available for use in North America at the time (Abrahamson and Shedlock, 1997).

The number and use of ground motion models for engineering and government seismic hazard studies in ENA has progressed rapidly over the last decade. The nuclear industry has relied mainly on models that were developed using either expert judgment (e.g., Budnitz *et al.*, 1997; Savy *et al.*, 1999; EPRI, 2004) or the stochastic method (e.g., EPRI, 1993; Silva *et al.*, 2003). The most recent versions of the expert-based models were formulated as composite relationships, wherein a single ground motion model is created from the weighted ground motion estimates of several existing ground motion models. The weights are varied based on the method that is used to develop the model and on the model's perceived validity over specific ranges of the explanatory variables. Epistemic uncertainty is included through the use of a separate probability distribution. Some ground motion models have been proposed and used only for academic research, although some of these models were considered for use in the EPRI (2004) composite model. Such ground motion models include the point-source stochastic model of Hwang and Huo (1997) and the hybrid empirical models of Abrahamson and Silva (2001) and Atkinson (2001). Site-specific studies will typically use a variety of models and methods in order to quantify epistemic uncertainty.

The engineering design and construction industries have relied mainly on the National Seismic Hazard Maps published by the U.S. Geological Survey (USGS) to define seismic loads, often through the use of seismic provisions in the national building codes (e.g., ICC, 2006). In recognition of the importance of epistemic uncertainty in the quantification of seismic hazard, the USGS has continued to expand the number and type of ENA ground motion models that it

has used in the production of these maps. For example, Frankel *et al*. (1996) used only two models to develop the 1996 edition of the National Seismic Hazard Maps and both of these models were derived using the single-corner point-source stochastic method (Frankel *et al*., 1996; Toro *et al*., 1997). This number was increased to five for the 2002 edition of the maps (Petersen *et al*., 2002). Two of these models were derived using the single-corner point-source stochastic method (Frankel *et al*., 1996; Toro *et al*., 1997), one was derived using the double-corner point-source stochastic method (Atkinson and Boore, 1995, 1997), one was derived using the numerical method (Somerville *et al*., 2001), and one was derived using the hybrid empirical method (Campbell, 2001b). Seven ENA ground motion models have tentatively been selected for use in the 2007 edition of the maps (NSHMP, 2007). Four of these models were derived using the stochastic method (Frankel *et al*., 1996; Toro, 2002; Silva *et al*., 2003; Atkinson and Boore, 2006), one was derived using the numerical method (Somerville *et al*., 2001), and two were derived using the hybrid empirical method (Campbell, 2003a, 2004; Tavakoli and Pezeshk, 2005). All of the stochastic models, except for Frankel *et al*. (1996), incorporate some form of finite-source effects, either by including them directly in the ground motion simulations (Atkinson and Boore, 2006) or by applying an empirical correction to the near-source attenuation term (Toro, 2002; Silva *et al*., 2003). Toro (2002) applied this correction to the single-corner model of Toro *et al.* (1997). Silva *et al*. (2003) developed four models using a combination of single-corner and double-corner source spectra and constant and variable stress drops. NSHMP (2007) has tentatively selected the single-corner constant stress drop model for the 2007 edition of the National Seismic Hazard Maps.

Background of the Hybrid Empirical Method

Campbell (1981) introduced a simple yet powerful method to develop a PGA ground motion model for ENA that involved modifying an empirical ground motion model for WNA. This method was intended to serve as an alternative to the intensity method that represented the paradigm at the time (e.g., Campbell, 1986). He used regional adjustment factors based on simple seismological models to account for differences in anelastic attenuation and magnitude measures between the two regions. This was the first application of what would later be called the hybrid empirical method (HEM). A year later, Campbell (1982) used the same method to develop a PGA ground motion model for Utah. Campbell (1987, 2000a) applied a more sophisticated version of the HEM to develop PGA and PGV ground motion models for north-central Utah that took into account differences in stress regime, fault mechanism, anelastic attenuation, and generic site conditions between California, the host region, and Utah, the target region. He used these ground motion models to estimate a near-source response spectrum and its associated epistemic uncertainty for a postulated large earthquake on the Wasatch fault in the vicinity of Salt Lake City, using the spectral shapes of Newmark and Hall (1982).

The HEM was further refined in the early 1990's when, at the request of the U.S. Nuclear Regulatory Commission (USNRC), I applied it to the development of alternative spectral ground

motion models used in the probabilistic risk assessments of two nuclear facilities in WNA that were currently under review by the USNRC. The USNRC staff wanted to use an HGMM to supplement the SGMM that the applicants were using to estimate the expected ground motion at these facilities. Based on its success in these studies, the HEM was selected as one of several ground motion estimation methods in several high-profile seismic hazard projects; namely, the Senior Seismic Hazard Analysis Committee (SSHAC) demonstration project for ENA (Budnitz *et al*., 1997), the Yucca Mountain High-Level Radioactive Waste Repository project in southwestern Nevada (Abrahamson and Becker, 1997; Stepp *et al*, 2001), and the Trial Implementation project in the southeastern United States (Savy *et al*., 1999). The HEM was used to develop alternative ground motion estimates for PGA, PGV and PSA to use as inputs to a probabilistic seismic hazard analysis (PSHA). For these applications, the HEM took into account differences in stress drop, magnitude measures, fault mechanism, anelastic attenuation, crustal velocity structure, and generic site conditions between WNA, the host region, and ENA and southwestern Nevada, the two target regions.

The first formal mathematical framework of the HEM was published in a Yucca Mountain project report (Abrahamson and Becker, 1997), a 1999 Nuclear Energy Agency workshop proceedings (Campbell, 2001a), and a FY2000 USGS research report (Campbell, 2001b). The present form of the method, which included a final version of the preliminary ENA ground motion models that had been presented in these earlier studies, was published in Campbell (2003a, 2004). Atkinson and Boore (1998) evaluated the HEM and independently concluded that an EGMM from California could be reliably modified using the HEM to predict strong ground motion in ENA from future large earthquakes. Atkinson (2001) and Abrahamson and Silva (2001) later applied a simple version of the method to develop ground motion models for ENA. Tavakoli and Pezeshk (2005) modified the HEM presented by Campbell (2003a, 2004) to correct what they believed to be inappropriate assumptions regarding the source spectrum, stress drop, and focal depth in the development of the ENA-to-WNA regional adjustment factors. More recently, the HEM has been used to develop ground motion models for Central Europe (Scherbaum *et al.*, 2005), the Pacific Northwest (Atkinson, 2005), and southern Spain and southern Norway (Douglas *et al.*, 2006).

Mathematical Framework

The implementation of the HEM requires five steps: (1) the selection of the host and target regions, (2) the calculation of empirical ground motion estimates for the host region, (3) the calculation of regional adjustment factors between the target and host regions, (4) the calculation of hybrid empirical ground motion estimates for the target region, and (5) the development of a hybrid empirical ground motion model for the target region.

The host region should have at least one reliable EGMM that can be used to estimate the ground motion parameters of interest. Both the host and the target regions should have one or

more seismological models that can be used to characterize their respective source spectra, crustal structure, wave propagation characteristics, and generic site conditions. Empirical ground motion estimates in the host region should be calculated for a suite of ground motion parameters and other explanatory variables that will be used to define the ground motion model in the target region. The seismological estimates of ground motion used to derive the adjustment factors can be computed using any appropriate ground motion simulation method. However, the stochastic method has been shown to be adequate in all such applications to date (Atkinson and Boore, 1998; Atkinson, 2001, 2005; Abrahamson and Silva, 2001; Campbell, 2003a, 2004; Tavakoli and Pezeshk, 2005; Scherbaum *et al.*, 2005; Douglas *et al.*, 2006).

One of the strengths of the HEM is its ability to easily provide the quantification of both aleatory and epistemic uncertainty. Aleatory uncertainty represents the inherent randomness in the predicted ground motion parameter. This randomness is the result of unknown or unevaluated characteristics of the underlying physical process. Epistemic uncertainty represents the lack of scientific knowledge or the difference in scientific opinion in the equations, algorithms, and parameters that are used to model this physical process. In the mathematical formulation given below summarized from Campbell (2001b, 2004), I use a lognormal distribution to describe the aleatory and epistemic uncertainty in the ground motion predictions and a Gaussian distribution to describe the epistemic uncertainty in the aleatory standard deviation. Following the convention of Benjamin and Cornell (1970), I refer to the mean of the natural logarithm of a lognormally distributed ground motion parameter as its median. In all cases, the standard deviations are defined in terms of the natural logarithm of ground motion.

The median hybrid empirical ground motion estimates for the target region can be calculated from the equation

$$\ln \breve{y}^t(\beta_{jk}) = \sum_{i=1}^{n} \left[w_i(\beta_{jk}) \ln y_i^t(\beta_{jk}) \right] \tag{1}$$

where

$$\ln y_i^t(\beta_{jk}) = \ln y_i^h(\beta_{jk}) + \ln \breve{F}(\beta_{jk}) \; ; \tag{2}$$

the superscripts t and h refer to the target and host regions, respectively; the subscript i refers to the ith of n empirical ground motion models; β_{jk} is the kth value of the jth explanatory variable used to derive the individual ground motion estimates, where k quantifies epistemic uncertainty in the mean value of the variable; $\ln y_i^h(\beta_{jk})$ is the ith empirical ground motion estimate in the host region; $\ln \breve{F}(\beta_{jk})$ is the median estimate of the target-to-host regional adjustment factor; and $w_i(\beta_{jk})$ is a set of weights whose sum over i must equal unity. As formulated above, multiple ground motion models can be used to estimate $\ln y_i^h(\beta_{jk})$ as an added element of epistemic uncertainty. However, the method can just as easily be applied to one EGMM at a time, in which case the resulting suite of individual hybrid empirical models will represent this epistemic uncertainty. The weights are allowed to vary depending on the particular ground

motion model, explanatory variable, and mean value of the explanatory variable. The set of model parameters should take into account the distribution of magnitude, distance, fault mechanism, local site conditions, and other explanatory variables that will eventually be used in the development of the HGMM.

The median value of the regional adjustment factor can be calculated from the equation

$$\ln \breve{F}(\beta_{jk}) = \sum_{l=1}^{n1}\sum_{m=1}^{n2}\sum_{o=1}^{n3}\sum_{p=1}^{n4}\left[w(\phi_{lm}^{t})w(\phi_{op}^{h})\ln F(\beta_{jk},\phi_{lm}^{t},\phi_{op}^{h})\right] \tag{3}$$

where

$$\ln F(\beta_{jk},\phi_{lm}^{t},\phi_{op}^{h}) = \ln Y^{t}(\beta_{jk},\phi_{lm}^{t}) - \ln Y^{h}(\beta_{jk},\phi_{op}^{h})\,; \tag{4}$$

$Y^{t}(\beta_{jk},\phi_{lm}^{t})$ is the seismological estimate of ground motion in the target region; $Y^{h}(\beta_{jk},\phi_{op}^{h})$ is the seismological estimate of ground motion in the host region; ϕ_{lm}^{t} is the *m*th value of the *l*th seismological parameter in the target region, where *m* quantifies epistemic uncertainty in the value of the parameter; $w(\phi_{lm}^{t})$ is the weight corresponding to ϕ_{lm}^{t}, which must equal unity when summed over *m*; ϕ_{op}^{h} is the *p*th value of the *o*th seismological parameter in the host region, where *o* quantifies epistemic uncertainty in the value of the parameter; $w(\phi_{op}^{h})$ is the weight corresponding to ϕ_{op}^{h}, which must equal unity when summed over *p*; and *n*1, *n*2, *n*3 and *n*4 are the total number of seismological parameters and their corresponding alternative values. ϕ_{lm}^{t} and ϕ_{op}^{h} include those seismological parameters that are required to estimate $Y^{t}(\beta_{jk},\phi_{lm}^{t})$ and $Y^{h}(\beta_{jk},\phi_{op}^{h})$ but that are not explicitly included in the set of explanatory variables, β_{jk} (e.g., stress drop). In the general formulation given above, the seismological parameters in the host region, ϕ_{op}^{h}, are allowed to have epistemic uncertainty. However, in many applications, this uncertainty is expected to be relatively small compared to the epistemic uncertainty in the target region, ϕ_{lm}^{t}, and can be neglected. This is because the values of the seismological parameters in the host region will usually be well constrained by weak and strong motion data. If this is not the case, this epistemic uncertainty should be formally included. The summations in Equation (3) assume that the values of the seismological parameters in the host and target regions are uncorrelated.

Equation (3) is structured as if ϕ_{lm}^{t} and ϕ_{op}^{h} are defined by a discrete set of values or models (defined by the indices *m* and *p* in the above equations) with weights of $w(\phi_{lm}^{t})$ and $w(\phi_{op}^{h})$, respectively. Discrete distributions are commonly used in the development of a logic tree, which serves as the typical technique by which epistemic uncertainty is incorporated in seismic hazard analysis (e.g., Thenhaus and Campbell, 2003; McGuire, 2004). It is also possible to model continuous variables in this way as long as they can be defined by a relatively small number of discrete values. If the number of alternative parameter values or logic-tree branches becomes too large, it is more efficient to sample ϕ_{lm}^{t} and ϕ_{op}^{h} using Monte Carlo simulation, in which case they can be defined by either discrete or continuous probability distributions. Further guidance on the use of logic trees in seismic hazard analysis is given in Reiter (1990), Kramer

(1996), Budnitz *et al.* (1997), Coppersmith (1991), Thenhaus and Campbell (2003), McGuire (2004), Bommer *et al.* (2005), and Scherbaum *et al.* (2005).

The mean aleatory standard deviation of $\ln \breve{y}^t(\beta_{jk})$ can be calculated from the equation

$$\bar{\sigma}^t_{\ln y}(\beta_{jk}) = \sum_{i=1}^{n} \left[w_i(\beta_{jk}) \sigma^t_i(\beta_{jk}) \right] \tag{5}$$

where

$$\sigma^t_i(\beta_{jk}) = \left[\left(\sigma^h_i(\beta_{jk}) \right)^2 + \left(\delta\sigma^h_i \right)^2 \right]^{1/2}; \tag{6}$$

$\sigma^h_i(\beta_{jk})$ is the aleatory standard deviation of $\ln y^h_i(\beta_{jk})$; $\delta\sigma^h_i$ is the additional aleatory standard deviation associated with an empirical ground motion estimate when it is evaluated for a specific value of an explanatory variable that is not included in the final HGMM; and all other variables are as defined in Equation (1).

The epistemic standard deviation of $\ln \breve{y}^t(\beta_{jk})$ can be calculated from the equation

$$\tau^t_{\ln y}(\beta_{jk}) = \left\{ \left(\tau_F(\beta_{jk}) \right)^2 + \sum_{i=1}^{n} \left[w_i(\beta_{jk}) \left(\ln y^t_i(\beta_{jk}) - \ln \breve{y}^t(\beta_{jk}) \right)^2 \right] \right\}^{1/2} \tag{7}$$

where $\tau_F(\beta_{jk})$ is the epistemic standard deviation of $\ln \breve{F}(\beta_{jk})$. This latter standard deviation accounts for uncertainty in the regional adjustment factor that is not accounted for in the aleatory standard deviation defined in Equation (5) and is given by the equation

$$\tau_F(\beta_{jk}) = \left\{ \sum_{l=1}^{n1} \sum_{m=1}^{n2} \sum_{o=1}^{n3} \sum_{p=1}^{n4} \left[w(\phi^t_{lm}) w(\phi^h_{op}) \left(\ln F(\beta_{jk}, \phi^t_{lm}, \phi^h_{op}) - \ln \breve{F}(\beta_{jk}) \right)^2 \right] \right\}^{1/2}. \tag{8}$$

If desired, the total dispersion in an individual estimate of $\ln \breve{y}^t(\beta_{jk})$ can be calculated by combining the aleatory and epistemic standard deviations by SRSS using the equation

$$\sigma^t_{tot}(\beta_{jk}) = \left[\left(\bar{\sigma}^t_{\ln y}(\beta_{jk}) \right)^2 + \left(\tau^t_{\ln y}(\beta_{jk}) \right)^2 \right]^{1/2}. \tag{9}$$

Although it is rarely used except for analyses involving high-risk facilities (e.g., Budnitz *et al.*, 1997; Savy *et al.*, 1999; Stepp *et al.*, 2001), the epistemic standard deviation of $\bar{\sigma}^t_{\ln y}(\beta_{jk})$ can be calculated from the equation

$$\tau^t_{\sigma}(\beta_{jk}) = \left\{ \sum_{i=1}^{n} \left[w_i(\beta_{jk}) \left(\sigma^t_i(\beta_{jk}) - \bar{\sigma}^t_{\ln y}(\beta_{jk}) \right)^2 \right] \right\}^{1/2}. \tag{10}$$

Ground Motion Model for Eastern North America

I have used the HEM to develop an updated HGMM for ENA using the general approach presented in Campbell (2003a, 2004) and summarized in the previous section. I selected for the target region the area of ENA that Toro *et al*. (1997) define as the Midcontinent. It includes the region of North America bounded on the west by the Rocky Mountain Front and on the south by the Gulf Coast region. ENA is a good candidate for the HEM because it has a relatively well-constrained seismological model. WNA was selected as the host region because of the availability of a well-constrained seismological model and a recently revised state-of-the-art EGMM. For this study, WNA represents the shallow crustal region of North America located west of the Rocky Mountain Front. Although most of the strong motion recordings used to develop the EGMM come from California, many other relevant recordings come from other parts of the world with tectonic characteristics similar to WNA.

Empirical Ground Motion Estimates in WNA

The original intent of this study was to use all of the revised ground motion models that were being developed for the Pacific Earthquake Engineering Research Center (PEER) Next Generation Attenuation (NGA) project (Power *et al.*, 2006, 2008). However, only the NGA ground motion model of Campbell and Bozorgnia (2007a, 2008) had been finalized by the conclusion of the current USGS grant period (after several extensions). As a result, only this model was used to derive the empirical ground motion estimates, $y_i^{wna}(\beta_{jk})$, and their corresponding aleatory standard deviations, $\sigma_i^{wna}(\beta_{jk})$, in the application of the HEM. It should be noted that the generic superscript *h* used to identify the host region in the general mathematical framework presented above has been replaced with *wna* to designate WNA as the host region. Similarly, the superscript *t* has been replaced by *ena* to designate ENA as the target region.

The empirical ground motion parameters were defined as the orientation-independent geometric mean of the two horizontal components of PGA and 5% damped PSA for periods ranging from 0.01 to 10 sec. This geometric mean is designated GMRotI50 by Boore *et al.* (2006). PGA was assumed to represent the value of PSA at the 0.01-sec period, consistent with the assumption made by Campbell (2003a, 2004) and Campbell and Bozorgnia (2007a, 2008), hereafter referred to as C03-ENA and CB07-WNA, respectively. CB07-WNA defines the magnitude measure as moment magnitude, **M**, and the distance measure as the closest distance to the coseismic rupture plane, R_{RUP}. Collectively, **M** and R_{RUP} and their corresponding values comprise the initial explanatory variable set, β_{jk}. These variables were evaluated for moment magnitudes ranging from 4.0–8.0 in increments of 0.2 and for rupture distances equal to 1, 2, 3, 5, 7, 10, 20, 30, 40, 50 and 70 km. The reason for restricting the calculations to near-source distances, defined as $R_{RUP} \leq 70$ km in this study, will become obvious during the discussion of the ENA seismological model. As indicated below, all of the remaining explanatory variables

were assigned values consistent with the median parameter values used in the WNA seismological model.

The shallow site response term in CB07-WNA was evaluated for $V_{S30} = 620$ m/sec, where V_{S30} (30-m velocity) is the time-averaged value of shear-wave velocity in the upper 30 m of the site profile. The basin response term was evaluated for $Z_{2.5} = 1$ km, where $Z_{2.5}$ is the depth to the 2.5 km/sec shear-wave velocity horizon in the site profile. Both of these values are consistent with the generic-rock site profile that was used to represent the site conditions in the WNA seismological model (Boore and Joyner, 1997). The fault mechanism term was evaluated for $F_{RV} = 0.5$ to represent an average of strike slip and reverse fault mechanism consistent with the use of a single median stress drop in both the ENA and WNA seismological models. Normal fault mechanisms are not expected to occur in the Midcontinent region due to the pervasive regional compressive stress field (e.g., Heidbach *et al.*, 2005). The hanging-wall term was evaluated for $\delta = 90°$ (i.e., assuming a vertical fault rupture plane) in order to exclude hanging-wall effects in the initial evaluation of the model. As discussed later, there is no reason to believe that the site response, fault mechanism, and hanging-wall terms in CB07-WNA are not also generically valid in ENA. Therefore, these terms were added to the final HGMM once the analysis was completed. In C03-ENA, the aleatory standard deviation of each model, $\sigma_i^{wna}(\beta_{jk})$, was increased by an additional incremental standard deviation, $\delta\sigma_i^{wna}$, for each EGMM in which some of the explanatory variables were treated as random variables in the empirical calculations. This was not necessary in this study, since all of the explanatory variables in the EGMM were evaluated for specific values and the terms involving these variables were included in the final HGMM.

ENA-to-WNA Regional Adjustment Factors

Based on its success in modeling a wide range of ground motion parameters (Boore, 2003), I selected the stochastic method together with a point-source single-corner ω-square (Brune) source spectrum (Brune, 1970, 1971) to calculate the median seismological estimates of the ground motion parameters $Y^{wna}(\beta_{jk}, \phi_{op}^{h})$ and $Y^{ena}(\beta_{jk}, \phi_{lm}^{t})$. The computer program SMSIM (Boore, 1996) was used to perform the calculations. Atkinson and Boore (1995, 1997), Frankel *et al*. (1996), Hwang and Huo (1997), Toro *et al.* (1997), and Silva *et al.* (2003) also used the point-source stochastic method to develop ground motion models for ENA. However, Atkinson and Boore (1995, 1997), and later Silva *et al.* (2003) for two of their four models, used a double-corner version of the point-source spectrum in their calculations, which resulted in significantly lower spectral amplitudes at large magnitudes and intermediate frequencies, or what has been called the "spectral sag" (Atkinson, 1993). Atkinson and Boore (2006) used a finite-source stochastic method to revise their previous ENA ground motion model and found that the spectral sag was significantly diminished. They suggested that this sag might have been an artifact of using a double-corner source spectrum to approximate finite-source effects. As I discuss later, the difference between a single-corner, double-corner, or finite-fault source spectrum should not have a significant impact on the HEM as long as the same spectral shape is used in ENA and

WNA. I calculated the stochastic ground motion simulations for the same values of **M** and R_{RUP} that were initially used to derive the empirical ground motion estimates, assuming that R_{RUP} corresponds to the hypocentral distance measure, *R*, used in the point-source stochastic model (Boore, 2003).

The stochastic method assumes that the Fourier amplitude spectrum (FAS) of ground motion can be modeled as Gaussian band-limited white noise using simple seismological models that describe the source, path, and site characteristics of this ground motion. It uses random process theory to derive the desired strong motion parameters from an estimate of the FAS and the duration of the time series. The salient features of this method are briefly summarized below for completeness. A more thorough description can be found in Boore (1983, 2003).

Using notation proposed by Boore (2003), the total FAS of displacement, $Y(M_0, R, f)$, can be calculated from the spectral contributions of the earthquake source, $E(M_0, f)$, the propagation path, $P(R, f)$, the site response, $G(f)$, and the type of motion, $I(f)$, from the relationship

$$Y(M_0, R, f) = E(M_0, f)\, P(R, f)\, G(f)\, I(f) \tag{11}$$

where M_0 is seismic moment, *f* is wave frequency, *R* is hypocentral distance, and moment magnitude is calculated from M_0 (dyne-cm) by the relationship (Hanks and Kanamori, 1979)

$$\mathbf{M} = \frac{2}{3}\log M_0 - 10.7\,. \tag{12}$$

The source term is given by the equation

$$E(M_0, f) = C\, M_0\, S(M_0, f) \tag{13}$$

where $S(M_0, f)$ is the source displacement spectrum and the constant *C* is given by the equation

$$C = \langle R_{\Theta\Phi} \rangle V F \big/ (4\pi\rho_s \beta_s^3 R_0) \tag{14}$$

where $\langle R_{\Theta\Phi} \rangle = 0.55$ is shear-wave radiation pattern averaged over the focal sphere; $V = 1/\sqrt{2}$ is the partition of the total shear-wave energy into orthogonal horizontal components; $F = 2$ is the effect of the free surface (which strictly speaking is only correct for SH waves); ρ_s and β_s are density and shear-wave velocity in the vicinity of the source; and R_0 is a reference distance. The source displacement spectrum for the assumed single-corner ω-square source spectrum is given by the equation (Brune, 1970, 1971)

$$S(M_0, f) = \frac{1}{1 + \left(f / f_0 \right)^2} \tag{15}$$

where corner frequency (Hz) is given by the equation

$$f_0 = 4.9 \times 10^6 \beta_s (\Delta\sigma / M_0)^{1/3} \tag{16}$$

where $\Delta\sigma$ is stress drop (bars), β_s is shear-wave velocity at the source (km/sec), and M_0 is seismic moment (dyne-cm).

For this study, the path term was calculated by multiplying a point-source geometric attenuation term, $Z(R)$, by a crustal damping term as given by the equation

$$P(R, f) = Z(R) \exp\left(\frac{-\pi f R}{Q(f) c_Q} \right) \tag{17}$$

where quality factor, $Q(f)$, represents anelastic attenuation and scattering within the crust and $c_Q = \beta_s$ is the shear-wave velocity used in the determination of $Q(f)$. The geometric attenuation term is modeled by a piecewise continuous function that takes into account critical reflections off the base of the crust (the so-called "Moho bounce"), which have been shown to be important in characterizing ground motions at intermediate distances in ENA (e.g., Burger *et al.*, 1987; Atkinson and Mereu, 1992; Somerville *et al.*, 1990, 2001; Atkinson, 2004), in Switzerland (Bay *et al.* (2003), and even under certain conditions in WNA (e.g., Somerville and Yoshimura, 1990; Campbell, 1991).

The site term was separated into its amplification, $A(f)$, and diminution, $D(f)$, components as given in the equation

$$G(f) = A(f) D(f) \tag{18}$$

where the amplification term was calculated using the quarter-wavelength method (Joyner *et al.*, 1981; Boore and Joyner, 1991) from the equation

$$A(f) = \sqrt{\frac{\rho_s \beta_s}{\bar{\rho}(f) \bar{\beta}(f)}} \tag{19}$$

where

$$\bar{\rho}(f) = \frac{1}{z(f)} \int_0^{z(f)} \rho(z) dz \, ; \tag{20}$$

$$\bar{\beta}(f) = z(f) \left[\int_0^{z(f)} \left(1/\beta(z) \right) dz \right]^{-1} ; \tag{21}$$

$$z(f) = \frac{\bar{\beta}(f)}{4f} ; \tag{22}$$

$\bar{\rho}(f)$ and $\bar{\beta}(f)$ are average density and shear-wave velocity to a depth of a quarter-wavelength, $z(f)$, for wave frequency *f*; ρ_s and β_s are as defined in Equation (14); and $\beta(z)$

is shear-wave velocity at some arbitrary depth, *z*. Because of the interdependence between $\overline{\beta}(f)$ and $z(f)$, these two parameters must be calculated iteratively.

The diminution term was calculated using the kappa filter of Anderson and Hough (1984) as given by the equation

$$D(f) = \exp(-\pi\kappa_0 f) \tag{23}$$

where the site attenuation parameter "kappa" (κ_0) represents the attenuation of ground motion as it propagates through the upper few kilometers of the site profile.

The type of ground motion depends on the ground motion parameter of interest. The calculation of PGA requires the estimation of the FAS of the acceleration time series. The calculation of PSA requires the estimation of the FAS of the pseudo-absolute acceleration time series. The term for ground acceleration is given by the equation

$$I(f) = (2\pi f)^2 \tag{24}$$

and that for the pseudo-absolute acceleration time series is given by the equation

$$I(f) = \frac{(2\pi f f_r)^2}{[(f^2 - f_r^2)^2 - (2 f f_r \varsigma)^2]^{1/2}} \tag{25}$$

where f_r and ζ are the undamped natural frequency and critical damping ratio of a single-degree-of-freedom oscillator.

Given the appropriate form of $I(f)$, the expected value of PGA and 5% damped PSA, which represent the peak values of the appropriate time series, can be calculated from $Y(M_0, R, f)$ using random process theory. According to Cartwright and Longuet-Higgins (1956), the peak of a random function can be calculated from its root-mean-square (rms) value by the approximate expression (valid for large N_z)

$$y_{max} = y_{rms}\left[\sqrt{2\ln N_z} + \left(\frac{0.5772}{\sqrt{2\ln N_z}}\right)\right] \tag{26}$$

where N_z is the number of zero crossings in the time domain. The more accurate form of the Cartwright and Longuet-Higgins relationship used in SMSIM is given by the equation

$$y_{max} = 2y_{rms}\int_0^\infty \left(1 - [1 - \xi\exp(-z^2)]N_e\right)dz \tag{27}$$

where N_e is the number of extrema in the time domain and $\xi = N_z / N_e$. From Parseval's Theorem, y_{rms} can be calculated from the equation

$$y_{rms} = \left[\frac{1}{T_{rms}} \int_0^\infty \left| Y(M_0, R, f) \right|^2 df \right]^{1/2} \tag{28}$$

where T_{rms} is the equivalent rms duration. One of the critical elements of the above relationship is the appropriate value to use for T_{rms}. This is particularly critical at long periods and small magnitudes where the natural period of the oscillator can be longer than the duration of the time series. Methods for estimating T_{rms} that take into account the period of the oscillator are discussed by Boore and Joyner (1984), Liu and Pezeshk (1999), and Boore (2003). According to Dave Boore (personal comm., 2001), SMSIM uses the method proposed by Boore and Joyner (1984), which is given by the equation

$$T_{rms} = T_{gm} + T_0 \left(\frac{\gamma^3}{\gamma^3 + \frac{1}{3}} \right) \tag{29}$$

where T_s is duration of the source; T_p is duration of the path; $T_{gm} = T_s + T_p$ is duration of the ground motion; $T_0 = 1/(2\pi f_r \zeta)$ is duration of the oscillator; and $\gamma = T_{gm}/T_0$.

For this study, representative stochastic parameters for WNA, with the exception of Q_0 and η, were taken from C03-ENA. The values for Q_0 and η were revised from those originally determined by Raoof *et al*. (1999) to better agree with the near-source attenuation characteristics of CB07-WNA for $\mathbf{M} = 5.0$ and $R_{RUP} < 200$ km (Figure 1). The plots in Figure 1 are shown only to 100 km to be consistent with the restriction of the HGMM to the near-source region in this study. The revised values are found to be more consistent with those determined by Atkinson and Silva (1997) from strong motion data ($Q_0 = 204, \eta = 0.56$) rather than those determined by Raoof *et al.* (1999) from weak motion data ($Q_0 = 180$, $\eta = 0.45$). However, these differences are not important for the short distances of interest in this study. I did not find it necessary to adjust the previously selected values for stress drop and kappa ($\Delta\sigma = 100$ bars, $\kappa_0 = 0.04$ sec) after comparing the empirical generic rock response spectrum predicted from CB07-WNA with the response spectrum predicted from the WNA point-source stochastic model for $\mathbf{M} = 5.0$ and $R_{RUP} = 10$ km (Figure 2). The comparison in Figure 2 is made for a relatively small magnitude and distance to be consistent with the point-source assumption in the stochastic model and to diminish the effects of geometric and anelastic attenuation.

Representative median values of the ENA stochastic model parameters were updated based on the seismological model of Atkinson (2004) as applied by Atkinson and Boore (2006). These latter investigators performed stochastic finite-source ground motion simulations for two different generic site profiles: a traditional ENA hard-rock profile and a softer NEHRP B-C ($V_{S30} = 760$ m/sec) profile. To be consistent with the generic site conditions used in the development of the National Seismic Hazard Maps (Frankel *et al*., 1996; Petersen *et al.*, 2002; NSHMP, 2007), I used the NEHRP B-C site profile in performing the ENA stochastic ground motion simulations. This is the same as the NEHRP B-C profile developed by Frankel *et al.* (1996) except that kappa was increased from 0.01 to 0.02 sec (Atkinson and Boore, 2006).

There are two notable differences between the stochastic parameters used by Atkinson and Boore (2006) and those used in C03-ENA: the median stress drop was reduced from 150 bars to 140 bars and the geometric spreading coefficient (n in the distance term R^n) was decreased from –1.0 to –1.3 for distances less than 70 km from the source. In addition, rupture dimensions and hypocentral depth were added as stochastic parameters to represent the location and finiteness of the earthquake rupture. Atkinson and Boore (2006) used a median hypocentral depth of 13 km (Ma and Atkinson, 2004) and a median rupture width and rupture length that was 0.6 times the rupture dimensions predicted from Wells and Coppersmith (1994) to account for the observation that source dimensions are generally smaller in ENA than in more tectonically active regions of the world. The selected ENA and WNA stochastic parameters are summarized in Table 1. A comparison of ENA and WNA amplification factors with and without the effects of the kappa filter is shown in Figure 3.

I have not incorporated epistemic uncertainty in the stochastic parameters used in this study. I recognize that epistemic uncertainty is important, especially in ENA, but the large number of calculations that are needed to evaluate this uncertainty did not seem warranted given the current use of a single EGMM to calculate empirical ground motion in WNA. Besides, the diverse set of ground motion models that are currently available in ENA are believed to adequately capture the breadth in the epistemic uncertainty associated with the estimation of ground motion in this region. Any additional epistemic uncertainty that might be associated with the application of the HEM to ENA must await the availability of additional NGA ground motion models and their subsequent use in the development of alternative hybrid ground motion models for ENA.

The dependence of the calculated median regional adjustment factors on magnitude and distance is shown in Figure 4. Their dependence on oscillator period is shown in Figure 5. Figure 4 indicates that the dependence of the adjustment factors on magnitude is relatively small compared to their dependence on distance. The abrupt change in slope at 70 km reflects the transition from a –1.3 to a +0.02 geometric spreading coefficient in the ENA seismological model that corresponds to the effects of the Moho bounce. The less abrupt change in slope that occurs at 40 km reflects the transition from a –1.0 to a –0.5 geometric spreading coefficient in the WNA seismological model. The dependence of the adjustment factors on oscillator period has a shape much like that of a typical response spectrum, with a peak occurring at periods ranging from 0.03 to 0.05 sec.

Hybrid Empirical Ground Motion Estimates in ENA

I calculated the median hybrid empirical estimates of ground motion, $\breve{y}^{ena}(\beta_{jk})$, from Equation (1) for the same set of magnitudes, distances, and ground motion parameters that I used to calculate the empirical estimates, $y_i^{wna}(\beta_{jk})$, and the regional adjustment factors, $F(\beta_{jk}, \phi_{lm}^t, \phi_{op}^h)$. The hybrid empirical estimate of the mean ENA aleatory standard deviation, $\bar{\sigma}_{\ln y}^{ena}(\beta_{jk})$, was calculated from Equations (5) and (6) assuming $\delta\sigma_i^{wna} = 0$. I also assumed that

the hypocentral distance used in the stochastic model, R, could be equated to the fault distance measure, R_{RUP}, used in CB07-WNA for purposes of applying the regional adjustment factors (Boore, 2003). R_{RUP} was calculated from the median hypocentral depth and the rupture width versus magnitude relationship listed in Table 1 assuming a vertical fault and a hypocenter located in the middle of the rupture plane.

One important limitation of the empirical ground motion estimates, and therefore the hybrid empirical estimates, is their restriction to distances of about 100–200 km. Because of the lower rate of attenuation in ENA, ground motion amplitudes of engineering significance can occur at distances of several hundred kilometers. In order to overcome this limitation, the hybrid empirical ground motion estimates used in C03-ENA were supplemented with stochastic ground motion simulations for distances ranging from 70 to 1000 km. This was done by scaling the stochastic simulations at $R = 70$ km for a given magnitude by a factor required to make them equal to the median hybrid empirical estimate at $R_{RUP} = 70$ km for the same magnitude. These adjusted stochastic ground motion estimates were then used together with the hybrid empirical ground motion estimates in the regression analysis to derive the HGMM. There is a significant amount of epistemic uncertainty associated with this extrapolation. Therefore, since epistemic uncertainty is not included as part of the present study, I chose not to supplement the hybrid empirical estimates with stochastic simulations for distances beyond 70 km at this time and, instead, limit the analysis to the near-source region. An approach for extrapolating these near-source estimates to larger distances is given in the next section.

Hybrid Empirical Ground Motion Model (HGMM)

I used nonlinear least squares regression to calibrate the HGMM using the hybrid empirical ground motion estimates within 40 km of the source. This restriction was used to avoid the increase in the rate of attenuation that occurs between distances of 40 and 70 km that is caused by the change in the geometric spreading coefficient from –1.0 to –0.5 in the WNA stochastic model that is not accompanied by a commensurate change in the spreading coefficient in the ENA model (Figure 4). Since the HGMM was restricted to near-source distances for other reasons, as discussed below, I decided not to incorporate this modeled increase in the rate of attenuation between 40 and 70 km in order to provide a better overall fit to the hybrid empirical estimates out to a distance of 100 km. If this modeled increase in attenuation had been included, the predicted ground motion amplitudes would have been less than those predicted from the preferred model beyond 40 km.

The functional form of the median ground motion model is identical to that used in CB07-WNA. The resulting ground motion model, valid for $4.0 \le \mathbf{M} \le 8.0$, $0 \le R_{RUP} \le 100$ km, and NEHRP B-C site conditions, is given by the general equation

$$\ln \hat{Y} = f_{mag} + f_{dis} + f_{flt} + f_{hng} + f_{site} + f_{sed} \tag{30}$$

where the magnitude and distance terms are given by

$$f_{mag} = \begin{cases} c_0 + c_1\mathbf{M}; & \mathbf{M} \le 5.5 \\ c_0 + c_1\mathbf{M} + c_2(\mathbf{M} - 5.5); & 5.5 < \mathbf{M} \le 6.5 \\ c_0 + c_1\mathbf{M} + c_2(\mathbf{M} - 5.5) + c_3(\mathbf{M} - 6.5); & \mathbf{M} > 6.5 \end{cases} \tag{31}$$

and

$$f_{dis} = (c_4 + c_5\mathbf{M}) \ln\left(\sqrt{R_{RUP}^2 + c_6^2}\right) \tag{32}$$

and $\ln \hat{Y}$ is the natural logarithm of the predicted median value of PGA (g) or PSA (g), defined in terms of the geometric mean horizontal component GMRotI50 (Boore *et al*., 2006); f_{flt} is the fault-mechanism term; f_{hng} is the hanging-wall term; f_{site} is the shallow site response term; f_{sed} is the basin response term; $\mathbf{M}$ is moment magnitude; R_{RUP} is closest distance to the coseismic rupture plane (km); and c_i are model coefficients (Table 2). All of the model coefficients, except for the alternative values for c_0 and c_4 listed in Table 2, were determined from the regression analysis. As explained later, the alternative values for c_0 and c_4 were conservatively estimated under the assumption that the near-source FAS attenuates as $R^{-1.0}$ rather than $R^{-1.3}$. The source terms f_{flt} and f_{hng} and the site response terms f_{site} and f_{sed} are presented in subsequent sections of this report.

The total aleatory standard deviation (natural log) of the geometric mean horizontal component (GM) of PGA and PSA is given by the equation

$$\sigma_{GM} = \sqrt{\sigma^2 + \tau^2 + \sigma_{Fit}^2} \tag{33}$$

where σ is the intra-event standard deviation, τ is the inter-event standard deviation, and σ_{Fit} is the standard deviation of the fit of the model to the hybrid empirical ground motion estimates (i.e., the standard error of regression).

Some engineering applications require an estimate of the arbitrary horizontal component rather than the geometric mean horizontal component of ground motion (Baker and Cornell, 2006). Studies have shown that the difference between the median amplitudes of the geometric mean horizontal component (GMRotI50) and the arbitrary horizontal component is small enough that it can be neglected (Beyer and Bommer, 2006; Campbell and Bozorgnia, 2007a, 2008; Watson-Lamprey and Boore, 2007). As a result, only the difference in the standard deviations of these two components needs to be considered as given by the equation

$$\sigma_{Arb} = \sqrt{\sigma_{GM}^2 + \sigma_C^2} \tag{34}$$

where σ_C is the standard deviation of the component-to-component variability (e.g., see Campbell and Bozorgnia, 2007a, 2008).

In CB07-WNA, the intra-event standard deviation was found to be dependent on the median value of PGA on reference rock and the 30-m velocity of the site profile in order to

account for a reduction in ground motion variability associated with nonlinear site response. However, it was also found that for the value of 30-m velocity that corresponds to NEHRP B-C site conditions, the model predicted only a relatively small degree of nonlinearity. As a result of this limited nonlinearity and the belief by some seismologists that aleatory uncertainty might be somewhat higher in ENA than in WNA, I have chosen to neglect any such reduction in intra-event standard deviation in this study. The final standard deviations are listed in Table 3.

Figures 6 and 7 display the attenuation and magnitude scaling characteristics predicted by the HGMM for PGA and PSA at periods of 0.1, 0.2, 1, 4 and 10 sec. In these and subsequent figures, the HGMM is evaluated for $F_{RV} = 1$ and $F_{SS} = 0$ (a reverse fault mechanism) except where noted. Figures 8 and 9 display the distance and magnitude scaling characteristics of the predicted response spectra predicted. Also shown on these plots are the hybrid empirical ground motion estimates that were used to derive the HGMM. These figures show that the error involved in fitting Equation (30) to the hybrid empirical estimates is relatively small and contributes only marginally to the total aleatory standard deviation (Table 3). The overestimation predicted at 70 km and the underestimation predicted at 100 km is the result of extrapolating the HGMM beyond the 40 km distance used in the regression. The misfit between 70 and 100 km is relatively small compared to the uncertainty in the geometric attenuation terms used in the WNA and ENA seismological models and, in my opinion, does not limit the efficacy of the model at these distances.

As discussed previously, epistemic uncertainty was not formally evaluated. It is the experience of this author that the epistemic uncertainty associated with an individual ground motion model is not generally used in practice. For most projects, this uncertainty is either evaluated by a panel of experts or is incorporated through the use of multiple ground motion models. There are many such models available for ENA, which alleviates the need to develop a separate epistemic uncertainty model. In other regions where multiple ground motion models do not exist, one should use the mathematical framework presented in Campbell (2003a, 2004) to formally evaluate epistemic uncertainty.

Incorporation of Site Effects

Campbell and Bozorgnia (2007a, 2008) included both a shallow site response term and a basin response term in their WNA ground motion model. The shallow site response term accounts for amplification in the shallow part of the site profile and is characterized by the explanatory variable V_{S30} (30-m velocity). The basin response term accounts for those aspects of site response that were not captured by the 30-m velocity, such as 3-D basin response and the inability of a very shallow site profile to fully amplify long-period ground motion. It is characterized by the explanatory variable $Z_{2.5}$ (basin or sediment depth). It is not known with certainty whether these site response terms are valid for ENA site profiles. However, based on the discussion the follows, I believe that they can be used to capture first-order site effects in

much the same way as the NEHRP site coefficients (BSSC, 2004), but they should not be used in place of a site-specific site response study when such a study is dictated by public policy, regulatory constraints, or best engineering practice.

Shallow Site Response Term

The HGMM presented in this study was developed for NEHRP B-C site conditions using the hypothetical site profile developed by Frankel *et al.* (1996) and the value of kappa (site attenuation, κ_0) recommended by Atkinson and Boore (2006). These later investigators suggested that the nonlinear site amplification model developed by Boore and Atkinson (2007) for WNA could be used to adjust their NEHRP B-C predictions to other site conditions. Although this is an interesting proposal, these investigators did not provide any evidence to support this recommendation. Nevertheless, their recommendation serves as precedence for a similar proposal in this study. Both the site amplification model of Boore and Atkinson (2007) and the alternative model developed by Campbell and Bozorgnia (2007a, 2008) quantify shallow site response in terms of 30-m velocity and the value of PGA on a generic reference rock site. Therefore, in order for the site factors from these models to be valid in ENA, the following two conditions must be met: (1) those layers of the site profiles above the reference-rock velocity horizon should have similar linear site response characteristics for the same value of 30-m velocity and (2) the soil nonlinearity of the site profiles should be similar for the same values of 30-m velocity and rock PGA. It is beyond the scope of this paper to validate these conditions for ENA. However, as indicated below, some data are available that suggests these conditions might be met, at least for relatively deep ENA site profiles.

Hwang *et al.* (1996) performed a series of site response analyses for several generic ENA site profiles that were designed to represent NEHRP Site Classes A, B, C, D and E. These Site Classes correspond to 30-m velocities of >1500, 760–1500, 360–760, 180–360, and <180 m/sec, respectively (BSSC, 2004). They developed time histories for Site Class A using the single-corner point-source stochastic method and seismological parameters appropriate for ENA and ran these time histories through the generic site profiles using the equivalent-linear site response computer program SHAKE91. Hwang *et al.* concluded from these analyses that their site factors for hard rock and rock (Site Classes A and B) were similar to those in the NEHRP *Provisions* (BSSC, 2004), but that their site factors for soft rock, stiff soil, and soft soil (Site Classes C, D and E) were generally higher and exhibited much less nonlinearity than those in the NEHRP *Provisions*. There was somewhat better agreement with the NEHRP intermediate-period site coefficient, F_v, than for the NEHRP short-period site coefficient, F_a.

EPRI (1993) performed a similar analysis for a generic ENA site profile with a 30-m velocity that corresponded to Site Class C. The input PGA values and the site amplification factors were calculated with respect to a reference rock site having a shear-wave velocity of 1830 m/sec. Input time histories were developed using the single-corner point-source stochastic

method and seismological parameters appropriate for ENA. EPRI calculated five sets of site factors for this generic site profile by truncating the profile at different depths. In each case the bedrock at the base of the profile was assigned a shear-wave velocity of 1830 m/sec. The site factors used in the comparisons presented below are for the deepest (>122 m) site profile. In order to compare these site factors with the site factors in CB07-WNA and with the site coefficients in the NEHRP *Provisions*, I adjusted the input PGA values and site factors used by EPRI to represent a Site Class B reference site using simple corrections based on the quarter-wavelength method. The site factors for CB07-WNA were evaluated for Site Class C by setting $V_{S30} = 525$ m/sec, which corresponds to the median (logarithmic average) 30-m velocity for this Site Class. The resulting site factors were found to exhibit similar nonlinearity with values that were within about 5–15% of the site factors calculated from CB07-WNA. Both sets of site factors were also relatively consistent with those in the NEHRP *Provisions*. Silva *et al.* (1999) found a similar agreement between the NEHRP site coefficients and the site factors that they calculated using stochastic ground motion simulations, seismological models, and deep site profiles typical of ENA and WNA.

A comparison of the site factors from the five EPRI site profiles clearly shows that their linear and nonlinear site response is strongly dependent on the depth of the site profile. The linear (low amplitude) site factors at short periods were found to increase with the depth of the profile; whereas, those at intermediate periods were found to decrease with profile depth. The nonlinear (high amplitude) site factors at short periods were found to exhibit less nonlinearity as the depth of the profile decreases, becoming nearly linear for the shallowest (3–10 m) profile. The nonlinear site factors at intermediate periods were found to exhibit a small amount of nonlinearity for the deep profile, but were found to increase with ground motion amplitude for the shallower profiles. This latter behavior represents a progressive shift in the predominant period of the site profile to longer periods with a corresponding increase in amplification as the ground motion amplitude increases, which for relatively shallow profile depths is not offset by site attenuation. Similar results were found by Savy *et al.* (1987) for shallow site profiles in ENA and by Silva *et al.* (1999) for shallow site profiles in both WNA and ENA. Hwang *et al.* (1996) found similar results to those of EPRI, which is consistent with their use of relatively shallow site profiles.

The general agreement among the site factors for Site Class C between CB07-WNA, the NEHRP *Provisions*, and the deep profile of EPRI (1993), together with the conclusions by Silva *et al.* (1999) that site response is similar in ENA and WNA for similar NEHRP Site Classes, suggests that it might be reasonable to use the shallow site response term of CB07-WNA to modify the ENA ground motions predicted by C07-ENA. However, as the above results indicate, this model is not necessarily appropriate for site profiles shallower than 50–100 m either in ENA or WNA. Interestingly, this same caveat apparently applies to the NEHRP site coefficients as well (e.g., Anderson *et al.*, 1996). Nevertheless, the NEHRP *Provisions* (BSSC, 2004) and the *International Building Code* (ICC, 2006) recommend the use of the same NEHRP

site coefficients for site profiles of any depth throughout the United States, even though they were developed for relatively deep profiles in WNA (Dobry *et al.*, 2000). Furthermore, the NEHRP site coefficients for the softer Site Classes might need to be revised in lieu of more recent stochastic and empirical results (e.g., Silva *et al.*, 1999; Choi and Stewart, 2005; Campbell and Bozorgnia, 2007b). Considering the relatively large degree of uncertainty that is involved in applying WNA site response results to ENA, it would seem that either the CB07-WNA site factors or the NEHRP site coefficients can be used to account for the approximate generic site response characteristics of relatively deep site profiles in ENA.

In order to use the CB07-WNA site factors with the HGMM developed in this study, one needs an estimate of the median value of PGA on reference rock corresponding to $V_{S30} = 1100$ m/sec (represented by the variable A_{1100}). Although this adjustment is nonlinear, the nonlinear effects are relatively small and can be neglected, such that A_{1100} can be estimated from the equation

$$A_{1100} = 0.88 A_{760} \tag{35}$$

where A_{760} is the median value of PGA for a site with $V_{S30} = 760$ m/sec from Equation (30) and the 0.88 coefficient was calculated from the linear (second) term in the equation for f_{site} given below. Once A_{1100} has been estimated, the shallow site response term can be calculated form the equation (Campbell and Bozorgnia, 2007a, 2008)

$$f_{site} = \begin{cases} k_3 \ln\left(\dfrac{V_{S30}}{k_1}\right) + k_2 \left\{ \ln\left[A_{1100} + c\left(\dfrac{V_{S30}}{k_1}\right)^n \right] - \ln\left[A_{1100} + c\right] \right\}; & V_{S30} < k_1 \\ (k_3 + k_2 n) \ln\left(\dfrac{V_{S30}}{k_1}\right); & k_1 \le V_{S30} < 1830 \\ (k_3 + k_2 n) \ln\left(\dfrac{1830}{k_1}\right); & V_{S30} \ge 1830 \end{cases} \tag{36}$$

where V_{S30} is 30-m velocity (m/sec); c, n, k_1 and k_2 are theoretically constrained coefficients as defined in CB07-WNA; and $k_3 = c_{10}$, where c_{10} is an empirically constrained coefficient from CB07-WNA. The coefficients c, n, k_1, k_2 and k_3 are listed in Table 4. In the above equation, the restriction by Campbell and Bozorgnia (2007a, 2008) that site amplification should be held constant for $V_{S30} > 1100$ m/sec has been relaxed to $V_{S30} > 1830$ m/sec. This later 30-m velocity corresponds to the median shear-wave velocity of bedrock beneath soil profiles of typical sites located in ENA (Savy *et al.*, 1987; EPRI, 1993) and, when substituted into the above equation, results in site factors similar to those given in the NEHRP *Provisions* and in Silva *et al.* (1999) for Site Class A. Site factors for harder sites can be calculated by stochastic simulation using the quarter-wavelength method (e.g., Boore, 2003) or by some other suitable method.

Basin Response Term

I am not aware of any studies of 3-D basin response in ENA, so there is no means of validating the use in ENA of the basin response term developed by Campbell and Bozorgnia (2007a, 2008). The term was based on intermediate-to-long-period numerical ground motion simulations of 3-D basin response in the Los Angeles, San Fernando, San Gabriel, and Ventura sedimentary basins of Southern California (Day *et al.*, 2006, 2008). CB07-WNA extended these results to shorter periods and to very shallow depths using empirical regression. The term is considered to be generic to the extent that it is averaged over multiple earthquake scenarios both inside and outside the basins, multiple sedimentary basins, and multiple site locations within each basin. However, it should be used in ENA with caution until it can be validated.

The basin response term is given by the equation (Campbell and Bozorgnia, 2007a, 2008)

$$f_{sed} = \begin{cases} k_4(Z_{2.5} - 1); & Z_{2.5} < 1 \\ 0; & 1 \le Z_{2.5} \le 3 \\ k_5 e^{-0.75}\left[1 - e^{-0.25(Z_{2.5}-3)}\right]; & Z_{2.5} > 3 \end{cases} \tag{37}$$

where $Z_{2.5}$ is the basin or sediment depth (km), $k_4 = c_{11}$ and $k_5 = c_{12}k_3$, where c_{11}, c_{12} and k_3 are empirically and theoretically constrained coefficients from CB07-WNA. The coefficients k_4 and k_5 are listed in Table 4. The shear-wave velocity that defines the sediment-depth horizon is close to the value that Atkinson and Boore (2006) define as ENA hard rock. Therefore, depth to hard rock can be used as an analog for $Z_{2.5}$ when this latter depth is unknown. Campbell and Bozorgnia (2007a, 2008) did not find basin effects to be important for depths ranging from 1 to 3 km. Apparently, the shallow site response term is sufficient to model both shallow site response and basin response over this depth range.

Incorporation of Source Effects

Campbell and Bozorgnia (2007a, 2008) include both a fault mechanism and a hanging-wall term in their WNA ground motion model. The fault mechanism term accounts for differences in ground motion between earthquakes with strike-slip, reverse, and normal fault mechanisms. The reverse-faulting term also distinguishes between buried and near-surface rupture. The hanging-wall term accounts for amplification due to geometric wave-propagation effects for sites located on the hanging wall of the rupture plane. It cannot be known with certainty whether these source terms are valid for ENA earthquakes, although ground motion simulations conducted by Hermann and Malagnini (2005) do indicate that there are differences in near-source attenuation and source excitation between reverse and strike-slip fault mechanisms. Hanging-wall effects are believed to be a geometric aspect of wave-propagation from a dipping fault and; therefore, are not necessarily restricted to a specific tectonic regime.

Therefore, I believe that the source terms in CB07-WNA can be used to capture first-order source effects in ENA. However, they should be used with caution until they can be validated.

Fault Mechanism Term

The fault mechanism term is given by the equation (modified from Campbell and Bozorgnia, 2007a, 2008)

$$f_{flt} = k_6 (F_{RV} f_{hng,Z} + F_{SS}) \tag{38}$$

where

$$f_{flt,Z} = \begin{cases} 1 - Z_{TOR}; & Z_{TOR} < 1 \\ 0; & Z_{TOR} \geq 1 \end{cases}; \tag{39}$$

F_{RV} is an indicator variable representing a reverse or reverse-oblique fault mechanism, where $F_{RV} = 1$ for $30° < \lambda < 150°$, $F_{RV} = 0$ otherwise, and λ is the rake angle, defined as the average angle of slip measured in the plane of rupture between the strike direction and the slip vector; F_{SS} is an indicator variable representing a strike-slip fault mechanism, where $F_{SS} = 1$ for $-30° < \lambda < 30°$, $-180° < \lambda < -150°$, or $150° < \lambda < 180°$ and $F_{SS} = 0$ otherwise; Z_{TOR} is the depth to the top of the coseismic rupture plane (km); and $k_6 = -c_7$, where c_7 is an empirically constrained coefficient from CB07-WNA. The coefficient k_6 is listed in Table 4. The minus sign in front of c_7 is needed because the term is being used to go from a buried-reverse (the base case for the analysis) to a strike-slip fault mechanism; whereas, the term in CB07-WNA was used to go from a strike-slip to a buried-reverse fault mechanism. The depth term, $f_{flt,Z}$, has also been modified so that the correction is performed only for reverse faults with near-surface rupture (i.e., $Z_{TOR} < 1$). Such events are rare in ENA, so this latter correction should not be used unless there is a valid reason to suspect that rupture will propagate to the surface.

Hanging-Wall Term

The hanging-wall term is given by the equation (Campbell and Bozorgnia, 2007)

$$f_{hng} = k_7 f_{hng,R} f_{hng,M} f_{hng,Z} f_{hng,\delta} \tag{40}$$

where

$$f_{hng,R} = \begin{cases} 1; & R_{JB} = 0 \\ \left[\max\left(R_{RUP}, \sqrt{R_{JB}^2 + 1}\right) - R_{JB} \right] \Big/ \max\left(R_{RUP}, \sqrt{R_{JB}^2 + 1}\right); & R_{JB} > 0, Z_{TOR} < 1; \\ (R_{RUP} - R_{JB}) / R_{RUP}; & R_{JB} > 0, Z_{TOR} \geq 1 \end{cases} \tag{41}$$

$$f_{hng,M} = \begin{cases} 0; & \mathbf{M} \le 6.0 \\ 2(\mathbf{M} - 6.0); & 6.0 < \mathbf{M} < 6.5 \\ 1; & \mathbf{M} \ge 6.5 \end{cases}; \tag{42}$$

$$f_{hng,Z} = \begin{cases} 0; & Z_{TOR} \ge 20 \\ (20 - Z_{TOR})/20; & 0 \le Z_{TOR} < 20 \end{cases}; \tag{43}$$

$$f_{hng,\delta} = \begin{cases} 1; & \delta \le 70 \\ (90 - \delta)/20; & \delta > 70 \end{cases}; \tag{44}$$

R_{JB} is closest distance to the surface projection of the coseismic rupture plane (km), also known as Joyner-Boore distance; δ is average dip of the rupture plane (°); $k_7 = c_9$, where c_9 is an empirically constrained coefficient from CB07-WNA; and Z_{TOR} is as defined previously. The coefficient k_7 is listed in Table 4. The location of the hanging-wall was found by Campbell and Bozorgnia (2007a, 2008) and by Chiou and Youngs (2007) to be completely defined in terms of the relationship between the distance measures R_{RUP} and R_{JB}, which is additional evidence in support of the hypothesis that hanging-wall effects are primarily geometric in nature.

Model Evaluation

A comparison of the HGMM developed in this study with all of the ground motion models that are currently available in ENA is beyond the scope of this study. Instead, two sets of comparisons are presented. In Figures 10 to 13, the HGMM developed in this study (C07-ENA) is compared with two sets of ground motion estimates: (1) ground motion simulations calculated from the single-corner point-source stochastic method using the ENA seismological parameters listed in Table 1 (STO-ENA), and (2) ground motion estimates from the stochastic finite-source ground motion model developed by Atkinson and Boore (2006) using these same seismological parameters (AB06-ENA). Since all three models used the same ENA seismological model, their comparison isolates differences due to the three methodologies. In Figures 14 to 17, the HGMM developed in this study is compared with the author's previous HGMM (C03-ENA), as summarized in Campbell (2003a, 2004), and with the EGMM (CB07-WNA) used to derive the empirical ground motion estimates in the present study (Campbell and Bozorgnia, 2007a, 2008). This later comparison isolates the effects of the regional adjustment factors.

Comparison with Stochastic Models

The model comparisons for $\mathbf{M} = 5.0$ in Figures 10 to 13 show remarkable agreement amongst the stochastic point-source simulations (STO-ENA), the stochastic finite-source ground motion model (AB06-ENA), and the HGMM developed in this study (C07-ENA). The one exception is for $R_{RUP} < 3$ km, where C07-ENA predicts lower ground motions than the other two

models. The empirical ground motion estimates used to develop C07-ENA are not constrained at such short distances for such a small earthquake, so the comparison at these near-field distances is not meaningful. Fortunately, deaggregation studies have shown that design ground motions in ENA come from events located more than 3 km from the site. It is not surprising, although it is comforting, to find that the two stochastic models agree so well when the earthquake is small enough to be reasonably represented by a point source. The fact that both stochastic models agree so closely with C07-ENA in both amplitude and scaling characteristics implies that the ENA and WNA seismological models used in this study accurately represent differences in generic source, path, and site characteristics between the two regions.

All three of the models are also found to agree at large magnitudes for distances approaching 70 km. Where the agreement breaks down is at large magnitudes and close distances. The amplitudes of the stochastic point-source simulations continue to increase unabated with increasing magnitude and decreasing distance. This lack of "saturation" is a well-known weakness of the point-source model and is the reason that many investigators have included empirical saturation terms in ground motion models that have been developed using this method (e.g., Toro, 2002; Silva *et al.*, 2003). Although the stochastic finite-source model and the HGMM have similar magnitude scaling characteristics, the HGMM exhibits a larger degree of saturation at short distances, especially at short periods. For example, whereas C07-ENA predicts a constant PGA of ~1g for an event of $\mathbf{M} \geq 6.5$ at $R_{RUP} = 1$ km, AB06-ENA predicts a constant PGA of ~4g for such an event. This difference diminishes at longer periods where, for example, both models predict a 4-sec spectral acceleration of ~0.2g for an event of $\mathbf{M} = 8.0$ at $R_{RUP} = 1$ km.

Comparison with Hybrid and WNA Models

The model comparisons in Figures 16 and 17 show that there is a significant difference in the spectral shapes of the C03-ENA and C07-ENA hybrid empirical models. For this comparison, C03-ENA was adjusted to Site Class B-C using the magnitude- and distance-independent adjustment factors recommended in Frankel *et al*. (1996). These adjustment factors were applied to the ENA hard-rock ground motions predicted from the ground motion models of Toro *et al.* (1997), Somerville *et al.* (2001), and Campbell (2001b, 2003b, 2004) in the 1996, 2002 and 2007 National Seismic Hazard Maps (Frankel *et al*., 1996; Petersen *et al*., 2002; NSHMP, 2007). For example, the predicted C03-ENA spectral accelerations peak near periods (T) of around 0.02–0.04 sec; whereas, the predicted C07-ENA spectral accelerations peak near periods of 0.1–0.2 sec. This difference is due principally to the difference in the value of kappa that was used to characterize the ENA B-C site profiles in the two models ($\kappa_0 = 0.2$ sec for C07-ENA and $\kappa_0 = 0.1$ sec for C03-ENA). Figure 3 shows the relatively large impact that kappa can have on the site amplification characteristics of the FAS. A similar plot that isolates the effect of kappa on the site amplification characteristics of the FAS is given in Figure 12 of Boore (2003). The impact of kappa on spectral accelerations predicted using the stochastic method is

demonstrated in Figure 3.11 of Boore *et al*. (1993). The difference in spectral shapes between $\kappa_0 = 0.2$ sec and $\kappa_0 = 0.1$ sec exhibited in this latter figure is consistent with the observed difference in spectral shapes between C03-ENA and C07-ENA.

Figure 13 shows that the difference between the two models at the longer distances and larger magnitudes is due to the greater near-source attenuation predicted by C07-ENA. This directly reflects the difference in the near-source geometric spreading coefficients between the ENA seismological model used in developing C07-ENA (–1.3) and that used in developing C03-ENA (–1.0). The larger difference in attenuation at large magnitudes reflects the difference in the functional forms between CB07-WNA and the empirical ground motion models that were used to develop C03-ENA. Figure 14 shows that the magnitude scaling predicted by the two models is similar at very short distances. However, at longer distances C03-ENA exhibits much less magnitude saturation. This difference in magnitude scaling also reflects the difference in functional forms between CB07-WNA and the previous ground motion models.

One of the more interesting comparisons is between C07-ENA and CB07-WNA. Because C07-ENA uses CB07-WNA to derive the empirical ground motion estimates in the host region, the differences between the two models correspond directly to the differences between the ENA and WNA seismological models as reflected in the ENA-to-WNA regional adjustment factors. Figures 16 and 17 show that the difference in spectral shapes is consistent with the larger stress drop ($\Delta\sigma = 140$ versus $\Delta\sigma = 100$ bars) and the lower site attenuation ($\kappa_0 = 0.02$ versus $\kappa_0 = 0.04$ sec) associated with the ENA seismological model. However, the observed difference in spectral amplitudes was not anticipated based on the current seismological paradigm. Although the predicted value of PSA at a distance of 1 km is larger in ENA than in WNA for $T < 1$ sec and about the same at longer periods, at a distance of 10 km the WNA spectra are higher than the ENA spectra for $T > 0.2$ sec. At a distance of 30 km the WNA spectra are higher for $T > 0.08$ sec and at a distance of 70 km the WNA spectra are higher at virtually all periods. Figure 15 shows that magnitude scaling is very similar between the two models, which suggests that this behavior is due to the difference in the geometric attenuation between the two regions as noted in Figure 14. The higher attenuation in C07-ENA is a direct result of the difference in near-source geometric spreading coefficients between the ENA seismological model (–1.3) and the WNA seismological model (–1.0). This difference gets even greater between distances of 40 and 70 km, where the WNA seismological model has a geometric spreading coefficient of –0.5.

Discussion

The model comparisons presented in the previous section point to three factors as the principal contributors to differences between the HGMM developed in this study and that developed previously by Campbell (2003a, 2004). These factors are: (1) the difference in site attenuation (κ_0) used in the previous and revised ENA seismological models, (2) the difference

in near-source geometric attenuation (R^n) used in the previous and revised ENA seismological models, and (3) the difference in functional forms used in the previous and revised WNA empirical ground motion models. A fourth issue suggested by Tavakoli and Pezeshk (2005) is whether the single-corner source spectrum that is used to calculate the regional adjustment factors is valid in view of studies that have shown that a double-corner source spectrum better matches observed spectral amplitudes at large magnitudes and short distances (Atkinson and Silva, 1997, 2000; Atkinson and Boore, 1995, 1997). Each of these issues is discussed below.

Site Attenuation

Frankel *et al*. (1996) used a kappa of 0.01 sec to develop the site amplification factors that Petersen *et al*. (2002) used to adjust the predicted C03-ENA ground motions on hard-rock to NEHRP B-C site conditions. Atkinson and Boore (2006) revised this value to 0.02 sec, but gave no basis for this revision. NSHMP (2007) attributes the value used by Frankel *et al*. (1996) to "ground shaking studies by J. Fletcher of the USGS observed in a borehole characterized by bedrock underlying a stiff soil condition with shear-wave velocity similar to that defining NEHRP B-C site conditions." However, no specific reference is given for these studies. Since there is insufficient documentation to validate either of the proposed kappa values, I used published assessments of κ_0 from the literature to assess which of these two candidate values might be more appropriate.

Kappa is considered to represent the frequency independent attenuation within the top few kilometers of the crust (Anderson and Hough, 1984). It is typically calculated from the high-frequency slope of the FAS after correcting for crustal damping. However, Chapman *et al.* (2003) show that it can also be calculated from the quality factor, Q, through the relationship

$$\kappa_0 = \int_0^z \frac{dz}{Q(z)\beta(z)} \tag{45}$$

where $Q(z)$ and $\beta(z)$ are the quality factor and shear-wave velocity at an arbitrary depth, z, within the site profile.

Before embarking on a quest for an appropriate kappa value for NEHRP B-C site conditions, it is useful to review the kappa values that have been proposed for ENA hard rock. Silva and Darragh (1995) estimated kappa from template fits of response spectral shapes of strong motion recordings in ENA. They determined a median kappa of 0.007 (0.004–0.016) sec from 16 recordings located on ENA hard rock described as granitic plutons, carbonates, and Precambrian rock of the Canadian Shield. This value is somewhat higher than the upper-bound estimate of 0.004 sec that Atkinson (1996) determined for the Canadian Shield from small earthquakes recorded by the Eastern Canadian Telemetered Network (ECTN). However, the Canadian Shield sites are likely to be underlain by higher quality rock than the average ENA hard rock site. Rock quality can have a significant affect on the value of kappa. For example,

Atkinson (1996) reported kappa values ranging from 0.02–0.04 sec, more typical of soft-to-hard rock sites in WNA, for sites in the Charlevoix and Sudbury areas of southeastern Canada, which are located on fractured Precambrian rock within an ancient meteor impact crater. Silva and Darragh (1995) found a kappa of 0.025 sec for a "sheared" hard rock site in the 1988 Nahanni earthquake area. Chapman *et al.* (2003) analyzed recordings of 25 very shallow microearthquakes near Monticello Reservoir, South Carolina, and found kappa values that ranged from 0–0.018 sec, depending on the parameters used to filter the ground motion, for a site that was located on metamorphic and igneous rock. The travel paths used by Chapman *et al.* were somewhat longer than the "few kilometers" assumed to represent κ_0, so the actual value is expected to be somewhat smaller than these estimates. For the assessments of kappa presented below for a generic NEHRP B-C site profile, I will use the median hard-rock value ($\kappa_0 = 0.007$ sec) estimated by Silva and Darragh (1995) to represent the site attenuation in the hard-rock part of the site profile. According to Equation (45), this value of kappa corresponds to an average Q of 145–215 for a site profile of 2–3 km and an average shear-wave velocity of 2 km/sec. Alternatively, if the travel path extends to the hypocentral region of earthquakes in ENA (typically around 10 km) and the average shear-wave velocity is assumed to be around 3 km/sec, the implied value of Q is estimated to be 475, similar to the value assigned by Cramer *et al.* (2004) to Paleozoic and older rock beneath the city of Memphis, Tennessee.

There have been several studies that can be used to infer the value of kappa for a site profile representative of NEHRP B-C site conditions in ENA. Darragh and Silva (1995) analyzed three ENA strong motion recordings on sandstone and claystone (ENA soft rock) and found a median kappa of 0.017 (0.015–0.018) sec. Boore and Joyner (1991) developed a generic deep soil profile for the Mississippi Embayment to which they assigned a kappa of 0.03 sec to that part of the profile located above hard rock. This profile yields a kappa of 0.015 sec for the 550 m of the profile that falls below the $V_{S30} = 760$ m/sec horizon, corresponding to NEHRP B-C site conditions. The kappa for the hard-rock part of the profile that extends from 550 m to a depth of 2500 m (i.e., a "few kilometers) beneath the site is estimated by multiplying 0.007 sec by the ratio 550/1950, which corresponds to a kappa of 0.005 sec. Adding this incremental hard-rock kappa to the value of kappa estimated for the sedimentary column yields a total kappa of approximately 0.02 sec. Silva *et al.* (1999) struggled with this same issue in their effort to reevaluate the NEHRP site coefficients in the NEHRP *Provisions*. They concluded that, although $\kappa_0 = 0.01$ sec might be an appropriate value for a relatively shallow (≤ 91 m) generic NEHRP B-C profile in ENA, a more realistic deeper profile, typical of Gulf Coast sandstones and of mudstones, claystones, and siltstones in South Carolina and the Denver Basin of Colorado, should have a kappa of about 0.02 sec. The hypothetical NEHRP B-C profile used in the present study (Frankel *et al.*, 1996) has a depth of 175 m to the 2000 m/sec velocity horizon and 455 m to the 2800 m/sec velocity horizon. Therefore, this profile would correspond to a deep profile according to Silva *et al.* (1999).

Wen and Wu (2001) present generic site profiles for the cities of Memphis (Tennessee), Carbondale (Illinois), and St. Louis (Missouri). These profiles have depths to hard rock (shear-wave velocity > 2000 m/sec) of 1000, 165 and 16 m, respectively. Carbondale and St. Louis have relatively low velocities of 310 m/sec or less above these depths. Wen and Wu report kappa values of 0.063, 0.043, and 0.0076 sec for Memphis, Carbondale and St. Louis, which they attribute to Herrmann and Akinci (1999). Since the Carbondale and St. Louis profiles do not have any layers above hard rock with shear-wave velocities greater than 760 m/sec, they cannot be used to estimate kappa for NEHRP B-C site conditions. However, they can be used to check the reasonableness of the assumed hard-rock value of kappa. Using Q values typical of similar deposits in Memphis (Cramer *et al.*, 2004), the total kappa for both the Carbondale and St. Louis profiles is found to be consistent with a hard-rock kappa of 0.007 ± 0.001 sec if the Mississippian Limestone geologic unit that underlies both of these profiles is assumed to have a Q of 100 and the profile for St. Louis is assumed to be composed only of Mississippian Limestone (i.e., no soft soils). Also using Q values typical of Memphis (Cramer *et al.*, 2004), slightly adjusted to give the correct total kappa, the 580-m thickness of the Wen and Wu Memphis profile that falls below the $V_{S30} = 760$ m/sec horizon is estimated to contribute a value of 0.018 sec to the total kappa of the profile. Adding to this that part of the kappa attributable to hard rock to a depth of 2500 m yields a total kappa of approximately 0.024 sec.

Park and Hashash (2004) used ground motion recordings in the Mississippi Embayment from the 2001 Enola, Arkansas, earthquake together with a generic 1000-m deep Mississippi Embayment shear-wave velocity profile developed by Romero and Rix (2001) to back-calculate a small strain damping profile. They used these velocity and damping profiles to estimate a kappa of 0.053 sec for the entire sedimentary column above Paleozoic bedrock. Using these same profiles, I calculated a kappa of 0.009 sec for the 473-m thickness of the Romero and Rix sedimentary column that falls below the $V_{S30} = 760$ m/sec velocity horizon. Adding to this the kappa of 0.006 sec attributable to the 2027 m of hard rock beneath the sedimentary profile gives a total kappa of 0.015 sec.

Using recordings from microearthquakes in the Summerville-Middleton Place seismic zone, Chapman *et al*. (2003) found kappa values that ranged from 0.035–0.049 sec for a 775-m unconsolidated sedimentary profile in the Charleston, South Carolina, area. Later, Chapman *et al*. (2006) compiled a detailed 830-m deep shear-wave velocity profile for a nearby site in downtown Charleston, based on velocity measurements and geophysical investigations conducted by several investigators. Using this velocity profile and the Q values that are consistent with the kappa values determined by Chapman *et al*. (2003) and for similar sedimentary deposits in Memphis (Cramer *et al.*, 2004), I calculated a kappa of 0.050 sec for the entire Charleston profile and 0.008 sec for the 327-m section of the profile that falls below the $V_{S30} = 760$ m/sec velocity horizon. Adding to this the kappa of 0.006 sec attributable to the 2173 m of hard rock beneath the sedimentary column gives a total kappa of 0.014 sec.

Cramer *et al.* (2004) used *in-situ* measurements to estimate the shear-wave velocities and *Q* values for various geologic units that underlie the city of Memphis and Shelby County, Tennessee. They used these estimates together with the lithology of the Memphis area described by Gomberg *et al.* (2003) to construct a series of site profiles to use in the development of a regional site-specific seismic hazard map. Using a typical 1000-m site profile from these studies, I calculated a kappa of 0.049 sec, which when combined with the 0.004 sec value attributable to the 1500 m of hard rock below the sedimentary column yields a total kappa of 0.053 sec. This estimate is similar to values found by others for the Mississippi Embayment. I estimated the 588-m section of the profile that falls below the $V_{S30} = 760$ m/sec velocity horizon to have a kappa of 0.013 sec. Combining this with the kappa of 0.006 sec for the 1912 m of hard rock beneath this NEHRP B-C sedimentary column gives a total kappa of 0.019 sec.

All of the assessments given above indicate that the kappa associated with a typical deep NEHRP B-C site profile in the Mississippi Embayment and the Charleston area can be expected to have a value ranging between 0.014 and 0.024 sec. This range is consistent with the kappa of 0.02 sec recommended by Silva *et al.* (1999) for a generic NEHRP B-C site profile in ENA. However, as Wen and Wu (2001) have found, shallower profiles can have much smaller kappa values.

Looking beyond ENA, perhaps a reasonable kappa analog to a NEHRP B-C site in ENA is the 0.026 (0.01–0.060) sec value typical of WNA hard rock (Darragh and Silva, 1995) or the range of values (0.016–0.03 sec) typical of volcanic rock in western Nevada (Hough *et al.*; 1989; Su *et al.*; 1996; Ichinose *et al.*; 1989), all of which have near-surface shear-wave velocities that are consistent with NEHRP B-C site conditions. The lower end of the range of kappa values for these WNA hard-rock sites are similar to the range of values found for deep NEHRP B-C profiles in ENA.

The hypothetical NEHRP B-C site profile proposed by Frankel *et al.* (1996) has a much steeper velocity gradient than either the Mississippi Embayment or the Charleston profiles below the $V_{S30} = 760$ m/sec velocity horizon that defines NEHRP B-C site conditions. The hypothetical profile attains a shear-wave velocity in excess of 2000 m/sec, or what Atkinson and Boore (2006) classify as ENA hard rock, at a depth of 175 m, whereas the Memphis, Mississippi Embayment, and Charleston profiles reach this velocity at depths ranging from 800–1000 m. The Carbondale profile has about the same depth to hard rock as the hypothetical profile, but lacks the steep velocity gradient. I calculated an independent estimate of kappa for the Frankel *et al.* (1996) hypothetical profile from the inferred values of *Q* and kappa measured or estimated for the deeper NEHRP B-C site profiles. Using *Q* values of 25, 50 and 100 for shear-wave velocities ranging from 648–1000, 1000–2000, and 2000–3000 m/sec, respectively, I calculate a kappa of 0.006 sec for the hypothetical profile. Adding to this the fraction of hard-rock kappa attributable to the remainder of the profile to a depth of 2500 m (0.005 sec) gives a total kappa of 0.011 sec, similar to the value used by Frankel *et al.* (1996).

Therefore, it appears that the kappa of 0.01 sec used by Frankel *et al.* (1996) is consistent with his relatively shallow hypothetical NEHRP B-C profile. The issue is whether the profile itself is appropriate for defining generic NEHRP B-C site conditions in ENA. The NEHRP site coefficients that are used with the Seismic Design Maps use this generic site condition as its reference site condition (BSSC, 2004; ICC, 2006), but they were developed for a typical deep soil profile in WNA (Borcherdt, 1994; Dobry *et al.*, 2000). Therefore, the steep velocity gradient and relatively low site attenuation in the hypothetical profile can lead to unrealistically high amplification factors at short oscillator periods if coupled with these deep-site-based NEHRP site coefficients. In my opinion, additional research is needed to find an appropriate combination of site attenuation and velocity gradient to use in defining a more reasonable generic NEHRP B-C site profile in ENA for purposes of seismic hazard mapping. Until then, I suggest that it is more reasonable to use $\kappa_0 = 0.02$ sec rather than $\kappa_0 = 0.01$ sec to quantify the site attenuation in the hypothetical NEHRP B-C profile defined by Frankel *et al.* (1996) in order to estimate ground motions for generic NEHRP B-C site conditions (i.e., Site Class B-C) in ENA.

Near-Source Geometric Attenuation

An empirical near-source geometric spreading coefficient of –1.0 was used in both ENA (Atkinson and Mereu, 1992) and WNA (Raoof *et al*., 1999) to develop the regional adjustment factors in C03-ENA. As a result, the near-source ground motions predicted by C03-ENA were found to be consistently larger than those predicted by the WNA ground motion models. This can be seen by comparing the attenuation rates between C03-ENA and CB07-WNA in Figure 14. Atkinson (2004), using an expanded weak and strong motion database of 1700 vertical components from 186 earthquakes in southeastern Canada and northeastern United States, revised the ENA near-source spreading coefficient to –1.3. By adopting this higher rate of attenuation in this study, I found C07-ENA to predict lower ground motions in ENA than in WNA at distances ranging from a few kilometers for PSA at $T = 4$ sec to a few tens of kilometers for PGA and PSA at $T = 0.1$ sec (Figure 14).

As noted previously, it is actually the relative difference and not the absolute values of geometric attenuation in ENA and WNA that is important in applying the HEM. Therefore, the issue is whether the regional difference in geometric attenuation found by Raoof *et al.* (1999) for Southern California and Atkinson (2004) for southeastern Canada and northeastern United States is both scientifically defensible and extrapolative to other regions of WNA and ENA. In order to address this issue, I searched the literature to see if I could find other studies that could either support or refute a similar difference in geometric attenuation between these two regions. First, I will present results for WNA. I found that Malagnini *et al*. (2007) provided additional support for the Raoof *et al.* (1999) geometric attenuation term. They evaluated 5769 horizontal waveforms from 281 small-to-moderate earthquakes in the San Francisco Bay Area and found a geometric spreading coefficient of –1.0 for $R < 30$ km and –0.6 for larger distances. Recall that Raoof *et al.* (1999) found a spreading coefficient of –1.0 for $R < 40$ km and –0.5 for larger

distances from 820 three-component broadband recordings from 140 moderate-to-large earthquakes in Southern California. Neither study found a near-zero spreading coefficient at intermediate distances that would be indicative of a strong crustal reflector. This might be due to the heterogeneous nature of the crustal structure in California; although, the crossover distance from body-wave-like to surface-wave-like geometric spreading found at such short distances in both regions could also be caused by a combination of weak crustal reflections from a relatively thin low-velocity crustal layer and the arrival of surface wave phases (e.g., Boatwright *et al.*, 2003). Atkinson and Silva (1997) analyzed 1000 horizontal strong motion components from 43 moderate-to-large earthquakes in California and found a preferred spreading coefficient of –1.0 for $R < 50$ km, 0 for $50 \le R \le 170$ km, and –0.5 for $R > 170$ km, although they recognized that the data could have been just as easily interpreted as having a constant spreading coefficient of –0.5 beyond 50 km, consistent with the results of Raoof *et al.* (1999) and Malagnini *et al*. (2007). Further support for a near-source spreading coefficient of –1.0 in WNA is provided by Samiezade-Yazd (1993) for the Southern Great Basin (California and Nevada), Atkinson (1995) for crustal earthquakes in the Cascadia region (Pacific Northwest and southeastern British Columbia), and Herrmann and Dutt (1999) for crustal earthquakes in the Pacific Northwest.

I also found several supporting studies for relatively steep near-source geometric attenuation in ENA. Sonley and Atkinson (2006) found a relatively low near-source spreading coefficient (corresponding to relatively high attenuation) from an analysis of 800 three-component short-period and broadband recordings from 350 small-to-moderate earthquakes in the Charlevoix seismic zone of eastern Canada. They found a spreading coefficient of –1.36 within 70 km of the source similar to that found by Atkinson (2004) using a more geographically diverse dataset in southeastern Canada and northeastern United States. Atkinson (2004) compared the limited number of horizontal recordings to her model based on vertical components and concluded that any differences in attenuation were not statistically significant. Jeon and Herrmann (2006) also found a relatively high rate of near-source geometric attenuation in southeastern Canada from an empirical analysis of 4519 three-component seismograms recorded by the ECTN, but they concluded that the attenuation rate depended on the type of component. They found that the two horizontal components, the vertical component, and a combination of all three components had spreading coefficients of –1.3, –1.0 and –1.3 for $R < 40$ km and –1.2, –1.2 and –1.0 for $40 \le R < 60$ km. The vertical-component results of Atkinson (2004) are consistent with the vertical-component results of Jeon and Herrmann (2006) only if her results are dominated by distances greater than 40 km. Similarly, the three-component results of Sonley and Atkinson (2006) are consistent with the three-component results of Jeon and Herrmann (2006) only if their results are dominated by distances less than 40 km. Allen *et al*. (2007) found a geometric spreading coefficient of –1.3 within 90 km of the source using 1200 vertical-component seismograms from 84 small earthquakes in southeastern Australia, a Stable Continental Region (SCR) that is considered analogous to southeastern Canada for travel paths less than 100 km and frequencies less than 10 Hz (Atkinson and Allen, 2007). These results

would appear to support the vertical-component results of Atkinson (2004) and Jeon and Herrmann (2006) only if they are dominated by distances greater than 40 km.

The above discussion appears to lend additional support for a difference in near-source attenuation rates between Coastal California (and possibly other regions of the West Coast) and southeastern Canada and northeastern United States, although this conclusion depends on whether there is a consistency in both the ground motion components and the distance ranges that were used to derive the spreading coefficients (Jeon and Herrmann, 2006), factors that are not easily verified from the references. Furthermore, there is other evidence to suggest that the difference in geometric attenuation between horizontal ground motion components in these two regions, even if validated, might not be representative of other areas within the same general tectonic regions. For example, relatively high near-source geometric attenuation rates (typically spreading coefficients of –1.2 to –1.1) have been observed not only for Switzerland (Bay *et al*., 2003), a region that some consider to be a SCR like ENA, but also for the Erzincan region of Turkey (Akinci *et al*., 2001), the Friuli-Venezia Giulia region of northeastern Italy (Malagnini *et al*., 2002), and the Wasatch Front in Utah (Jeon and Herrmann, 2004), areas considered to be in regions of active tectonics. Conversely, spreading coefficients of around –1.0 have been found for other SCRs, such as Central Europe (Malagnini *et al*., 2000), the Kachchh Basin of southwestern India (Bodin *et al*., 2004), eastern Sicily (Scognamiglio *et al*., 2005), and the Burakin region of southwestern Western Australia (Allen *et al*., 2006). It is particularly interesting that Samiezade-Yazd *et al*. (1997) found a near-source geometric spreading coefficient of –1.0 for vertical-component seismograph data in the New Madrid region, location of the 1811–1812 New Madrid earthquakes (**M** 7.5–8.0), and not the stronger attenuation rate that was found for southeastern Canada and northeastern United States.

One possible explanation for the observed regional differences in near-source geometric attenuation noted above is offered by Herrmann and Malagnini (2005). Using numerical ground motion modeling studies for a crustal model typical of the central United States, these authors found that the factors most responsible for controlling near-source ($R < 40$ km) geometric attenuation were fault mechanism and component type. Their analysis for the two horizontal, the vertical, and the combination of all three components of ground motion resulted in geometric spreading coefficients of –1.3, –1.7 and –1.5 for 45°-dipping normal and reverse fault mechanisms and –1.3, –1.0 and –1.1 for vertically dipping strike-slip mechanisms. Interestingly, the simulated results for both types of fault mechanisms and the empirical results from southeastern Canada (Jeon and Herrmann, 2006) for reverse fault mechanisms consistently give a near-source spreading coefficient of around –1.3 for the horizontal components of ground motion. The simulated results also appear to be generally consistent with the spreading coefficients reported above for strike-slip events in Southern California (–1.1 vs. –1.0 for all three components) and for strike-slip events in New Madrid (–1.0 vs. –1.0 for vertical components). However, the simulated results do not seem to be consistent with the spreading coefficients reported above for strike-slip events in San Francisco (–1.3 vs. –1.0 for horizontal

components) and for normal-faulting events in Utah (–1.5 vs. –1.2 for all three components), although these latter results do both support attenuation rates steeper than one.

Stress maps developed for the United States by Herrmann (2007) and for the world by Heidbach *et al.* (2005) demonstrate the potential impact of the Herrmann and Malagnini (2005) simulation results on the attenuation of horizontal ground motion. According to these maps, southeastern Canada and northeastern United States are dominated by reverse fault mechanisms, which is consistent with the spreading coefficient of –1.3 used in this study and in Atkinson and Boore (2006). California is dominated by strike-slip faulting, which is consistent with a predicted spreading coefficient of –1.3 based on the simulations of Herrmann and Malagnini (2005) but is inconsistent with the –1.0 spreading coefficients found by Raoof *et al.* (1999) and Malagnini *et al*. (2007). The limited stress data that are available for the Atlantic Coastal Plain suggest that this region is likely to be dominated by reverse fault mechanisms, like the region to the north, and might be expected to exhibit a relatively high rate of near-source attenuation. The oddity is the Midwest, where the New Madrid area is observed to have a mixture of strike-slip and reverse fault mechanisms and the region north of New Madrid is observed to have predominantly strike-slip fault mechanisms. Therefore, according to Hermann and Malagnini (2005), these regions would likely have lower near-source geometric attenuation rates than other parts of ENA.

One can only conclude from this diverse range of observed and theoretical geometric spreading coefficients that there are large regional differences in attenuation that are not easily quantified in terms of simple tectonic environments, such as ENA and WNA. This means that the potential difference in geometric attenuation between WNA and ENA should be treated as a significant source of epistemic uncertainty. It appears that the –1.3 near-source geometric spreading coefficient used in ENA in this study is generally appropriate for horizontal ground motions in southeastern Canada, northeastern United States, and the Atlantic Coastal Plain, and if the theoretical modeling results of Herrmann and Malagnini (2005) are correct, even in the Midwest (including the New Madrid region). However, Herrmann and Malagnini (2005) also predict a horizontal near-source geometric spreading coefficient of –1.3 for California, in direct contradiction to the results of Raoof *et al.* (1999) and Malagnini *et al*. (2007), which appear to indicate that the predominantly strike-slip earthquakes in California have a near-source spreading coefficient of around –1.0.

I have attempted to assess the impact of the potentially higher near-source geometric attenuation in WNA predicted by Herrmann and Malagnini (2005) by adding the difference between the two spreading coefficients (0.3) to the model coefficient c_4 and adjusting c_0 to make the predicted ground motion from the alternative model equal to that of the original (base) model at a specified reference distance. I conservatively selected $R_{RUP} = 0$ as the reference distance to make the ground motion amplitudes for the two models the same at the closest point on the rupture plane. Therefore, the only difference in the two models is the constant regional near-source geometric spreading coefficient assumed in the alternative model (Herrmann and

Malagnini, 2005). A comparison of the attenuation characteristics predicted by the base HGMM, the alternative HGMM, and the WNA ground motion model developed by Campbell and Bozorgnia (2007a, 2008) is shown in Figure 18. This figure demonstrates that the constant rate of near-source attenuation inferred for the alternative ENA model, as compared to the steeper ENA versus WNA near-source attenuation used to develop the base ENA model, results in ground motion predictions that are either similar to or greater than those from the WNA model. Therefore, the alternative model is a conservative choice given that it always predicts higher near-source ground motion. I leave it to the user to decide how the base and alternative models should be weighted for their specific application. The alternative HGMM can be evaluated by replacing the coefficients c_0 and c_4 in Equation (32) by the alternative coefficients c_0' and c_4' listed in Table 2.

Functional Form

The functional form used to derive C03-ENA for distances within 70 km of the source was the same as that used in the Campbell and Bozorgnia (2003a, 2003b, 2003c, 2004) empirical ground motion model (CB03-WNA). On the other hand, the functional form used in this study was taken from the revised EGMM used to evaluate ground motions in the host region (CB07-WNA). These two empirical models have very different functional forms as demonstrated in Figure 19. The most notable difference is in the magnitude and distance scaling for $\mathbf{M} > 6.5$, where CB07-WNA has relaxed several of the constraints that were imposed by CB03-WNA and by a similar EGMM for PGV (C97-WNA) developed by Campbell (1997, 2000b) to compensate for the limited amount of near-source large-magnitude data that was available at the time. These constraints were: (1) imposing complete saturation of near-source ground motion with magnitude at zero distance for all oscillator periods and (2) imposing a constant far-source attenuation rate independent of magnitude. Using a significantly expanded strong motion database (Power *et al.*, 2006, 2008), Campbell and Bozorgnia (2007a, 2008) found that magnitude saturation occurred only at short-to-intermediate periods and that complete saturation occurred only for $\mathbf{M} > 6.5$, $R_{RUP} = 0$, and $T \leq 0.3$ sec. These investigators also found that the decay of ground motion with distance decreased with magnitude. Because these differences in functional forms had such a large impact on the predicted near-source ground motion from large earthquakes, during its review of the NGA project, the USGS applied several tests to determine whether the new functional form used in CB07-WNA was seismologically justified before it was accepted for use in the 2007 revision of the National Seismic Hazard Maps (NHSMP, 2007).

As part of the USGS review, Frankel (2007) used broadband ground motion simulations to test the dependence of ground motion attenuation on magnitude. He produced synthetic accelerograms for earthquakes with magnitudes of 6.5 and 7.5 and distances ranging from 2–200 km. He concluded from this study that the CB07-WNA functional form was consistent with the magnitude scaling and attenuation characteristics inferred from his broadband simulations. As an additional part of the USGS review, Jack Boatwright (written comm., 2005) used simple

seismological theory to provide constraints on the expected magnitude scaling of the far-field geometric attenuation term. These constraints were valid for large-magnitude earthquakes that were expected to exhibit near-source saturation at short periods. In all cases the far-field magnitude scaling predicted by CB07-WNA fell within Boatwright's theoretical constraints (Campbell and Bozorgnia, 2007a). The USGS also convened a distinguished panel of engineers and earth scientists to review the NGA models that were available at the time. This panel concluded from the extensive documentation that was provided to them, which included answers to USGS questions that were submitted prior to the panel meeting, that the CB07-WNA functional form was scientifically justified (NSHMP, 2007). The documentation that was provided to the panel is summarized in a comprehensive report by Campbell and Bozorgnia (2007a). Appendix B of that report also summarizes the USGS questions and responses as they pertain to CB07-WNA.

One major assumption in the present application of the HEM that has not been validated is whether the magnitude saturation characteristics predicted by CB07-WNA are directly transferable to ENA. The finite-source ground motion models of Atkinson and Boore (2006) and Somerville *et al.* (2001), both of which were developed specifically for ENA, do not predict the same degree of saturation that is predicted by CB07-WNA and the other NGA models (e.g., Abrahamson and Silva, 2007, 2008; Boore and Atkinson, 2007, 2008; Chiou and Youngs, 2007, 2008), or for that matter, by most of the other recent empirical ground motion models for WNA developed prior to the NGA project (e.g., Abrahamson and Shedlock, 1997; Campbell and Bozorgnia, 2003). Even theoretical finite-source models developed specifically for WNA (e.g., Somerville *et al.*, 2006) do not predict the same degree of saturation inferred by strong motion recordings from large earthquakes in active tectonic environments without imposing an additional constraint. Examples of such constraints include (1) a decreasing stress drop with magnitude (Atkinson and Silva, 1997, 2000), (2) a decreasing slip velocity with magnitude (Beresnev and Atkinson, 2002), (3) a decreasing "effective" source area with magnitude (Halldorsson and Papageorgiou, 2005), and (4) a decreasing strength of fault gauge with decreasing depth (Somerville and Pitarka, 2006). Several investigators offer possible physical mechanisms for these constraints. Somerville and Pitarka (2006) suggest that the observed saturation might be the result of rupture within the shallow part of the fault (upper few kilometers), which is controlled by velocity strengthening, larger slip weakening distance, larger fracture energy, larger energy absorption from the crack tip, lower rupture velocity, and lower slip velocity than rupture at greater depths on the fault. Using ground motion simulations from a dynamic rupture model, Schmedes and Archuleta (2007) found that near-field estimates of PGV increase to a maximum at a critical distance along the fault related to the rupture width and then decreases to an asymptotic value beyond this critical distance. Another physical mechanism that might result in ground motion saturation is the reduction in friction on the fault surface due to lubrication by rock melt (Di Toro *et al.*, 2006) and thermal dehydration (Hirose and Bystricky, 2007), properties that have been observed in laboratory experiments and inferred from exhumed faults.

The issue is whether the observed and modeled saturation of ground motion and the possible physical mechanisms that are used to explain this saturation is be expected in ENA. Beresnev and Atkinson (2002) noted that the slip velocity they found to be dependent on magnitude in WNA was randomly distributed with magnitude in ENA, suggesting that ENA earthquakes might not exhibit the same degree of saturation as WNA earthquakes. Halldorsson and Papgeorgiou (2005) did not see a need to invoke a decrease in "effective" source area for earthquakes in stable tectonic environments, such as ENA, as they did for earthquakes in active tectonic environments, also suggesting less saturation. However, there are very few recordings from large SCR earthquakes that can be used to test these hypotheses and those that are (e.g., 1976 $\mathbf{M} = 6.8$ Gazli, USSR; 1985 $\mathbf{M} = 6.8$ Nahanni, Canada) have very few recordings and are arguably located in more active tectonic environments or in transition zones between stable and active tectonic environments. Somerville and Pitarka (2006) argue that buried rupture, typical of ENA, is expected to produce higher ground motion than near-surface rupture, typical of WNA. This, however, does not rule out the same degree of saturation in the two regions. As a result of the lack of understanding on what physical mechanisms might lead to the ground motion saturation observed for large earthquakes in active tectonic environments and whether these mechanisms are also valid in stable tectonic environments, I consider the assumption in this study that the saturation predicted by WNA ground motion models is transferable to ENA to be a viable alternative hypothesis.

Source Spectral Shape

Tavakoli and Pezeshk (2005) argued that the use of a single-corner point-source stochastic model to develop the regional adjustment factors in C03-ENA caused this model to underestimate ground motion amplitudes at large magnitudes and short distances. This conclusion was based on several studies that found that a double-corner source spectrum used in conjunction with a stress drop that decreases with magnitude and a focal depth that increases with magnitude was required to match strong motion recordings from moderate-to-large earthquakes in California (Atkinson and Silva, 1997, 2000). They also noted that Atkinson and Boore (1995, 1997) proposed a double-corner source spectrum for ENA, except that this latter model assumed constant stress drop with magnitude. Tavakoli and Pezeshk went on to propose that using a double-corner source model would constitute an improvement in the HEM, at least as it was applied to ENA by Campbell (2003a, 2004) and, as a result, gave it significant weight in their application of the HEM. Although I do not agree with their hypothesis, for reasons given below, their ability to apply the double-corner model does demonstrate the flexibility of the HEM in accommodating a wide range of seismological modeling assumptions.

As mentioned previously, one of the strengths of the HEM is that the regional adjustment factors are not sensitive to the exact form of the source spectra or to the absolute amplitudes or functional relationships of the seismological parameters that are used in the stochastic simulations. What the HEM is sensitive to is the *difference* in the spectra and seismological

parameters between the host and target regions. This means that the seismological model does not need to produce correct absolute ground motion amplitudes for each region; it only needs to provide an accurate *ratio* of ground motion amplitudes between these regions. Accurate ratios will be obtained if the source spectra and other seismological parameters for each region have the same functional relationships, regardless of what these relationships are. For example, using a constant stress drop in each region will produce the same regional adjustment factors as using a stress drop that decreases with magnitude in each region as long as their ratios are the same. The reason that Tavakoli and Pezeshk obtained different results than C03-WNA was because their alternative double-corner source models in ENA and WNA did not produce ground motion ratios that were the same as those obtained using single-corner source models. The issue is whether these regional differences are real or just an artifact of how the seismological models were developed.

Tavakoli and Pezeshk (2005) adopted the Atkinson and Silva (2000) double-corner stochastic source model for WNA. Atkinson and Silva made two modifications to the standard Brune (1970, 1971) point-source stochastic model in order to better match California strong motion data: (1) they used a double-corner rather than a single-corner source spectrum and (2) they allowed the hypocentral depth of the equivalent point source to be an increasing function of magnitude. However, neither of these changes significantly affected the simulated ground motions at small magnitudes, where the single-corner and double-corner source models were found to give similar results. These modifications were only needed to match the finite-source effects of the strong motion recordings at large magnitudes and short distances. Although Atkinson and Silva found that the high-frequency amplitudes of their simulations were consistent with a constant stress drop of 80 bars, Tavakoli and Pezeshk incorrectly used a magnitude-dependent stress drop in conjunction with this double-corner source spectrum in their simulations, in direct violation of the model. Tavakoli and Pezeshk adopted the Atkinson and Boore (1995) double-corner stochastic source model for ENA. This model uses the double-corner source spectrum developed by Atkinson (1993), which has a different shape than the double-corner source spectrum used in WNA even after accounting for differences in stress drop. For their ENA model, Tavakoli and Pezeshk used the Atkinson (1993) double-corner source spectrum together with a constant stress drop and a hypocentral depth with the same dependence on magnitude as that used in WNA. All of the other seismological parameters were the same as those used by C03-ENA. Therefore, the cause of the difference in the ratios of simulated ENA-to-WNA ground motion amplitudes between Tavakoli and Pezeshk and C03-ENA is attributable to two factors: (1) the use of different double-corner source spectral shapes in ENA and WNA and (2) the use of a constant stress drop in ENA and a magnitude-dependent stress drop in WNA. The issue is whether these differences are warranted given the available data.

Due to the limited number of strong motion recordings in ENA, Atkinson (1993) used a diverse set of data to derive the double-corner source spectrum that was adopted by Atkinson and Boore (1995) and Tavakoli and Pezeshk (2005). The main database was a set of 1500 digital

seismograms ($2.5 \le \mathbf{M} < 6.0$) recorded by the ECTN, supplemented with moment magnitudes from other sources for the limited number of $\mathbf{M} > 4.5$ earthquakes. One-Hertz source spectral amplitudes for the larger earthquakes were taken from northeastern North American regional seismograms compiled by Street and Turcotte (1987) and worldwide intraplate teleseismic seismograms compiled by Boatwright and Choy (1992). High-frequency source spectral levels ($4 \le \mathbf{M} < 7$) were inferred from a relationship between high-frequency spectral level and felt area derived from ENA seismograms and MMI observations. The 1988 Nahanni, Canada, earthquake ($\mathbf{M} = 6.8$) and its aftershocks supplied the only set of large-magnitude strong motion recordings for her study. However, since the Nahanni events occurred along the Rocky Mountain Front, there is some question whether they truly represent an ENA tectonic environment or instead represent WNA tectonic conditions or a transition between WNA and ENA tectonic conditions. The relationship between the lower source-corner frequency (f_a) and magnitude was derived from the worldwide intraplate data of Boatwright and Choy (1992) and from corner frequencies inferred from the source durations of Somerville *et al.* (1987). The relationship between the higher source-corner frequency (f_b) and magnitude was derived from ECTN data and, according to Atkinson, was poorly constrained. The so-called sag in the double-corner source spectrum observed at intermediate frequencies was also poorly constrained by these data. One of the conclusions of the study was that most $\mathbf{M} > 4$ events have high-frequency spectral amplitudes that are consistent with a constant stress drop of approximately 150 bars. While the use of such a diverse set of seismological data by Atkinson is admirable, it cannot serve as a substitute for strong motion data. As a result, one needs to exercise caution when comparing her results to source models in WNA that are constrained by strong motion data. This caveat, together with the lack of adequate empirical constraints on the high-frequency corner and the intermediate-frequency spectral sag, and the questionable validity of the Nahanni earthquakes as representing a true ENA tectonic environment, results in a source spectral shape that is relatively poorly constrained and is not necessarily representative of ENA strong motion characteristics of near-source large-magnitude earthquakes.

Chen and Atkinson (2002) offered additional insight regarding the potential regional differences in source spectral shapes. They compared apparent earthquake source radiation for six different regions: Japan, Mexico, Turkey, California, British Columbia (western Canada), and ENA; and found that in all of these regions the apparent source spectra for small-to-moderate earthquakes ($\mathbf{M} < 6$) showed good agreement with the single-corner point-source omega-square (Brune) spectrum with a stress drop of around 100 bars. A two-corner source model was found to better match the spectra for large-magnitude earthquakes ($\mathbf{M} \ge 6$), especially at intermediate frequencies. For small-to-moderate events, the single-corner and double-corner source models were nearly equal and suggested a general similarity between the different tectonic regions studied. Although minor discrepancies appear in some cases, Chen and Atkinson did not find noticeable regional characteristics or depth effects associated with the apparent source spectra. They concluded that earthquakes of a given moment magnitude appear to have similar source spectral levels and shapes over different tectonic regions, where a mixture of tectonic styles may

be present within a region. This conclusion would appear to support a similarity in source spectral shapes in WNA and ENA.

Other investigators have also proposed that source spectral shapes in ENA and WNA might be similar or dependent only on differences in stress drop. Atkinson and Silva (1997) found that their empirical source spectrum for California was similar to that found for ENA by Atkinson and Boore (1995, 1997) at low frequencies, when differences in crustal properties were taken into account, implying that the two regions might have similar source spectra at these frequencies. They also found that the observed corner frequencies, f_a and f_b, of the double-corner source spectra in each region where virtually identical, but that the f_b–M relationship used in ENA predicted higher values of f_b in order to better match the large ENA spectral levels at high frequencies, relative to those at lower frequencies in ENA and those at all frequencies in WNA. This inconsistency between the high-frequency spectral amplitudes and the high-frequency corner frequencies in ENA might reflect an inconsistency in the different datasets that were used to derive these two parameters. These investigators also suggested that the enhanced high-frequency amplitudes in ENA are consistent with known differences in stress drop between the two regions. Therefore, these studies also suggest that differences in source spectra, aside from those caused by differences in stress drop, might not be important in the development of adjustment factors between WNA and ENA.

Atkinson (2001) went one step further and gave evidence to suggest that there is little, if any, difference in the apparent source radiation at both high and low frequencies between ENA and California earthquakes with the same moment magnitude. She cites a comparison of MMI data in WNA and ENA by Hanks and Johnston (1992) as suggesting that near-source damage levels, and by inference near-source ground motion amplitudes, are similar in the two regions for a given moment magnitude. However, Hanks and Johnston concluded that the MMI data, especially at the intensity VII level, are extremely limited and are not of themselves sufficient to rule out a possible factor of two higher stress drop in ENA. Bollinger *et al*. (1993) performed a similar study and concluded that the scatter in the MMI data was indeed large but that, in their opinion, it could support a possible factor of two higher stress drop in ENA.

Atkinson and Boore (1998) used the stochastic method to modify the empirical California source model of Atkinson and Silva (1997) for differences in crustal properties and generic rock characteristics between California and ENA and found that this modified model matched the limited ENA strong motion data almost as well as the stochastically derived ground motion model of Atkinson and Boore (1995) and better than many of the other stochastic ground motion models that had been developed for use in ENA up to that time. Beresnev and Atkinson (1999, 2002) performed finite-fault stochastic simulations of well-recorded moderate-to-large earthquakes in both California and ENA and suggested that the observed differences in ground motion between these two regions were largely caused by regional differences in crustal properties and anelastic attenuation.

All of the above studies point to the fact that one cannot disprove the hypothesis that source spectral shapes, aside from differences due to stress drop and crustal structure, are the same or very similar in ENA and WNA. One of the strengths of the HEM is that it is not sensitive to whether the source spectral shapes are single-corner, double-corner, or have some other arbitrary shape; it is only sensitive to whether these shapes are consistent. Certainly, there is ample evidence to support the hypothesis adopted in this study that ENA and WNA source spectra have similar shapes.

For their WNA stochastic model, Tavakoli and Pezeshk (2005) used a stress drop that decreased with magnitude in conjunction with the double-corner source spectrum of Atkinson and Silva (2000). Atkinson and Silva did not mention, nor did they require, the use of a stress drop parameter in their stochastic simulations. Moment magnitude, the corner frequencies f_a and f_b, and the weight (ε) of the two Brune single-corner source spectra that were derived from these frequencies, are the only parameters that were required to completely define the source spectrum. What they found was that the predicted high-frequency response spectral amplitudes from the stochastically simulated ground motions based on the double-corner point-source model were consistent with those from the single-corner point-source model when a constant stress drop of 80 bars was used over the entire magnitude range of interest ($5.0 \le \mathbf{M} \le 7.5$). They also found agreement amongst the high-frequency amplitudes of stochastic ground motion simulations and WNA strong motion data from three independent source models: (1) a single-corner source model with $\Delta\sigma = 80$ bars, (2) a double-corner source model, and (3) a finite-source model based on the FINSIM computer program of Beresnev and Atkinson (1998) with $s = 1.6$. Atkinson and Silva (1997) used the WNA strong motion database to derive parameters for a seismological model that was based on a single-corner source spectrum. They found that they needed to use stress drop and kappa values near 120 bars and 0.035 sec for $\mathbf{M} = 5.0$ and 50 bars and 0.05 sec for $\mathbf{M} = 7.5$ in order to fit these data. They suggested that the magnitude-dependence of stress drop might reflect saturation effects attributable to the point-source distance measure rather than to real stresses on the fault and that the magnitude-dependence of kappa could be interpreted as evidence of soil nonlinearity for typical California sites subjected to strong ground motion. None of these conclusions suggest the need to use a variable stress drop with the double-corner source spectrum in order to match strong motion data at large magnitudes. At magnitudes near 5.0, all three methods were found to give similar results, suggesting that the double-corner source spectrum and the source spectrum inferred from finite-source simulations are consistent with a single-corner source spectrum at small magnitudes (Atkinson and Silva, 1997, 2000).

Conclusions

The ENA ground motion model developed in this study represents a revision of the hybrid empirical ground motion model (HGMM) developed by Campbell (2003a, 2004). It uses an updated ENA seismological model developed by Atkinson (2004) and Atkinson and Boore

(2006) and an updated WNA empirical ground motion model (EGMM) developed by Campbell and Bozorgnia (2007a, 2008). The use of one rather than multiple WNA ground motion models was precipitated by a delay in the availability of the suite of empirical models that were being developed for the Next Generation Attenuation (NGA) project (Power *et al.*, 2006, 2008). However, there are several advantages of using a single EGMM in the implementation of the hybrid empirical method (HEM). For example, Scherbaum *et al.* (2005) proposed that stochastic model parameters should be tailored to a specific EGMM in order to account for differences that result from the melding of strong motion data from geographically diverse regions, even if these regions are located in similar tectonic environments. Scherbaum *et al.* (2006) proposed that the ground motion branches of a logic tree used for seismic hazard analysis should be treated as a single composite model representing the complete state-of-knowledge and belief of a particular ground motion analyst in a particular target region. As additional NGA models become available, they can be applied to ENA using the HEM framework to provide a more complete representation of uncertainty amongst this particular class of models.

The use of the revised ENA stochastic model resulted in a reduction in predicted short-period ground motions for NEHRP B-C site conditions compared to the previous model (Campbell, 2003a, 2004). This reduction is due mainly to the use of a larger kappa (κ_0), a stronger near-source geometric attenuation term (R^{-n}), and a lower median stress drop ($\Delta\sigma$) in the revised model. The use of the revised EGMM resulted in a reduction in near-source large-magnitude ground motions due mainly to the use of magnitude-dependent attenuation and the incorporation of greater magnitude saturation effects at short periods. An interesting outcome of these modifications is that the predicted ground motion in ENA at distances within 100 km of the source can be smaller than the predicted ground motion in WNA for NEHRP B-C site conditions if different spectral near-source geometric attenuation terms, derived from weak motion data, are used in ENA ($R^{-1.3}$) and WNA ($R^{-1.0}$). Using the more conservative alternative hypothesis, based on theoretical modeling studies, that spectral near-source geometric attenuation terms are the same in WNA and ENA ($R^{-1.3}$), the predicted near-source ground motions in ENA are similar to or larger than those in WNA at all distances. As a result of this uncertainty, the alternative model should be given significant weight in any seismic hazard analysis that uses the HGMM developed in this study. At larger distances, differences in geometric and anelastic attenuation will always result in higher ground motion amplitudes in ENA than in WNA regardless of what near-source geometric spreading coefficient is used.

Although there is a great deal of uncertainty in the values of the ENA stochastic model parameters I have used to develop the HGMM in this study, I have shown that the selected parameters together with the use of a single-corner source spectrum are reasonable given the limited amount of data that are available to constrain them. I have also shown that the use of single-corner source models in ENA and WNA do not lead to unreasonable near-source amplitudes, since magnitude saturation effects at large magnitudes are inherently accounted for through the use of an appropriate EGMM. Therefore, in my opinion, the HGMM developed in

this study represents a viable alternative to the ground motion models that are commonly used in seismic hazard evaluations in ENA as long as its use is restricted to $4.0 \le \mathbf{M} \le 8.0$, $R_{RUP} \le 100$ km, and NEHRP B-C site conditions (i.e., $V_{S30} = 760$ m/sec). Additional guidance is provided for extending the model to include the effects of fault mechanism, hanging-wall geometry, shallow site response, and basin response. If ground motion predictions at longer distances are required, they can be made by extrapolating the model using the distance (geometric and anelastic attenuation) scaling characteristics of one or more of the existing ENA ground motion models (e.g., Somerville *et al.*, 2001; Campbell, 2003a, 2004; Atkinson and Boore, 1995, 1997, 2006). This extrapolation can be done using the simplified method proposed by Campbell (2003a). If only one model is to be used for this extrapolation, I would recommend using that of Atkinson and Boore (2006), because it was developed using the same seismological parameters that were used in this study. The extrapolation should begin at a distance at which the attenuation characteristics begin to include the effects of critical reflections off the base of the crust (the Moho bounce), which for the Atkinson and Boore (2006) model occurs at 70 km.

Several seismological factors were found to have a significant impact on differences in the predicted ground motion between the revised and previous HGMM. These factors include: (1) the site profile and site attenuation that is used to represent NEHRP B-C site conditions in ENA, (2) the geometric spreading coefficient that is used to represent near-source attenuation in ENA, (3) the functional form that is used to characterize the ENA and WNA ground motion models, and (4) the assumption that source spectral shape aside from differences due to stress drop are similar in ENA and WNA. Item 2 is particularly important, since there are observed regional differences in the geometric spreading coefficients between the Midwest and the remainder of ENA that might infer differences in near-source ground motion attenuation in these two regions. More research is needed to reduce the epistemic uncertainty associated with these factors. In the meantime, the HGMM developed in this study, together with the diverse set of ground motion models that are already available for ENA, can be used to adequately represent the large epistemic uncertainty that characterizes the estimation of ground motion in this region.

References

Abrahamson, N. A., and A. M. Becker (1997). Ground motion characterization at Yucca Mountain, Nevada, Report submitted to the U.S. Geological Survey that fulfills Level 4 Milestone SPG28EM4 WBS No. 1.2.3.2.8.3.6.

Abrahamson, N. A., and K. M. Shedlock (1997). Overview, *Seism. Res. Lett.* **68**, 9–23.

Abrahamson, N. A., and W. Silva (2001). “Empirical” attenuation relations for central and eastern U.S. hard and soft rock and deep soil site conditions (abstract), *Seism. Res. Lett.* **72**, 282.

Abrahamson, N. A., and W. J. Silva (2007). *Abrahamson-Silva NGA Ground Motion Relations for the Geometric Mean Horizontal Component of Peak and Spectral Ground Motion*

Parameters, PEER Report No. 2007/03, Pacific Earthquake Engineering Research Center, University of California, Berkeley.

Abrahamson, N., and W. Silva (2008). Summary of the Abrahamson & Silva NGA ground motion relations, *Earthquake Spectra* **24**, in press.

Akinci, A., L. Malagnini, R. B. Herrmann, N. A. Pino, L. Scognamiglio, and H. Eyidogan (2001). High-frequency ground motion in the Erzincan region, Turkey: inferences from small earthquakes, *Bull. Seism. Soc. Am.* **91**, 1446–1455.

Allen, T. I., and G. M. Atkinson (2007). Comparison of earthquake source spectra and attenuation in eastern North America and southeastern Australia, *Bull. Seism. Soc. Am.* **97**, 1350–1354.

Allen, T. I., P. R. Cummins, and T. Dhu (2007). Empirical attenuation of ground-motion spectral amplitudes in southeastern Australia, *Bull. Seism. Soc. Am.* **97**, 1279–1292.

Allen, T. I., T. Dhu, P. R. Cummins, and J. F. Schneider (2006). Empirical attenuation of ground-motion spectral amplitudes in southwestern Western Australia, *Bull. Seism. Soc. Am.* **96**, 572–585.

Anderson, J. G. (2003). Strong motion seismology, in *International Handbook of Earthquake and Engineering Seismology*, W.H.K. Lee, H. Kanamori, P. C. Jennings, and C. Kisslinger (Editors), Academic Press, San Diego, California, Part B, 937–965.

Anderson, J. G., and S. E. Hough (1984). A model for the shape of the Fourier amplitude spectrum of acceleration at high frequencies, *Bull. Seism. Soc. Am.* **74**, 1969–1993.

Anderson, J. G., Y. Lee, Y Zeng, and S Day (1996). Control of strong motion by the upper 30 meters, *Bull. Seism. Soc. Am.* **86**, 1749–1759.

Atkinson, G. M. (1993). Earthquake source spectra in eastern North America, *Bull. Seism. Soc. Am.* **83**, 1778–1798.

Atkinson, G. M. (1995). Attenuation and source parameters of earthquakes in the Cascadia region, *Bull. Seism. Soc. Am.* **85**, 1327–1342.

Atkinson, G. M. (1996). The high-frequency shape of the source spectrum for earthquakes in eastern and western Canada, *Bull. Seism. Soc. Am.* **86**, 106–112.

Atkinson, G. M. (2001). An alternative to stochastic ground-motion relations for use in seismic hazard analysis in eastern North America, *Seism. Res. Lett.* **72**, 299–306.

Atkinson, G. M. (2004). Empirical attenuation of ground motion spectral amplitudes in southeastern Canada and the northeastern United States, *Bull. Seism. Soc. Am.* **94**, 1079–1095.

Atkinson, G. M. (2005). Ground motions for earthquakes in southwestern British Columbia and northwestern Washington: crustal, in-slab, and offshore events, *Bull. Seism. Soc. Am.* **95**, 1027–1044.

Atkinson, G. M., and D. M. Boore (1995). New ground motion relations for eastern North America, *Bull. Seism. Soc. Am.* **85**, 17–30.

Atkinson, G. M., and D. M. Boore (1997). Some comparisons between recent ground-motion relations, *Seism. Res. Lett.* **68**, 24–40.

Atkinson, G. M., and D. M. Boore (1998). Evaluation of models for earthquake source spectra in eastern North America, *Bull. Seism. Soc. Am.* **88**, 917–934.

Atkinson, G. M., and D. M. Boore (2006). Earthquake ground-motion prediction equations for eastern North America, *Bull. Seism. Soc. Am.* **96**, 2181–2205.

Atkinson, G. M., and R. F. Mereu (1992). The shape of ground motion attenuation curves in southeastern Canada, *Bull. Seism. Soc. Am.* **82**, 2014–2031.

Atkinson, G. M., and W. Silva (1997). An empirical study of earthquake source spectra for California earthquakes, *Bull. Seism. Soc. Am.* **87**, 97–113.

Atkinson, G. M., and W. Silva (2000). Stochastic modeling of California ground motions, *Bull. Seism. Soc. Am.* **90**, 255–274.

Atkinson, G. M., and E. Sonley (2000). Empirical relationships between modified Mercalli intensity and response spectra, *Bull. Seism. Soc. Am.* **90**, 537–544.

Baker, J. W., and C. A. Cornell (2006). Which spectral acceleration are you using?, *Earthquake Spectra* **22**, 293–312.

Bay, F., D. Fah, L. Malagnini, and D. Giardini (2003). Spectral shear-wave ground-motion scaling in Switzerland, *Bull. Seism. Soc. Am.* **93**, 414–429.

Benjamin, J. R., and C. A. Cornell (1970). *Probability, Statistics, and Decision for Civil Engineers*, McGraw-Hill, New York.

Beresnev, I. A., and G. M. Atkinson (1998). FINSIM: a FORTRAN program for simulating stochastic acceleration time histories from finite faults, *Seism. Res. Lett.* **69**, 27–32.

Beresnev, I. A., and G. M. Atkinson (1999). Generic finite-fault model for ground motion prediction in eastern North America, *Bull. Seism. Soc. Am.* **89**, 608–625.

Beresnev, I. A., and G. M. Atkinson (2002). Source parameters of earthquakes in eastern and western North America based on finite-fault modeling, *Bull. Seism. Soc. Am.* **92**, 695–710.

Boatwright, J. and G. Choy (1992). Acceleration source spectra anticipated for large earthquakes in northeastern North America, *Bull. Seism. Soc. Am.* **82**, 660–682.

Boatwright, J., H. Bundock, J. Luetgert, L. Seekins, L. Gee, and P. Lombard (2003). The dependence of PGA and PGV on distance and magnitude inferred from Northern California ShakeMap data, *Bull. Seism. Soc. Am.* **93**, 2043–2055.

Bodin, P., L. Malagnini, and A. Akinci (2004). Ground motion scaling in the Kachchh Basin, India, deduced from aftershocks of the 2001 M_W 7.6 Bhuj earthquake, *Bull. Seism. Soc. Am.* **94**, 1658–1669.

Bollinger, G. A., M. C. Chapman, and M. S. Sobol (1993). A comparison of earthquake damage areas as a function of magnitude across the United States, *Bull. Seism. Soc. Am.* **83**, 1064–1080.

Bolt, B. A. (1987). *Seismic Strong Motion Synthetics*, Academic Press, San Diego, California.

Bommer, J. J., F. Scherbaum, H. Bungum, F. Cotton, F. Sabetta, and N. A. Abrahamson (2005). On the use of logic trees for ground-motion prediction equations in seismic-hazard analysis, *Bull. Seism. Soc. Am.* **95**, 377–389.

Boore, D. M. (1983). Stochastic simulation of high-frequency ground motion based on seismological models of the radiated spectra, *Bull. Seism. Soc. Am.* **73**, 1865–1893.

Boore, D. M. (1996). SMSIM—Fortran programs for simulating ground motions from earthquakes: version 1.0, *U.S. Geol. Surv. Open-File Rept. 96-80-A.*

Boore, D. M. (2003). Prediction of ground motion using the stochastic method, *Pure Appl. Geophys.* **160**, 635–676.

Boore, D. M., and G. M. Atkinson (2007). *Boore-Atkinson NGA Ground Motion Relations for the Geometric Mean Horizontal Component of Peak and Spectral Ground Motion Parameters*, PEER Report No. 2007/01, Pacific Earthquake Engineering Research Center, University of California, Berkeley.

Boore, D. M., and G. M. Atkinson (2008). Ground-motion prediction equations for the average horizontal component of PGA, PGV, and 5%-damped PSA at spectral periods between 0.01 s and 10.0 s, *Earthquake Spectra* **24**, in press.

Boore, D. M., and W. B. Joyner (1984). A note on the use of random vibration theory to predict peak amplitudes of transient signals, *Bull. Seism. Soc. Am.* **74**, 2035–2039.

Boore, D. M., and W. B. Joyner (1991). Estimation of ground motion at deep-soil sites in eastern North America, *Bull. Seism. Soc. Am.* **81**, 2167–2185.

Boore, D. M., and W. B. Joyner (1997). Site amplification for generic rock sites, *Bull. Seism. Soc. Am.* **87**, 327–341.

Boore, D. M., K. W. Campbell, and R. B. Herrmann (1993). Estimation of ground motion in eastern North America, in *Hazard Assessment*, Central United States Earthquake Consortium, Memphis, Tennessee, 81–129.

Boore, D. M., W. B. Joyner, and T. E. Fumal (1997). Equations for estimating horizontal response spectra and peak acceleration from western North American earthquakes: a summary of recent work, *Seism. Res. Lett.* **68**, 128–153.

Boore, D. M., J. Watson-Lamprey, and N. Abrahamson (2006). Orientation-independent measures of ground motion, *Bull. Seism. Soc. Am.* **96**, 1502–1511.

Borcherdt, R. D. (1994). Estimates of site-dependent response spectra for design (methodology and justification), *Earthquake Spectra* **10**, 617–53.

Bozorgnia, Y., and K. W. Campbell (2004). Engineering characterization of ground motion, in *Earthquake Engineering from Engineering Seismology to Performance-Based Engineering*, Y. Bozorgnia and V. V. Bertero (Editors), CRC Press, Boca Raton, Florida, 5-1–5-74.

Brune, J. (1970). Tectonic stress and the spectra of seismic shear waves, *J. Geophys. Res.* **75**, 4997–5009.

Brune, J. (1971). Correction, *J. Geophys. Res.* **76**, 5002.

Budnitz, R. J., G. Apostolakis, D. M. Boore, L. S. Cluff, K. J. Coppersmith, C. A. Cornell, and P. A. Morris (1997). *Recommendations for Probabilistic Seismic Hazard Analysis: Guidance on Uncertainty and Use of Experts*, NUREG/CR-6372, U.S. Nuclear Regulatory Commission, Washington, D.C.

Burger, R. W., P. G. Somerville, J. S. Barker, R. B. Herrmann, and D. V. Helmberger (1987). The effect of crustal structure on strong ground motion attenuation relations in eastern North America, *Bull. Seism. Soc. Am.* **77**, 420–439.

Beyer, K., and J. J. Bommer (2006). Relationships between median values and between aleatory variabilities for different definitions of the horizontal component of motion, *Bull. Seism. Soc. Am.* **96**, 1512–1522.

Building Seismic Safety Council (BSSC) (2004). *NEHRP Recommended Provisions for Seismic Regulations for New Buildings and Other Structures (FEMA 450)*, 2003 Edition, National Institute of Building Sciences, Washington, D.C.

Campbell, K. W. (1981). A ground motion model for the central United States based on near-source acceleration data, in *Proceedings of the Conference on Earthquakes and Earthquake Engineering—the Eastern United States*, Ann Arbor Science Publishers, Ann Arbor, Michigan, Vol. 1, 213–232.

Campbell, K. W. (1982). A preliminary methodology for the regional zonation of peak ground acceleration, in *Proceedings of the 3rd International Earthquake Microzonation Conference*, Academic Press, San Diego, California, Vol. 1, 365–376.

Campbell, K. W. (1985). Strong motion attenuation relations: a ten-year perspective, *Earthquake Spectra* **1**, 759–804.

Campbell, K. W. (1986). An empirical estimate of near-source ground motion for a major, $m_b = 6.8$, earthquake in the eastern United States, *Bull. Seism. Soc. Am.* **76**, 1–17.

Campbell, K. W. (1987). Predicting strong ground motion in Utah, in *Assessment of Regional Earthquake Hazards and Risk Along the Wasatch Front, Utah*, P. L. Gori and W. W. Hays (Editors), *U.S. Geol. Surv, Open-File Rept. 87-585*, Vol. II, L1–L90.

Campbell, K. W. (1991). An empirical analysis of peak horizontal acceleration for the Loma Prieta, California, earthquake of 18 October 1989, *Bull. Seism. Soc. Am.* **81**, 1838–1858.

Campbell, K. W. (1997). Empirical near-source attenuation relationships for horizontal and vertical components of peak ground acceleration, peak ground velocity, and pseudo-absolute acceleration response spectra, *Seism. Res. Lett.* **68**, 154–179.

Campbell, K. W. (2000a). Predicting strong ground motion in Utah, in *Assessment of Regional Earthquake Hazards and Risk Along the Wasatch Front, Utah*, P. L. Gori and W. W. Hays (Editors), *U.S. Geol. Surv. Profess. Paper 1500-L*, L1–L31.

Campbell, K. W. (2000b). Erratum: empirical near-source attenuation relationships for horizontal and vertical components of peak ground acceleration, peak ground velocity, and pseudo-absolute acceleration response spectra, *Seism. Res. Lett.* **71**, 352–354.

Campbell, K. W. (2000c). Engineering seismology, in *Encyclopedia of Physical Science and Technology*, 3rd Edition, R. A. Meyers (Editor), Academic Press, San Diego, California.

Campbell, K. W. (2001a). Hybrid empirical model for estimating strong ground motion in regions of limited strong-motion recordings, in *Proceedings of the OECD/NEA Workshop on the Engineering Characterization of Seismic Input*, NEA/CSNI/R(2000)2, Nuclear Energy Agency, Paris, Vol. 1, 315–332.

Campbell, K. W. (2001b). Development of semi-empirical attenuation relationships for the CEUS, U.S. Geological Survey Award 01HQGR0011, Final report.

Campbell, K. W. (2003a). Prediction of strong ground motion using the hybrid empirical method and its use in the development of ground-motion (attenuation) relations in eastern North America, *Bull. Seism. Soc. Am.* **93**, 1012–1033.

Campbell, K. W. (2003b). Engineering models of strong ground motion, in *Earthquake Engineering Handbook*, W.-F. Chen and C. Scawthorn (Editors), CRC Press, Boca Raton, Florida, 5-1–5-75.

Campbell, K. W. (2003c). Strong motion attenuation relationships, in *International Handbook of Earthquake and Engineering Seismology*, W.H.K. Lee, H. Kanamori, P. C. Jennings, and C. Kisslinger (Editors), Academic Press, San Diego, California, Part B, 1003–1012.

Campbell, K. W. (2004). Erratum: prediction of strong ground motion using the hybrid empirical method and its use in the development of ground-motion (attenuation) relations in eastern North America, *Bull. Seism. Soc. Am.* **93**, 2418.

Campbell, K. W., and Y. Bozorgnia (2003a). Updated near-source ground motion (attenuation) relations for the horizontal and vertical components of peak ground acceleration and acceleration response spectra, *Bull. Seism. Soc. Am.* **93**, 314–331.

Campbell, K. W., and Y. Bozorgnia. (2003b). Erratum: updated near-source ground motion (attenuation) relations for the horizontal and vertical components of peak ground acceleration and acceleration response spectra, *Bull. Seism. Soc. Am.* **93**, 1413.

Campbell, K. W., and Y. Bozorgnia. (2003c). Erratum: updated near-source ground motion (attenuation) relations for the horizontal and vertical components of peak ground acceleration and acceleration response spectra, *Bull. Seism. Soc. Am.* **93**, 1872.

Campbell, K. W., and Y. Bozorgnia. (2004). Erratum: updated near-source ground motion (attenuation) relations for the horizontal and vertical components of peak ground acceleration and acceleration response spectra, *Bull. Seism. Soc. Am.* **94**, 2417.

Campbell, K. W., and Y. Bozorgnia (2007a). *Campbell-Bozorgnia NGA Ground Motion Relations for the Geometric Mean Horizontal Component of Peak and Spectral Ground Motion Parameters*, PEER Report No. 2007/02, Pacific Earthquake Engineering Research Center, University of California, Berkeley.

Campbell, K. W., and Y. Bozorgnia (2007b). Nonlinear site effects predicted by the 2006 Campbell-Bozorgnia NGA empirical ground motion model (abstract), *Seism. Res. Lett.* **78**, 272.

Campbell, K. W., and Y. Bozorgnia (2008). NGA ground motion model for the geometric mean horizontal component of PGA, PGV, PGD and 5% damped linear elastic response spectra for periods ranging from 0.01 to 10 s, *Earthquake Spectra* **24**, in press.

Cartwright, D. E., and M. S. Longuet-Higgins (1956). The statistical distribution of the maxima of a random function, *Proc. Roy. Soc. London, Ser. A237*, 212–232.

Chapman, M. C., J. R. Martin, C. G. Olgun, and J. N. Beale (2006). Site-response models for Charleston, South Carolina, and vicinity developed from shallow geotechnical investigations, *Bull. Seism. Soc. Am.* **96**, 467–489.

Chapman, M. C., P. Talwani, and R. C. Cannon (2003). Ground-motion attenuation in the Atlantic Coastal Plain near Charleston, South Carolina, *Bull. Seism. Soc. Am.* **93**, 998–1011.

Chen, S.-Z., and G. M. Atkinson (2002). Global comparisons of earthquake source spectra, *Bull. Seism. Soc. Am.* **92**, 885–895.

Chiou, B. S.-J., and R. R. Youngs (2007). *Chiou-Youngs NGA Ground Motion Relations for the Geometric Mean Horizontal Component of Peak and Spectral Ground Motion Parameters*, PEER Report No. 2007/04, Pacific Earthquake Engineering Research Center, University of California, Berkeley.

Chiou, B. S.-J., and R. R. Youngs (2008). Chiou-Youngs NGA ground motion relations for the geometric mean horizontal component of peak and spectral ground motion parameters, *Earthquake Spectra* **24**, in press.

Choi, Y., and J. P. Stewart (2005). Nonlinear site amplification as function of 30 m shear wave velocity, *Earthquake Spectra* **21**, 1–30.

Coppersmith, K. J. (1991). Seismic source characterization for engineering seismic hazard analysis, in *Proceedings of the 4th International Conference on Seismic Zonation*, Earthquake Engineering Research Institute, Palo Alto, California, Vol. 1, 3–60.

Cramer, C. H., J. S. Gomberg, E. S. Schweig, B. A. Waldron, and K. Tucker (2004). The Memphis, Shelby Country, Tennessee, seismic hazard maps, *U.S. Geol. Surv, Open-File Rept. 04-1294.*

Day, S. M., J. Bielak, D. Dreger., R. Graves, S. Larsen, K. Olsen., A. Pitarka, and L. Ramirez-Guzman (2006). Numerical simulation of basin effects on long-period ground motion, in *Proceedings of the 8th National Conference on Earthquake Engineering*, Paper No. 1857, Earthquake Engineering Research Institute, Oakland, California.

Day, S. M., R. Graves, J. Bielak, D. Dreger, S. Larsen, K. B. Olsen, A. Pitarka, and L. Ramirez-Guzman (2008). Model for basin effect on long-period response spectra, *Earthquake Spectra* **24**, in press.

Di Toro, G., T. Hirose, S. Nielsen, G. Pennacchioni., and T. Shimamoto (2006). Natural and experimental evidence of melt lubrication of faults during earthquakes, *Science* **311,** 647–649.

Dobry, R., R. D. Borcherdt, C. B. Crouse, I. M. Idriss, W. B. Joyner, G. R. Martin, M. S. Power, E. E. Rinne, and R. B. Seed (2000). New site coefficients and site classification system used in recent building seismic code provisions, *Earthquake Spectra* **16**, 41–67.

Douglas, J. (2003). Earthquake ground motion estimation using strong-motion records: a review of equations for the estimation of peak ground acceleration and response spectral ordinates, *Earth-Science Reviews* **61**, 43–104.

Douglas, J. (2006). *Errata of and Additions to 'Ground Motion Estimation Equations 1964-2003'*, BRGM/RP-54603-FR, Bureau de Recherches Géologiques et Minières (BRGM), Orléans, France, 103 pp.

Douglas, J., H. Bungum, and F. Scherbaum (2006). Ground-motion prediction equations for southern Spain and southern Norway obtained using the composite model perspective, *J. Earthquake Eng.* **10**, 33–72.

Ebel, J. E., and D. J. Wald (2003). Bayesian estimations of peak ground acceleration and 5% damped spectral acceleration from modified Mercalli Intensity data, *Earthquake Spectra* **19**, 511–529.

Electrical Power Research Institute (EPRI) (1993). Methods and guidelines for estimating earthquake ground motion in eastern North America, in *Guidelines for Determining Design Basis Ground Motions*, EPRI TR-102293, Palo Alto, California, Vol. 1.

Electrical Power Research Institute (EPRI) (2004). *CEUS Ground Motion Project Final Report*, EPRI TR-1009684, Palo Alto, California.

Frankel, A. D. (2007). Do the next generation attenuation relations make physical sense? (abstract), *Seism. Res. Lett.* **78**, 287.

Frankel, A., C. Mueller, T. Barnhard, D. Perkins, E. Leyendecker, N. Dickman, S. Hanson, and M. Hopper (1996). National seismic hazard maps: documentation June 1996, *U.S. Geol. Surv, Open-File Rept. 96-532.*

Gomberg, J., B. Waldron, E. Schweig, H. Hwang, A. Webbers, R. VanArsdale, K. Tucker, R. Williams, R. Street, P. Mayne, W. Stephenson, J. Odum, C. Cramer, R. Updike, S. Hutson, and M. Bradley (2003). Lithology and shear-wave velocity in Memphis, Tennessee, *Bull. Seism. Soc. Am.* **93**, 986–997.

Halldorsson, B., and A. S. Papgeorgiou (2005). Calibration of the specific barrier model to earthquakes of different tectonic regions, *Bull. Seism. Soc. Am.* **95,** 1276–1300.

Hanks, T. C., and A. C. Johnston (1992). Common features of the excitation and propagation of strong ground motion for North American earthquakes, *Bull. Seism. Soc. Am.* **82**, 1–23.

Hanks, T. C., and H. Kanamori (1979). A moment-magnitude scale, *J. Geophys. Res.* **84**, 2348–2350.

Hanks, T. C., and R. K. McGuire (1981). The character of high-frequency strong ground motion, *Bull. Seism. Soc. Am.* **71**, 2071–2095.

Heidbach, O., K. Fuchs, B. Müller, J. Reinecker, B. Sperner, M. Tingay, and F. Wenzel (2005). World stress map, WSM Release 2005, Commission for the Geological Map of the World, Heidelberg Academy of Sciences and Humanities, Heidelberg, Germany.

Herrmann, R. B. (2007). www.eas.slu.edu/Earthquake_Center/MECH.NA/MECHFIG.

Herrmann, R. B., and A. Akinci (1999). Mid-America ground motion models, www.eas.slu.edu/People/RBHerrmann/MAEC/maecgnd.html.

Herrmann, R. B., and J. Dutt (1999). High frequency vertical ground motion in the Pacific Northwest using PNSN data (abstract), *Seism. Res. Lett*. **70**, 216.

Herrmann, R., and L. Malagnini (2005). Interpretation of high frequency ground motion from regional seismic network observations, *Bull. Seism. Soc. Am*. (submitted).

Hirose, T., and M. Bystricky (2007). Extreme dynamic weakening of faults during dehydration by coseismic shear heating, *Geophs. Res. Lett.* **34**, L14311, doi:10.1029/2007GL030049.

Hough, S. E., J. G. Anderson, and H. J. Patton (1989). Attenuation in western Nevada: preliminary results from earthquake and explosion sources, *Geophs. Res. Lett.* **34**, 207–210.

Hwang, H., and J.-R. Huo (1997). Attenuation relations of ground motion for rock and soil sites in eastern United States, *Soil Dyn. Earthquake Eng.* **16**, 363–372.

Hwang, H.H.M., L. Huigie, and J.-R. Huo (1996). Site coefficients for design of buildings in eastern United States, *Soil Dyn. Earthquake Eng.* **16**, 29–40.

International Code Committee (ICC) (2006). *International Building Code 2006*, Falls Church, Virginia.

Ichinose, G. A., K. D. Smith, and J. G. Anderson (1997). Source parameters of the 15 November 1995 Border Town, Nevada, earthquake sequence, *Bull. Seism. Soc. Am.* **87**, 652–667.

Jeon, Y.-S., and R. B. Herrmann (2004). High-frequency earthquake ground-motion scaling in Utah and Yellowstone, *Bull. Seism. Soc. Am.* **94**, 1644–1657.

Jeon, Y.-S., and R. B. Herrmann (2006). High frequency earthquake ground motion scaling in southeastern Canada, *Bull. Seism. Soc. Am.* (submitted).

Joyner, W. B., R. E. Warrick, and T. E. Fumal (1981). The effect of Quaternary alluvium on strong ground motion in the Coyote Lake, California, earthquake of 1979, *Bull. Seism. Soc. Am.* **71**, 1333–1349.

Kaka, S. I., and G. M. Atkinson (2004). Relationships between instrumental ground-motion parameters and modified Mercalli Intensity in eastern North America, *Bull. Seism. Soc. Am.* **94**, 1828–1736.

Kramer, S. L. (1996). *Geotechnical Earthquake Engineering*, Prentice Hall, Upper Saddle River, New Jersey.

Liu, L., and S. Pezeshk (1999). An improvement on the estimation of pseudoresponse spectral velocity using RVT method, *Bull. Seism. Soc. Am.* **89**, 1384–1389.

Ma, S., and G. M. Atkinson (2006). Focal depths for small to moderate earthquakes ($m_N \geq 2.8$) in western Quebec, southern Ontario, and northern New York, *Bull. Seism. Soc. Am.* **96**, 609–623.

Malagnini, L., R. B. Herrmann, and K. Koch (2000). Regional ground-motion scaling in Central Europe, *Bull. Seism. Soc. Am.* **90**, 1052–1061.

Malagnini, L., A. Akinci, R. B. Herrmann, N. A. Pino, and L. Scognamiglio (2002). Characteristics of the ground motion in northeastern Italy, *Bull. Seism. Soc. Am.* **92**, 2186–1389.

Malagnini, L., K. Mayeda, R. Uhrhammer, A. Akinci, and R. B. Herrmann (2007). A regional ground-motion excitation/attenuation model for the San Francisco region, *Bull. Seism. Soc. Am.* **97**, 843–862.

McGuire, R. K. (2004). *Seismic Hazard and Risk Analysis*, Earthquake Engineering Research Institute, Palo Alto, California.

McGuire, R. K., and T. C. Hanks (1980). RMS accelerations and spectral amplitudes of strong ground motion during the San Fernando, California, earthquake, *Bull. Seism. Soc. Am.* **70**, 1907–1919.

Motazedian, D., and G. M. Atkinson (2005). Stochastic finite-fault modeling based on a dynamic corner frequency, *Bull. Seism. Soc. Am.* **95**, 995–1010.

Newmark, N. M., and W. J. Hall (1982). *Earthquake Spectra and Design*, Earthquake Engineering Research Institute, Berkeley, California.

Nuttli, O. W., and R. B. Herrmann (1984). Ground motion of Mississippi Valley earthquakes, *J. Tech. Topics Civil Eng.* **110**, 54–69.

Park, D., and Y.M.A. Hashash (2004). Evaluation of seismic site factors in the Mississippi Embayment. I. Estimation of dynamic properties, *Soil Dyn. Earthquake Eng.* **25**, 133–144.

Power, M., B. Chiou, N. Abrahamson, and C. Roblee. (2006). The next generation of ground motion attenuation models (NGA) project: an overview, in *Proceedings of the 8th National Conference on Earthquake Engineering*, Paper No. 2022, Earthquake Engineering Research Institute, Oakland, California.

Power, M., B. Chiou, N. Abrahamson, Y. Bozorgnia, T. Shantz, and C. Roblee (2008). An overview of the PGA project, *Earthquake Spectra* **24**, in press.

Raoof, M., R. Herrmann, and L. Malagnini (1999). Attenuation and excitation of three-component ground motion in southern California, *Bull. Seism. Soc. Am.* **89**, 888–902.

Reiter, L. (1990). *Earthquake Hazard Analysis: Issues and Insight*, Columbia University Press, New York.

Romero, S. M., and G. J. Rix (2001). *Ground Motion Amplification in the Upper Mississippi Embayment*, GIT-CEE/GEO-01-1, School of Civil and Environmental Engineering, Georgia Institute of Technology, Atlanta, Georgia.

Samiezade-Yazd, M. R. (1993). Ground motion studies in the southern Great Basin of Nevada and California, *Ph.D. Thesis*, Saint Louis University, St. Louis, Missouri.

Samiezade-Yazd, M., R. B. Herrmann, L. Malagnini, and W. Liu (1997). A regional comparison of vertical ground motion in North America, 1434-94-G-2403, Saint Louis University, St. Louis, Missouri, www.eas.slu.edu/People/RBHerrmann/GroundMotion.

Savy, J. B., D. L. Bernreuter, and J. C. Chen (1987). A methodology to correct for effect of the local site characteristics in seismic hazard analyses, in *Ground Motion and Engineering Seismology*, A. S. Cakmak (Editor), Elsevier, Amsterdam, Developments in Geotechnical Engineering, Vol. 44, 243–255.

Savy, J., W. Foxall, and N. Abrahamson (1999). *Guidance for Performing Probabilistic Seismic Hazard Analysis for a Nuclear Plant Site: Example Application to the Southeastern United States*, NUREG/CR-6607, U.S. Nuclear Regulatory Commission, Washington, D.C.

Scherbaum, F., J. J. Bommer, H. Bungum, F. Cotton, and N. A. Abrahamson (2005). Composite ground-motion models and logic trees: methodology, sensitivities, and uncertainties, *Bull. Seism. Soc. Am.* **95**, 1575–1593.

Scherbaum, F., F. Cotton, and H. Staedtke (2006). The estimation of minimum-misfit stochastic models from empirical ground-motion prediction equations, *Bull. Seism. Soc. Am.* **96**, 427–445.

Schmedes, J., and R. J. Archuleta (2007). Oversaturation of peak ground velocity along strike slip faults (abstract), *Seism. Res. Lett.* **78**, 272.

Scognamiglio, L., L. Malagnini, and A. Akinci (2005). Ground-motion scaling in eastern Sicily, Italy, *Bull. Seism. Soc. Am.* **95**, 568–578.

Silva, W. J, and R. Darragh (1995). *Engineering Characterization of Earthquake Strong Ground Motion Recorded at Rock Sites*, EPRI TR-102261, Electric Power Research Institute, Palo Alto, California.

Silva, W., R. Darragh, N. Gregor, G. Martin, N. Abrahamson, and C. Kircher (1999). Reassessment of site coefficients and near-fault factors for building code provisions, U.S. Geological Survey Award 98HQGR1010, Final report.

Silva, W., N. Gregor, and R. Darragh (2003). *Development of Regional Hard Rock Attenuation Relations for Central and Eastern North America, Mid-continent and Gulf Coast Areas*, Pacific Engineering and Analysis, El Cerrito, California.

Somerville, P. (1993). Engineering applications of strong ground motion simulation, in *New Horizons in Strong Motion: Seismic Studies and Engineering Practice*, F. Lund (Editor), *Tectonophysics* **218**, 195–219.

Somerville, P., and A. Pitarka (2006). Differences in earthquake source and ground motion characteristics between surface and buried faulting earthquakes, in *Proceedings of the 8th U.S. National Conference on Earthquake Engineering*, Paper No. 977, Earthquake Engineering Research Institute, El Cerrito, California.

Somerville, P., and J. Yoshimura (1990). The influence of critical MOHO reflections on strong ground motions recorded in San Francisco and Oakland during the 1989 Loma Prieta earthquake, *Geophys. Res. Lett.* **17**, 1203–1206.

Somerville, P., N. Collins, N. Abrahamson, R. Graves, and C. Saikia (2001). Ground motion attenuation relations for the central and eastern United States, U.S. Geological Survey Award 99HQGR0098, Final report.

Somerville, P., N. Collins, R. Graves, A. Pitarka, W. Silva, and Y. Zeng (2006). Simulation of ground motion scaling characteristics for the NGA-E project, in *Proceedings of the 8th U.S. National Conference on Earthquake Engineering*, Paper No. 1789, Earthquake Engineering Research Institute, El Cerrito, California.

Somerville, P., J. McLaren, L. Leevre, R. Burger, and D. Helmberger (1987). Comparison of source scaling relations of eastern and western North American earthquakes, *Bull. Seism. Soc. Am.* **77**, 322–346.

Somerville, P., J. McLaren, C. Saikia, and D. Helmberger (1990). The Nov. 25, 1988 Saguenay, Quebec earthquake: source parameters and the attenuation of strong ground motion, *Bull. Seism. Soc. Am.* **80**, 1118–1143.

Su, F., J. G. Anderson, J. N. Brune, and Y. Zeng (1996). A comparison of direct *S*-wave and coda-wave site amplification determined from aftershocks of the Little Skull Mountain earthquake, *Bull. Seism. Soc. Am.* **86**, 1006–1018.

Stepp, J. C., I. Wong, J. Whitney, R. Quittmeyer, N. Abrahamson, G. Toro, R. Youngs, K. Coppersmith, J Savy, T. Sullivan, and Yucca Mtn. PSHA Project Members (2001). Probabilistic seismic hazard analyses for ground motions and fault displacement at Yucca Mountain, Nevada, *Earthquake Spectra* **17**, 113–151.

Street, R., and F. Turcotte (1977). A study of northeastern North American spectral moments, magnitudes, and intensities, *Bull. Seism. Soc. Am.* **67**, 599–614.

Tavakoli, B., and S. Pezeshk (2005). Empirical-stochastic ground-motion prediction for eastern North America, *Bull. Seism. Soc. Am.* **95**, 2283–2296.

Thenhaus, P. C., and K. W. Campbell (2003). Seismic hazard analysis, in *Earthquake Engineering Handbook*, W.-F. Chen and C. Scawthorn (Editors), CRC Press, Boca Raton, Florida, 8-1–8-50.

Toro, G. R. (2002). *Modification of the Toro et al. (1997) Attenuation Equations for Large Magnitudes and Short Distances*, Risk Engineering, Boulder, Colorado.

Toro, G. R., N. A. Abrahamson, and J. F. Schneider (1997). Model of strong ground motions from earthquakes in central and eastern North America: best estimates and uncertainties, *Seism. Res. Lett.* **68**, 41–57.

Trifunac, M. D., and V. W. Lee (1989). Empirical models for scaling pseudo relative velocity spectra of strong earthquake accelerations in terms of magnitude, distance, site intensity and recording site conditions, *Soil Dyn. Earthquake Eng.* **8**, 126–144.

Trifunac, M. D., and V. W. Lee (1992). A note on scaling peak acceleration, velocity and displacement of strong earthquake shaking by modified Mercalli Intensity (MMI) and site soil and geologic conditions, *Soil Dyn. Earthquake Eng.* **11**, 101–110.

Wald, D. J., V. Quitoriano, T. H. Heaton, and H. Kanamori (1999). Relationships between peak ground acceleration, peak ground velocity, and modified Mercalli Intensity in California, *Earthquake Spectra* **15**, 557–564.

Watson-Lamprey, J. A., and D. M. Boore (2007). Beyond Sa_{GMRotI}: conversion to Sa_{Arb}, Sa_{SN}, and Sa_{MaxRot}, *Bull. Seism. Soc. Am.* **97** (in press).

Wells, D. L., and K. J. Coppersmith (1994). New empirical relationships among magnitude, rupture length, rupture width, rupture area, and surface displacement, *Bull. Seism. Soc. Am.* **84**, 974–1002.

Wen, Y. K., and C. L. Wu (2001). Uniform hazard ground motions for mid-America cities, *Earthquake Spectra* **17**, 359–384.

Bibliography of Published Reports

Campbell, K. W. (2007). Revision of the Campbell hybrid-empirical ground motion model for eastern North America (abstract), *Seism. Res. Lett.* **78**, 264.

Campbell, K. W. (2007). Prediction of near-source ground motion in eastern North America using the hybrid empirical method, *Bull. Seism. Soc. Am.* (submitted).

Table 1

Median Seismological Parameters Used in the Stochastic Models

Parameter	Western North America (WNA)	Eastern North America (ENA)
Source spectrum	Brune ω-square point source	Brune ω-square point source
Shear velocity, β_s (km/s)	3.5	3.7
Density, ρ_s (gm/cc)	2.8	2.8
Stress drop, $\Delta\sigma$ (bars)	100	140
Focal depth (km)	8.0	13.0
Fault width (km)	Wells and Coppersmith	0.6 × Wells and Coppersmith
Source duration, T_s (sec)	$1/f_0$	$1/f_0$
Geometric attenuation, $Z(R)$	$R^{-1.0}$; $R < 40$ km $R^{-0.5}$; $R \geq 40$ km	$R^{-1.3}$; $R < 70$ km $R^{+0.2}$; $70 \leq R < 140$ km $R^{-0.5}$; $R \geq 140$ km
Path duration, T_p (sec)	$0.05R$	0; $R \leq 10$ km $+0.16R$; $10 < R \leq 70$ km $-0.03R$; $70 < R \leq 130$ km $+0.04R$; $R > 130$ km
Path attenuation, Q	$200 f^{0.65}$	$893 f^{0.32}$ (1000 minimum)
Site profile[a] (30-m velocity)	WNA generic rock (620 m/sec)	ENA NEHRP B-C (760 m/sec)
Site amplification, $A(f)$[b]	Quarter–wavelength	Quarter–wavelength
Site attenuation, κ_0 (sec)	0.04	0.02

[a] WNA generic rock (Boore and Joyner, 1997); ENA NEHRP B-C (Frankel *et al.*, 1996).

[b] WNA (Boore and Joyner, 1997); ENA (Atkinson and Boore, 2006).

Table 2

Coefficients for the Base and Alternative Median Hybrid Empirical Ground Motion Models

T (sec)	c_0	c_0'	c_1	c_2	c_3	c_4	c_4'	c_5	c_6
0.000	0.780	0.311	0.273	-0.427	-0.191	-2.833	-2.533	0.221	4.77
0.010	0.723	0.256	0.285	-0.435	-0.189	-2.814	-2.514	0.218	4.75
0.020	1.293	0.822	0.234	-0.405	-0.179	-2.882	-2.582	0.223	4.81
0.030	1.555	1.080	0.241	-0.401	-0.183	-2.867	-2.567	0.217	4.87
0.050	1.200	0.725	0.326	-0.477	-0.192	-2.814	-2.514	0.214	4.87
0.075	0.981	0.506	0.392	-0.525	-0.233	-2.794	-2.494	0.209	4.87
0.10	0.703	0.228	0.453	-0.552	-0.264	-2.736	-2.436	0.199	4.87
0.15	-0.202	-0.677	0.583	-0.595	-0.299	-2.524	-2.224	0.173	4.87
0.20	-1.064	-1.539	0.665	-0.537	-0.382	-2.359	-2.059	0.158	4.87
0.25	-1.560	-2.007	0.677	-0.462	-0.448	-2.299	-1.999	0.157	4.43
0.30	-1.949	-2.371	0.684	-0.394	-0.510	-2.250	-1.950	0.157	4.08
0.40	-2.315	-2.704	0.677	-0.266	-0.616	-2.238	-1.938	0.158	3.66
0.50	-3.388	-3.750	0.812	-0.350	-0.584	-2.235	-1.935	0.160	3.34
0.75	-5.441	-5.764	1.058	-0.528	-0.497	-2.243	-1.943	0.166	2.93
1.0	-6.813	-7.137	1.228	-0.653	-0.419	-2.266	-1.966	0.169	2.94
1.5	-8.826	-9.154	1.476	-0.875	-0.273	-2.328	-2.028	0.177	2.98
2.0	-9.670	-10.002	1.531	-0.819	-0.279	-2.391	-2.091	0.186	3.02
3.0	-10.357	-10.697	1.504	-0.533	-0.453	-2.489	-2.189	0.198	3.11
4.0	-10.900	-11.246	1.495	-0.251	-0.685	-2.546	-2.246	0.204	3.17
5.0	-11.314	-11.664	1.491	-0.028	-0.878	-2.575	-2.275	0.207	3.21
7.5	-12.069	-12.424	1.488	-0.046	-0.539	-2.596	-2.296	0.209	3.26
10.0	-12.615	-12.971	1.484	-0.041	-0.322	-2.594	-2.294	0.208	3.28

PGA is equivalent to PSA at $T = 0$ sec; model coefficients with a prime should be used with the alternative ground motion model that assumes WNA near-source geometric attenuation proportional to $R^{-1.3}$ rather than to $R^{-1.0}$.

Table 3

Standard Deviations of the Hybrid Empirical Ground Motion Model

T (sec)	σ	τ	σ_{Fit}	σ_C	σ_{GM}	σ_{Arb}
0.000	0.478	0.219	0.063	0.166	0.530	0.555
0.010	0.478	0.219	0.061	0.166	0.529	0.554
0.020	0.480	0.219	0.061	0.166	0.531	0.556
0.030	0.489	0.235	0.059	0.165	0.546	0.570
0.050	0.510	0.258	0.052	0.162	0.574	0.596
0.075	0.520	0.292	0.050	0.158	0.598	0.619
0.10	0.531	0.286	0.051	0.170	0.605	0.628
0.15	0.532	0.280	0.053	0.180	0.604	0.630
0.20	0.534	0.249	0.051	0.186	0.591	0.620
0.25	0.534	0.240	0.046	0.191	0.587	0.617
0.30	0.544	0.215	0.042	0.198	0.586	0.619
0.40	0.541	0.217	0.036	0.206	0.584	0.619
0.50	0.550	0.214	0.041	0.208	0.592	0.627
0.75	0.568	0.227	0.035	0.221	0.613	0.652
1.0	0.568	0.255	0.038	0.225	0.624	0.663
1.5	0.564	0.296	0.042	0.222	0.638	0.676
2.0	0.571	0.296	0.046	0.226	0.645	0.683
3.0	0.558	0.326	0.052	0.229	0.648	0.687
4.0	0.576	0.297	0.055	0.237	0.650	0.692
5.0	0.601	0.359	0.056	0.237	0.702	0.741
7.5	0.628	0.428	0.057	0.271	0.762	0.809
10.0	0.667	0.485	0.056	0.290	0.827	0.876

PGA is equivalent to PSA at $T = 0$ sec.

Table 4

Coefficients for the Hybrid Empirical Ground Motion Model Source and Site Response Terms

T (sec)	c	n	k_1	k_2	k_3	k_4	k_5	k_6	k_7
0.000	1.88	1.18	865	-1.186	1.058	0.040	1.122	-0.280	0.490
0.010	1.88	1.18	865	-1.186	1.058	0.040	1.122	-0.280	0.490
0.020	1.88	1.18	865	-1.219	1.102	0.040	1.122	-0.280	0.490
0.030	1.88	1.18	908	-1.273	1.174	0.040	1.123	-0.280	0.490
0.050	1.88	1.18	1054	-1.346	1.272	0.040	1.124	-0.280	0.490
0.075	1.88	1.18	1086	-1.471	1.438	0.040	1.125	-0.280	0.490
0.10	1.88	1.18	1032	-1.624	1.604	0.040	1.127	-0.280	0.490
0.15	1.88	1.18	878	-1.931	1.928	0.040	1.130	-0.280	0.490
0.20	1.88	1.18	748	-2.188	2.194	0.040	1.132	-0.280	0.490
0.25	1.88	1.18	654	-2.381	2.351	0.040	1.303	-0.280	0.490
0.30	1.88	1.18	587	-2.518	2.460	0.040	1.399	-0.280	0.490
0.40	1.88	1.18	503	-2.657	2.587	0.040	1.593	-0.280	0.490
0.50	1.88	1.18	457	-2.669	2.544	0.040	1.663	-0.280	0.490
0.75	1.88	1.18	410	-2.401	2.133	0.077	1.906	-0.280	0.490
1.0	1.88	1.18	400	-1.955	1.571	0.150	1.929	-0.255	0.490
1.5	1.88	1.18	400	-1.025	0.406	0.253	1.974	-0.161	0.490
2.0	1.88	1.18	400	-0.299	-0.456	0.300	2.019	-0.094	0.371
3.0	1.88	1.18	400	0.000	-0.820	0.300	2.110	0.000	0.154
4.0	1.88	1.18	400	0.000	-0.820	0.300	2.200	0.000	0.000
5.0	1.88	1.18	400	0.000	-0.820	0.300	2.291	0.000	0.000
7.5	1.88	1.18	400	0.000	-0.820	0.300	2.517	0.000	0.000
10.0	1.88	1.18	400	0.000	-0.820	0.300	2.744	0.000	0.000

PGA is equivalent to PSA at $T = 0$ sec.

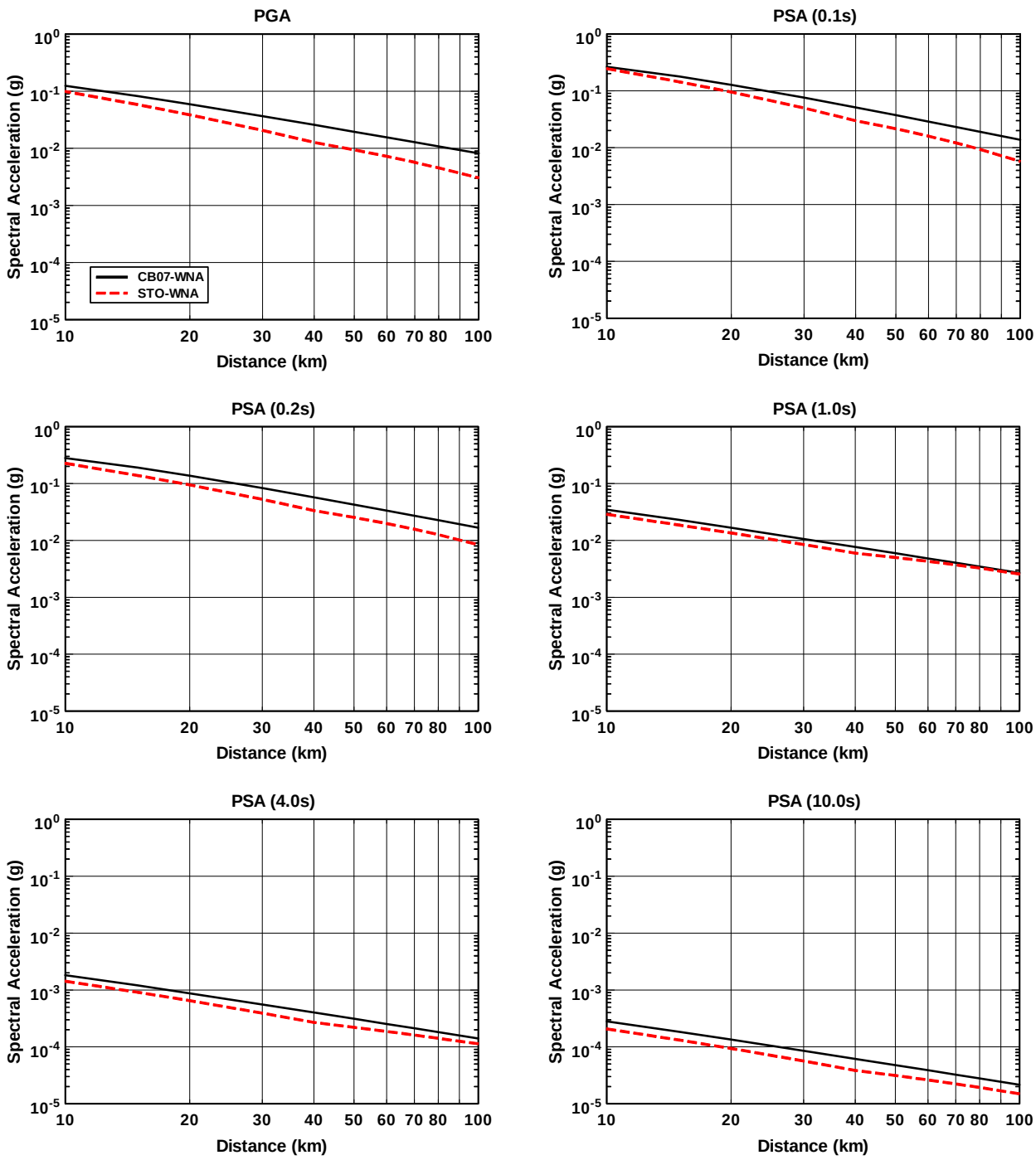

Figure 1. Predicted near-source attenuation characteristics for a magnitude 5.0 earthquake in WNA. CB07-WNA, empirical ground motion model used to represent the host region (Campbell and Bozorgnia, 2007a, 2008); STO-WNA, single-corner point-source stochastic model based on the WNA seismological parameters listed in Table 1 (this study).

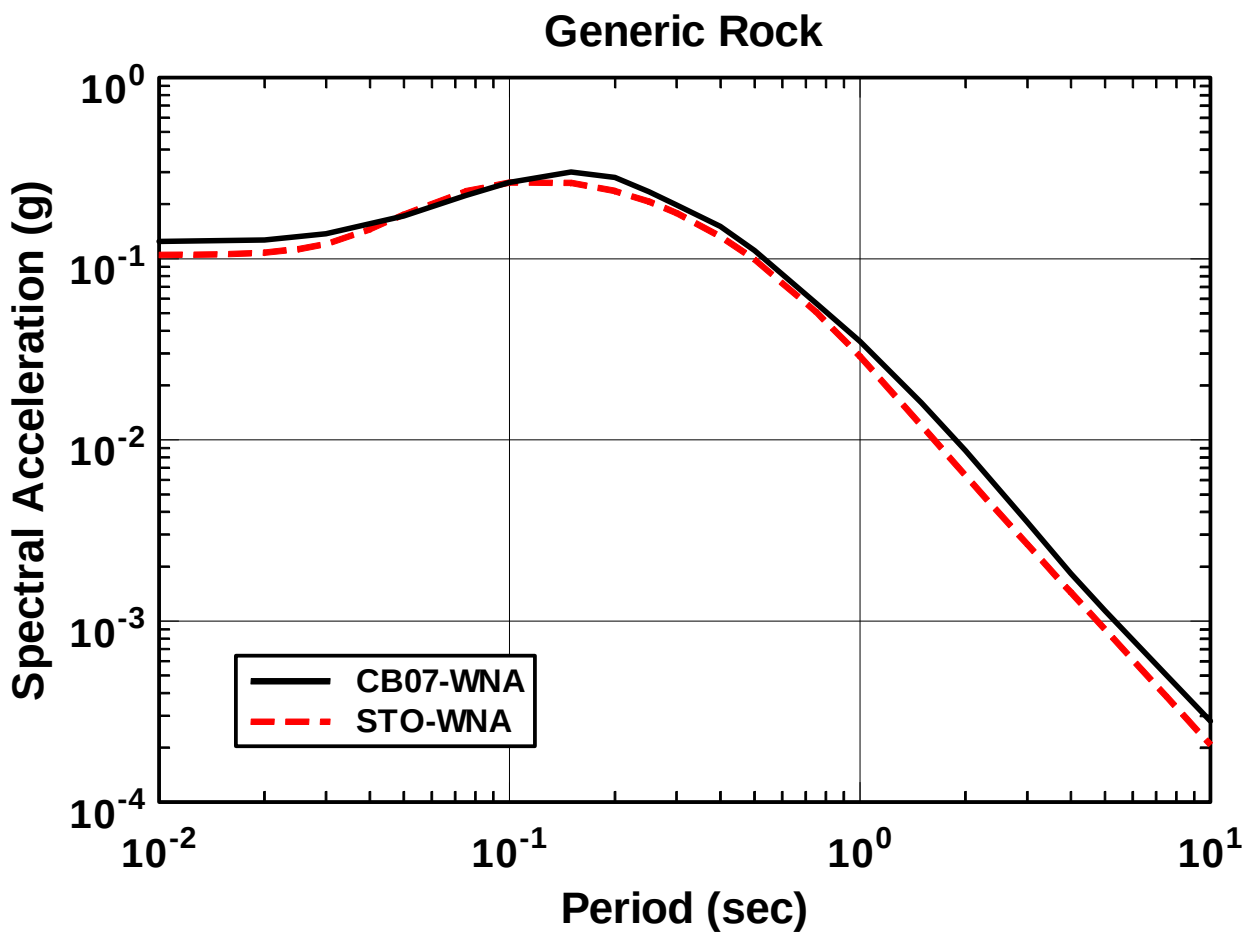

Figure 2. Predicted response spectra for a site located 10 km from a magnitude 5.0 earthquake in WNA. CB07-WNA, empirical ground motion model used to represent the host region (Campbell and Bozorgnia, 2007a, 2008); STO-WNA, single-corner point-source stochastic model based on the WNA seismological parameters listed in Table 1 (this study).

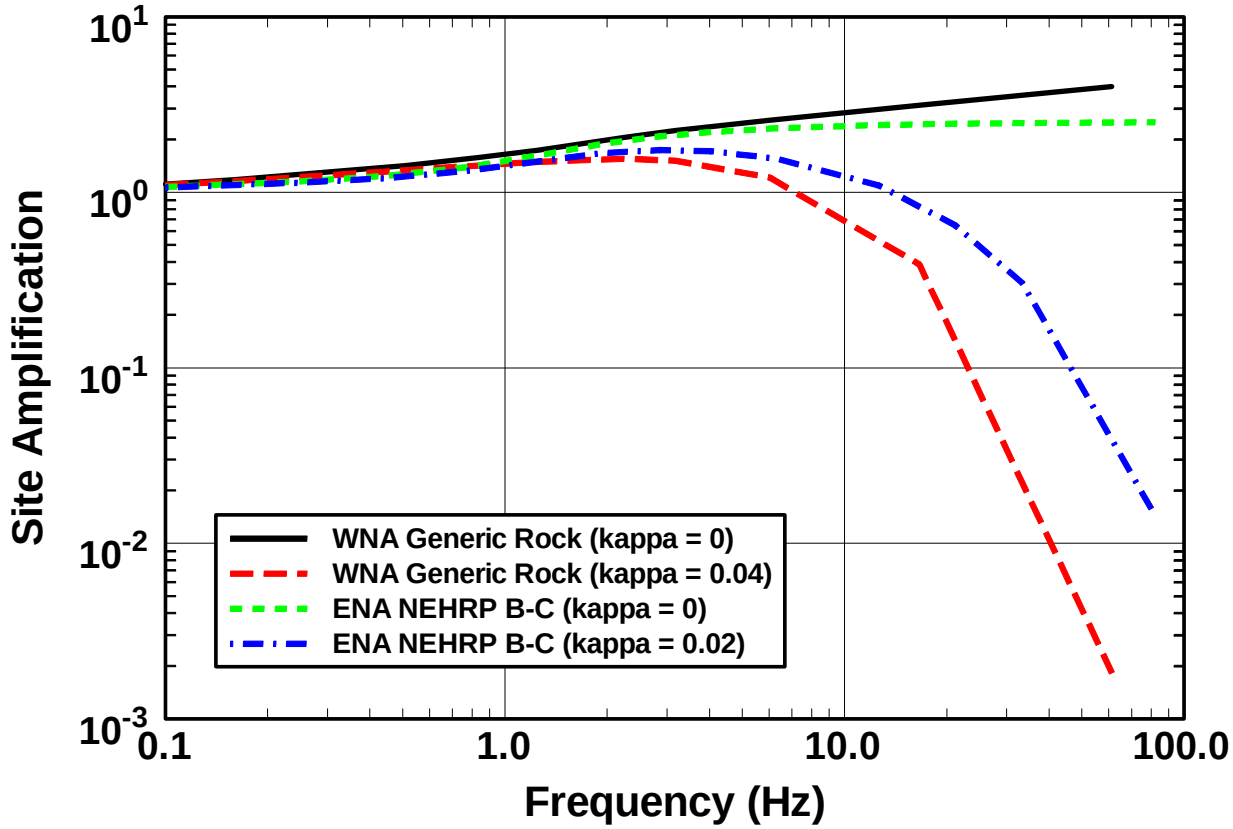

Figure 3. The effects of site attenuation (kappa, κ_0) on site amplification factors of Fourier amplitude spectra used in the ENA and WNA seismological models (Table 1).

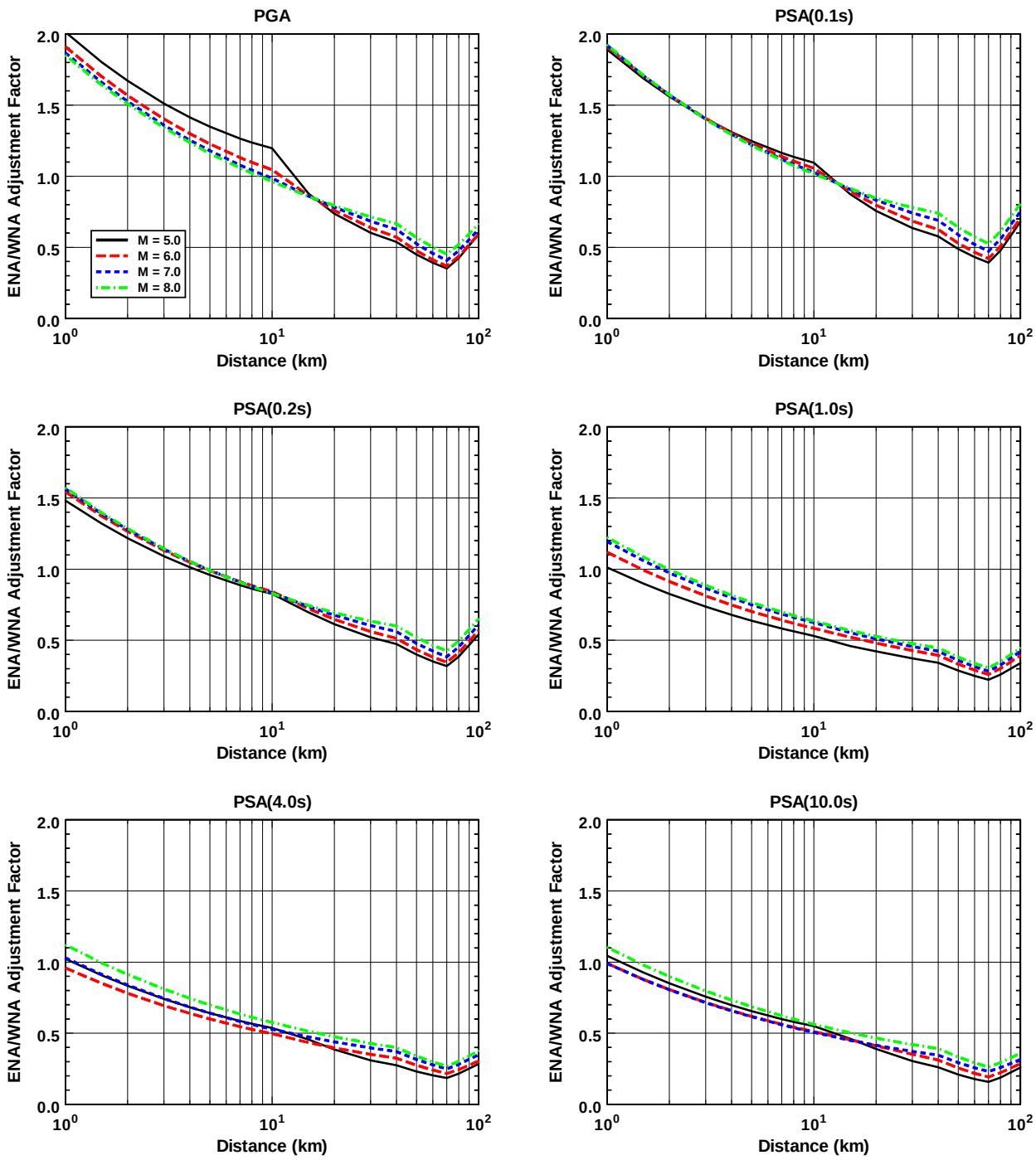

Figure 4. The dependence of ENA-to-WNA regional adjustment factors on magnitude and distance calculated from the seismological parameters in Table 1. Note that the magnitude dependence is relatively small compared to the distance dependence.

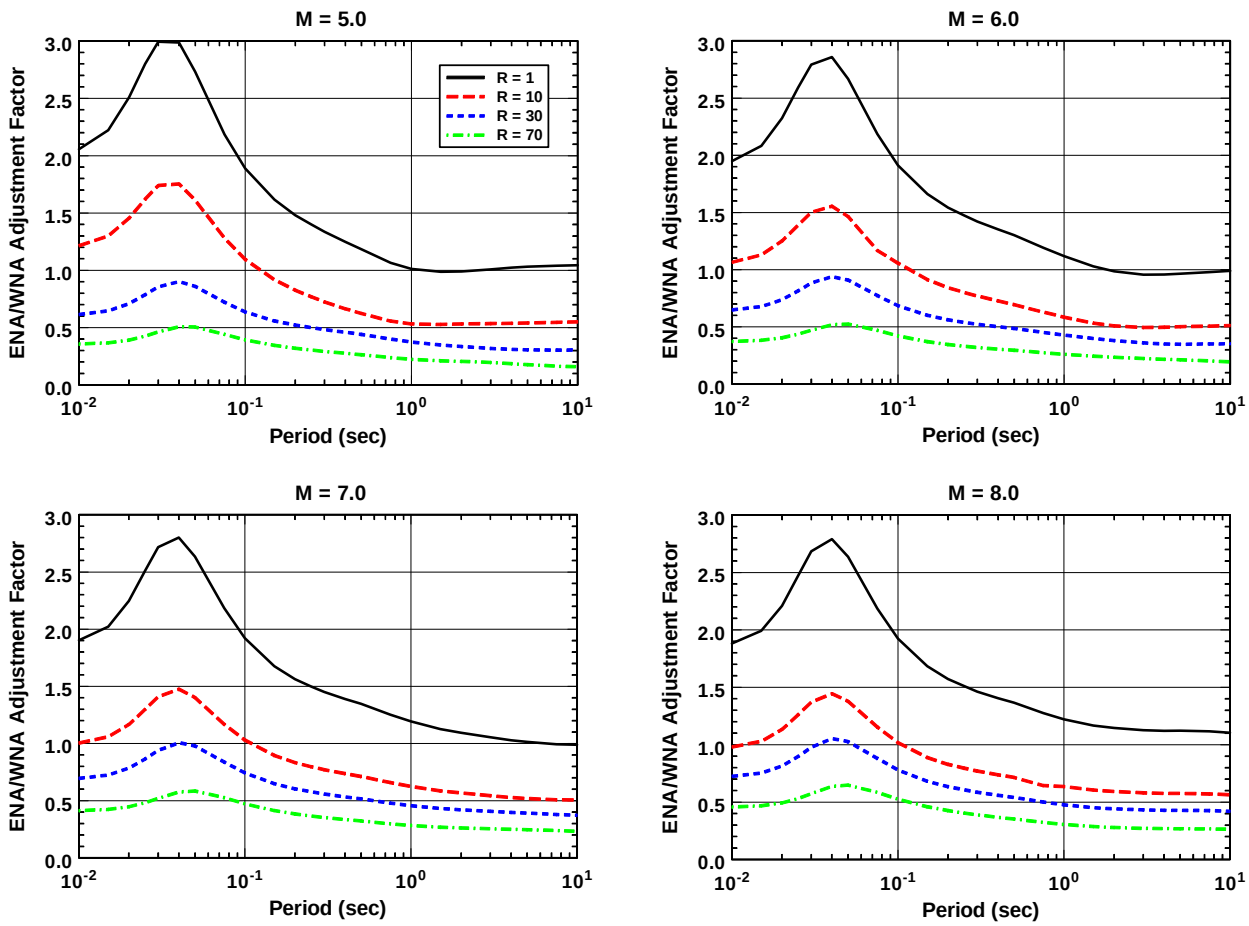

Figure 5. The dependence of ENA-to-WNA regional adjustment factors on oscillator period calculated from the seismological parameters listed in Table 1. Note that the maximum difference occurs at periods between 0.03 and 0.05 sec.

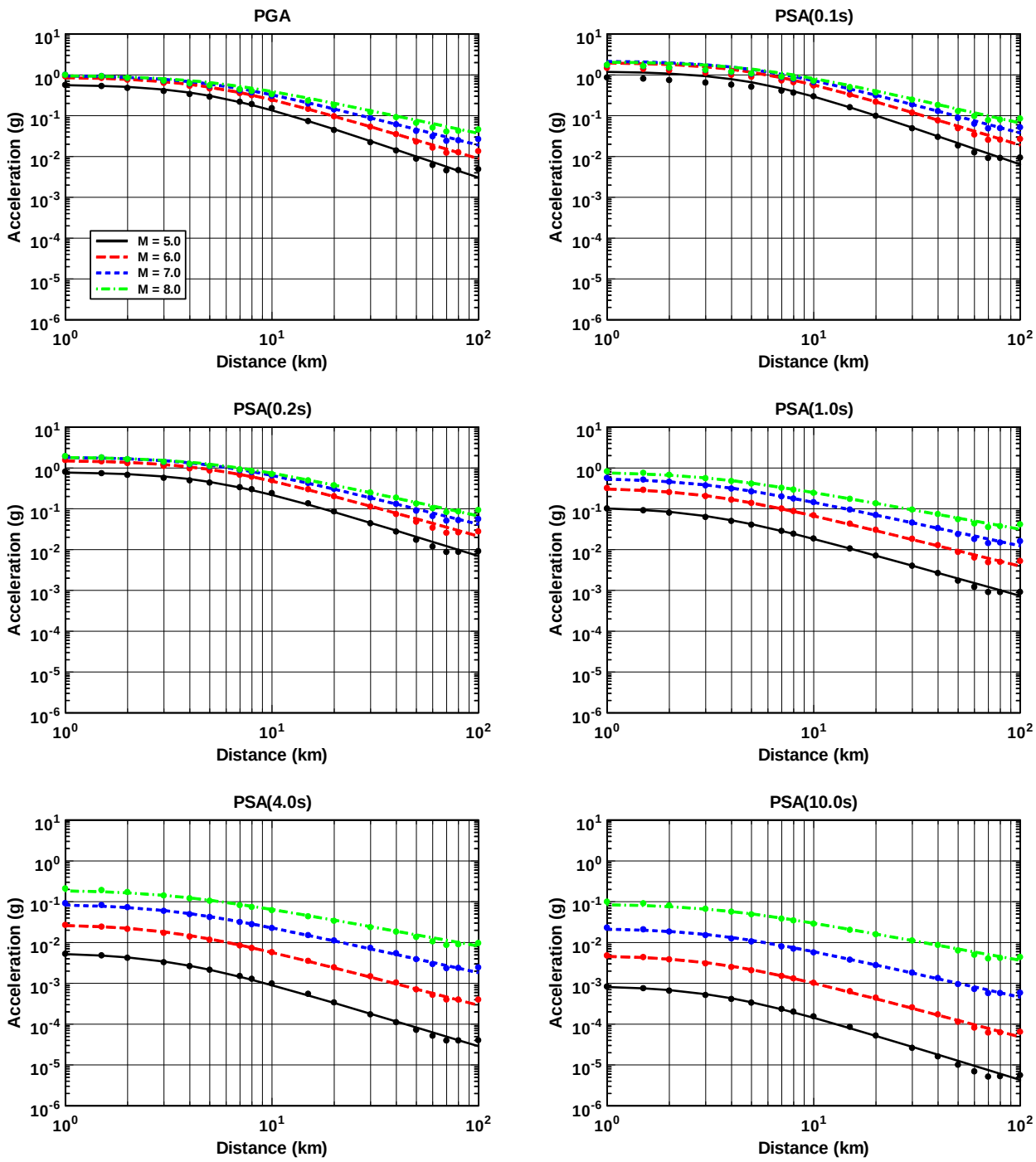

Figure 6. Ground motion attenuation characteristics predicted by the base hybrid empirical ground motion model developed in this study: (solid lines) median ground motion model; (solid circles) individual hybrid empirical estimates.

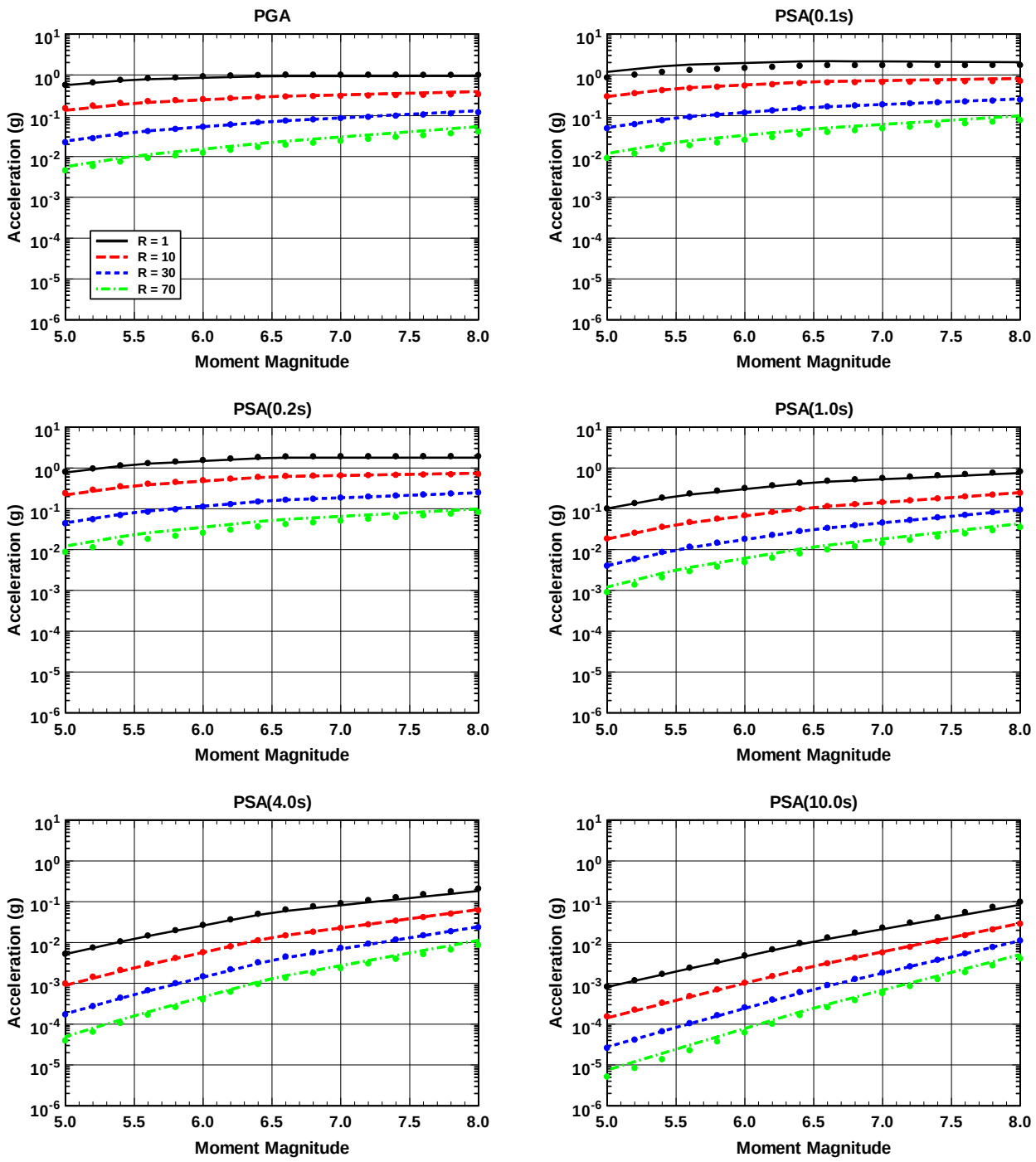

Figure 7. Ground motion magnitude scaling characteristics predicted by the base hybrid empirical ground motion model developed in this study: (solid lines) median ground motion model; (solid circles) individual hybrid empirical estimates.

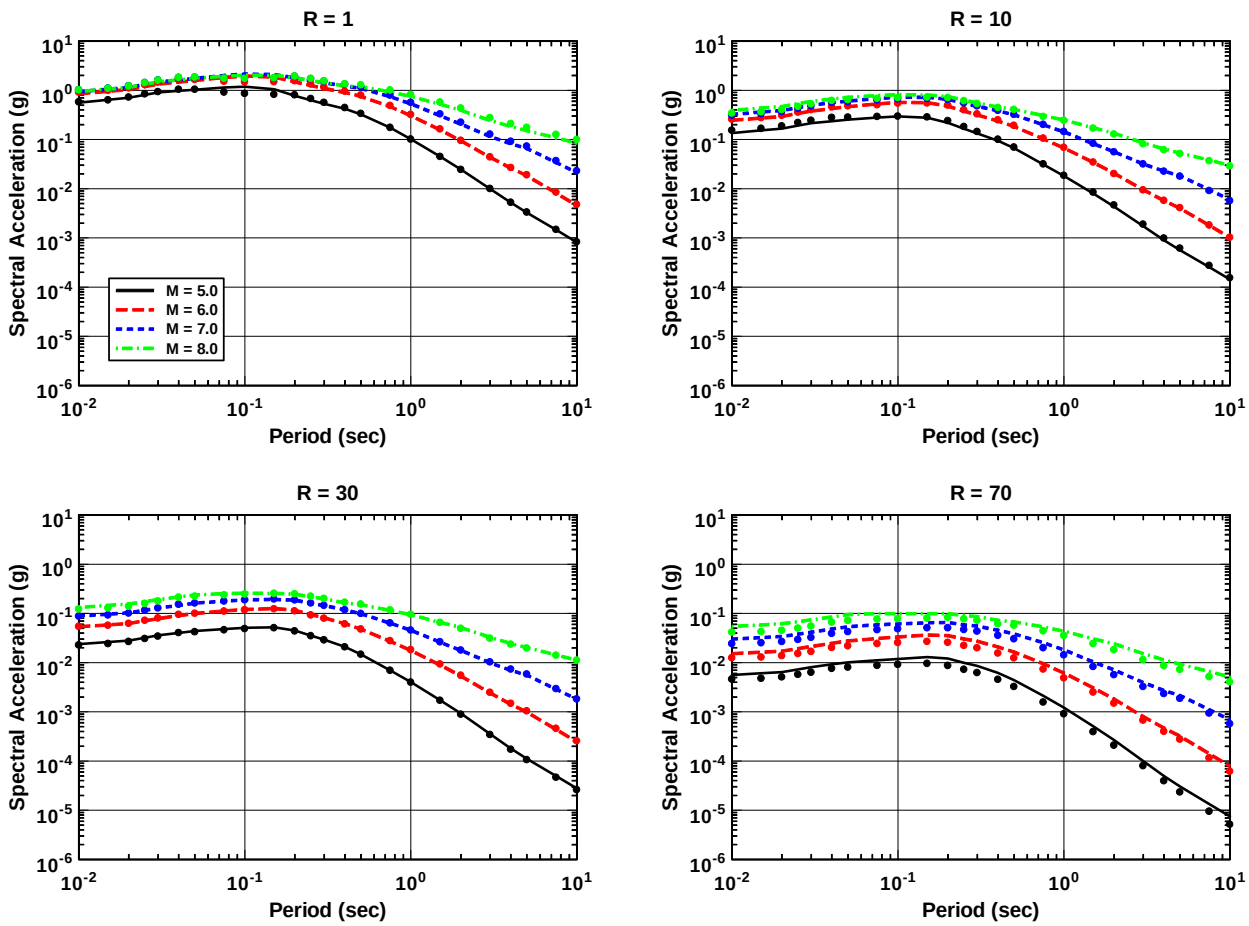

Figure 8. Response spectra predicted by the base hybrid empirical ground motion model developed in this study showing their dependence on magnitude at distances of 1, 10, 30, and 70 km: (solid lines) median ground motion model; (solid circles) individual hybrid empirical estimates.

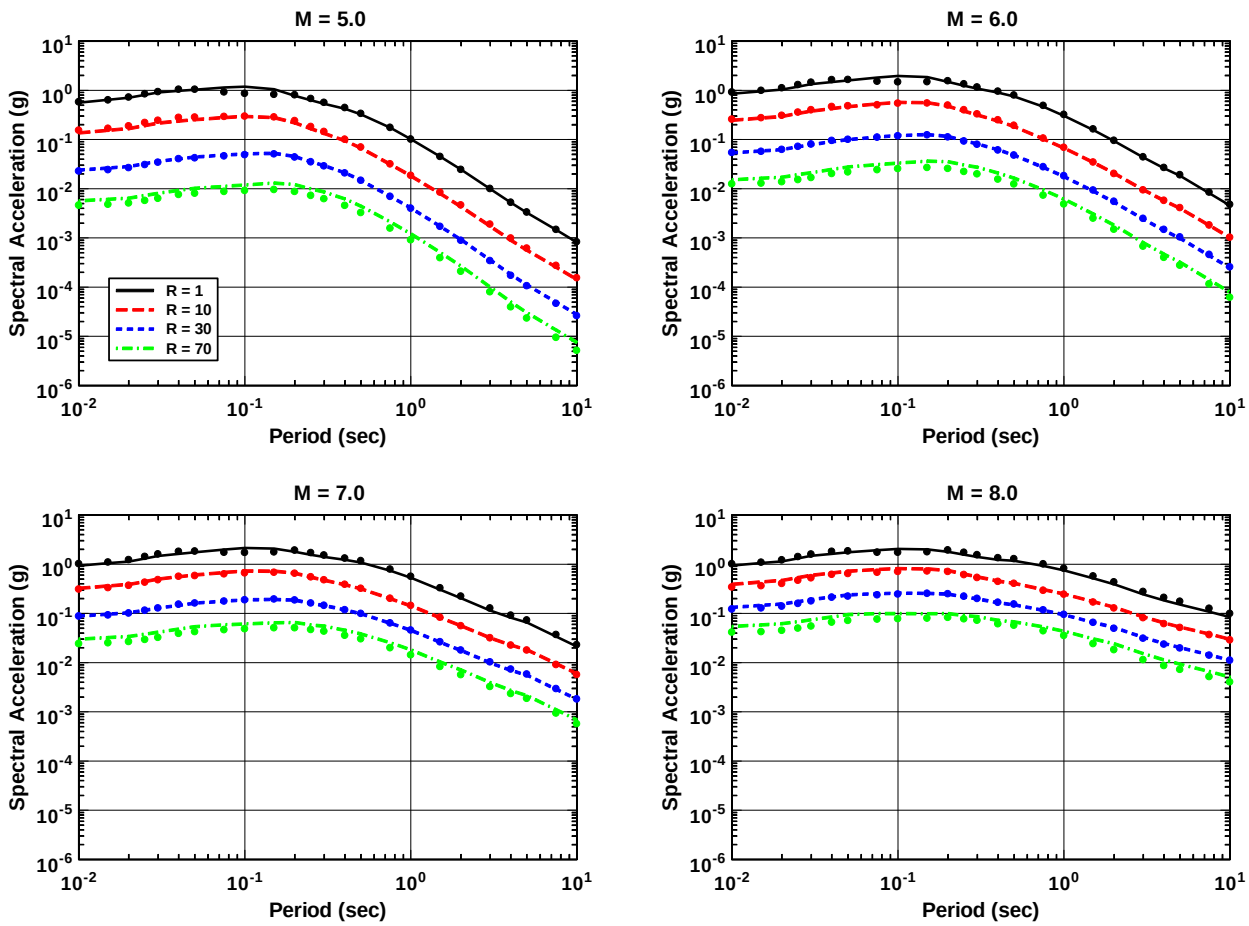

Figure 9. Response spectra predicted by the base hybrid empirical ground motion model developed in this study showing their dependence on distance for magnitudes of 5.0, 6.0, 7.0, and 8.0: (solid lines) median ground motion model; (solid circles) individual hybrid empirical estimates.

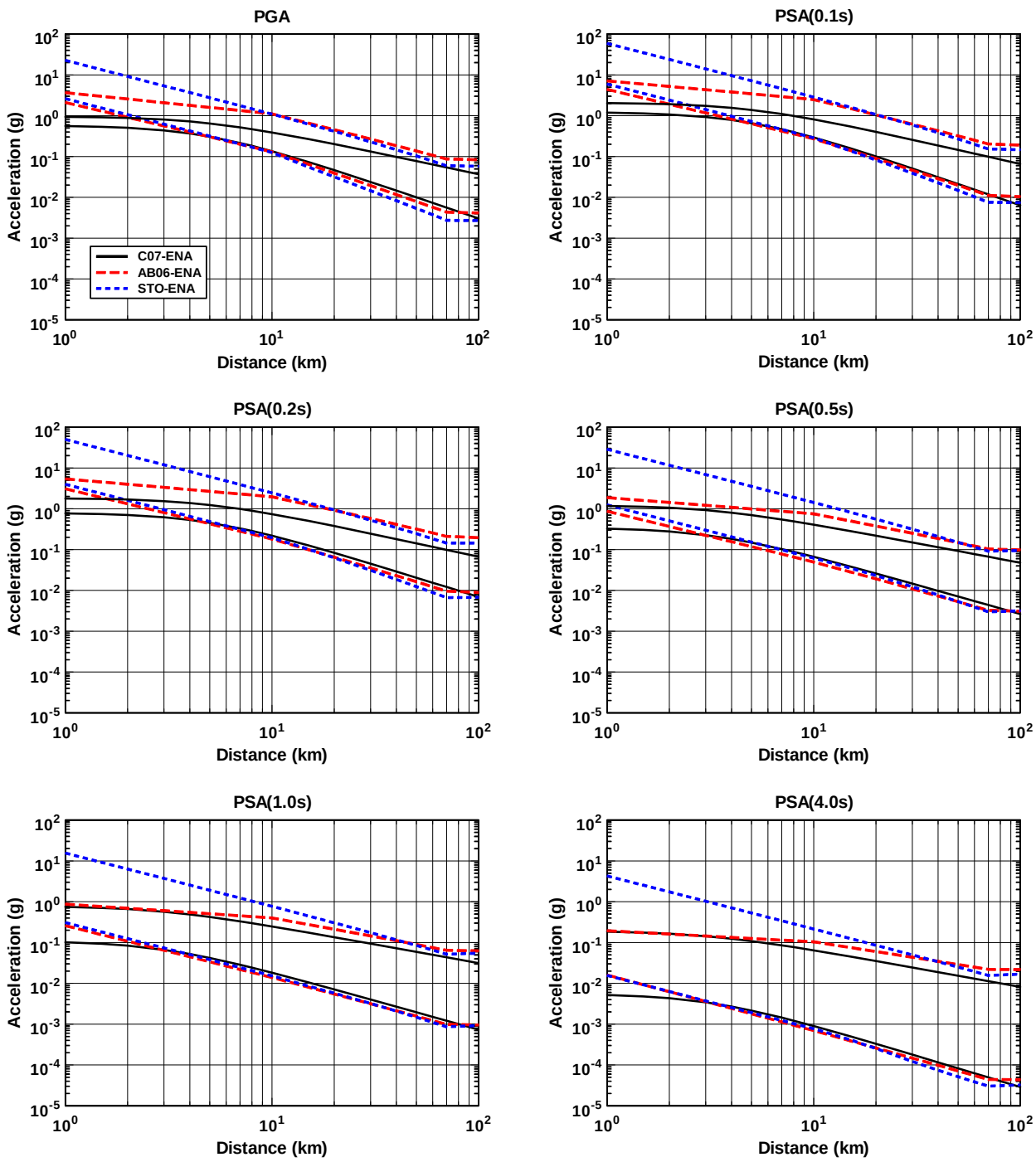

Figure 10. Attenuation characteristics predicted by three ground motion models that were derived from the same set of ENA stochastic model parameters listed in Table 1 using different methodologies: (lower curve) magnitude 5.0; (upper curve) magnitude 7.0. C07-ENA, hybrid empirical method (this study); AB06-ENA, finite-source stochastic method (Atkinson and Boore, 2006); STO-ENA, single-corner point-source stochastic method (this study).

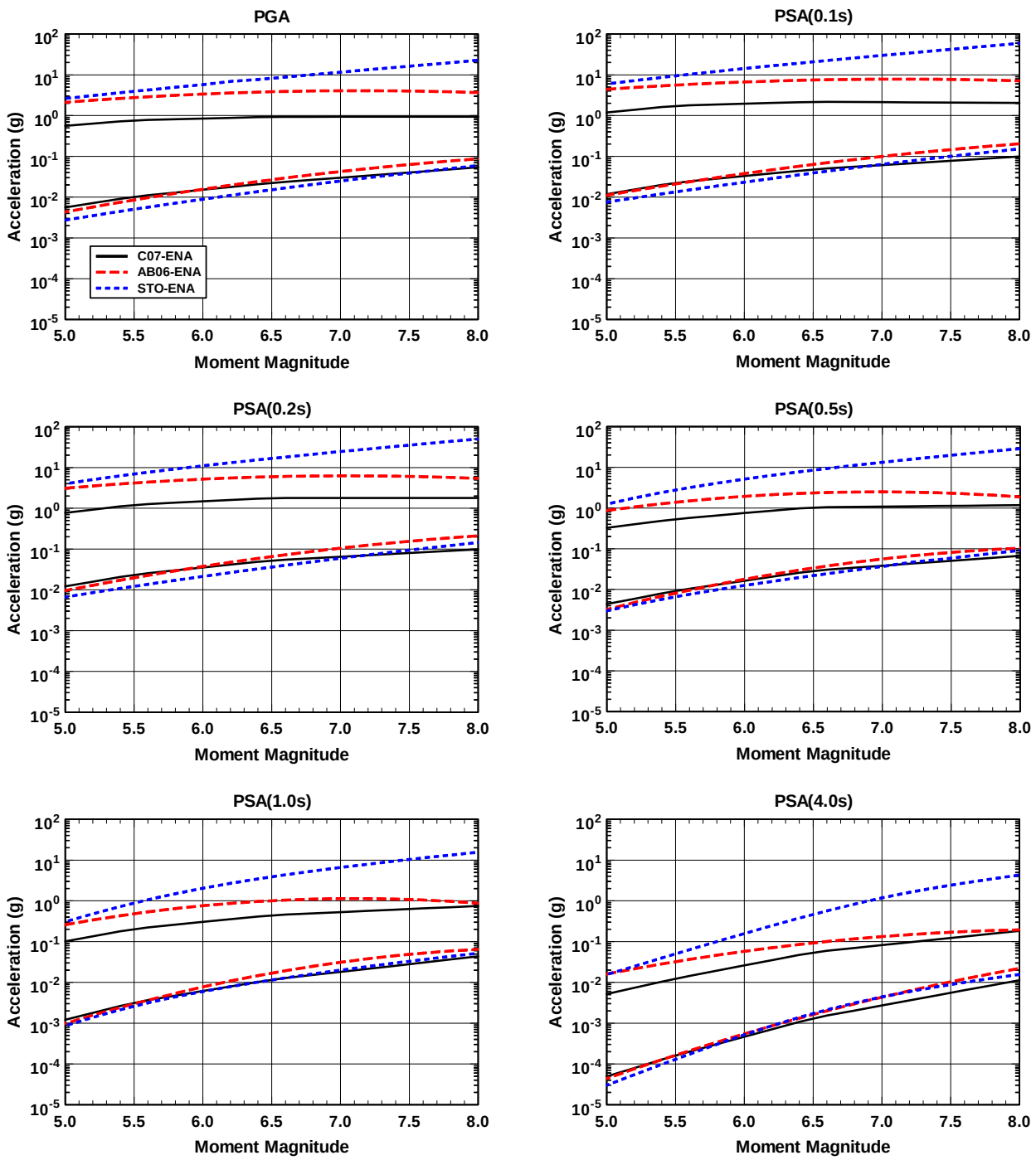

Figure 11. Magnitude scaling characteristics predicted by three ground motion models that were derived from the same set of ENA stochastic model parameters listed in Table 1 using different methodologies: (lower curve) 70 km distance; (upper curve) 1 km distance. C07-ENA, hybrid empirical method (this study); AB06-ENA, finite-source stochastic method (Atkinson and Boore, 2006); STO-ENA, single-corner point-source stochastic method (this study).

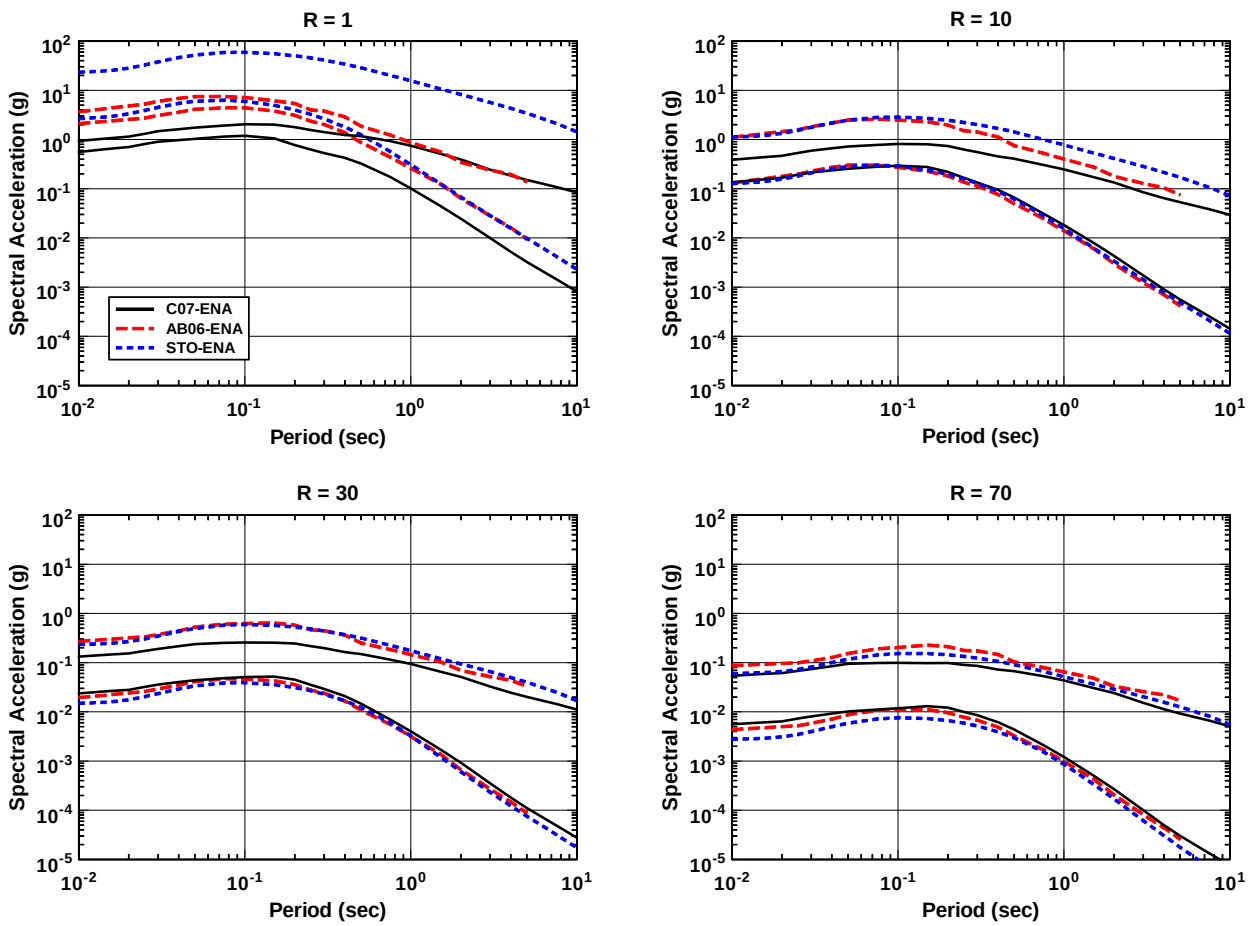

Figure 12. Response spectra predicted by three ground motion models that were derived from the same set of ENA stochastic model parameters listed in Table 1 using different methodologies: (lower curve) magnitude 5.0; (upper curve) magnitude 7.0. C07-ENA, hybrid empirical method (this study); AB06-ENA, finite-source stochastic method (Atkinson and Boore, 2006); STO-ENA, single-corner point-source stochastic method (this study).

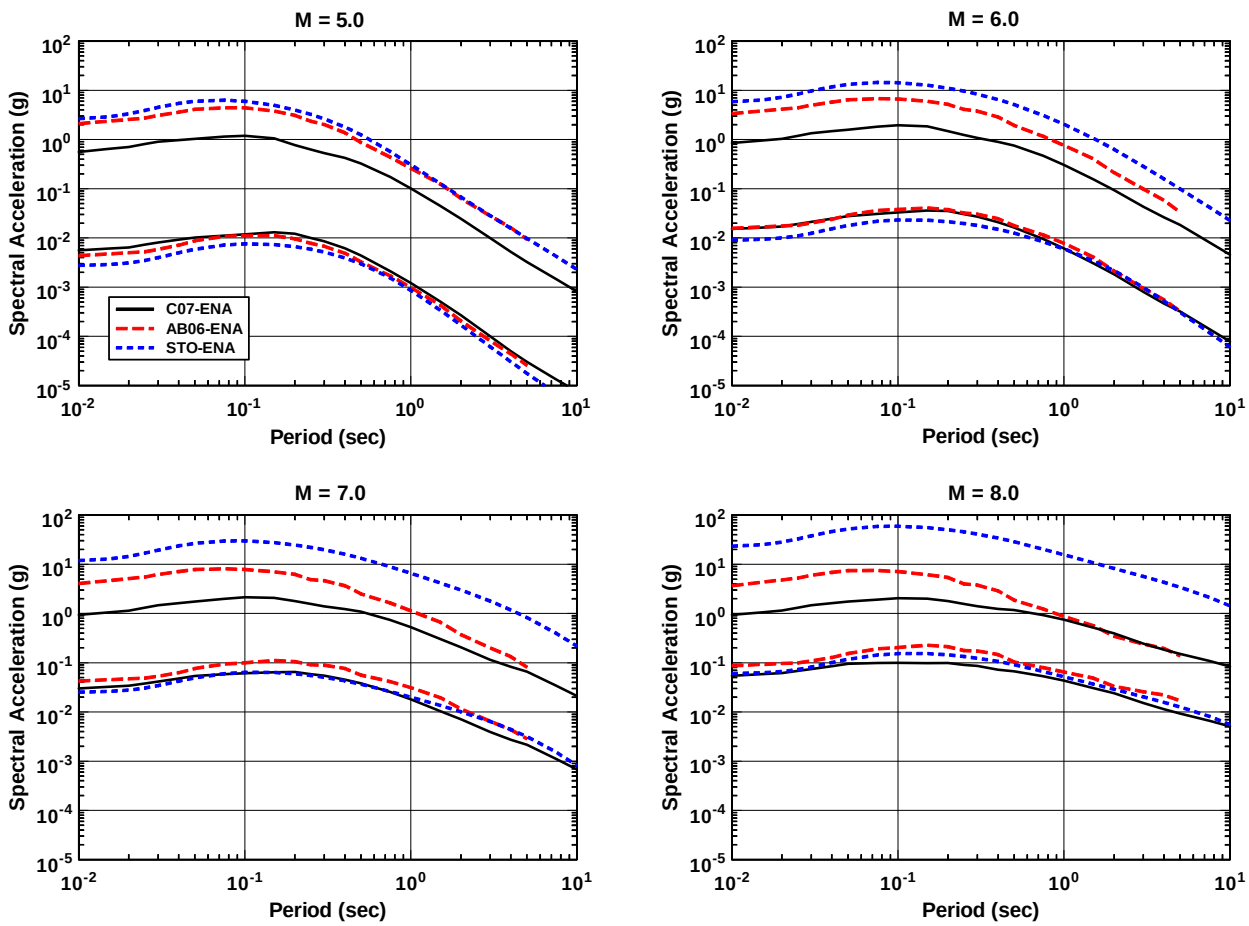

Figure 13. Response spectra predicted by three ground motion models that were derived from the same set of ENA stochastic model parameters listed in Table 1 using different methodologies: (lower curve) 70 km distance; (upper curve) 1 km distance. C07-ENA, hybrid empirical method (this study); AB06-ENA, finite-source stochastic method (Atkinson and Boore, 2006); STO-ENA, single-corner point-source stochastic method (this study).

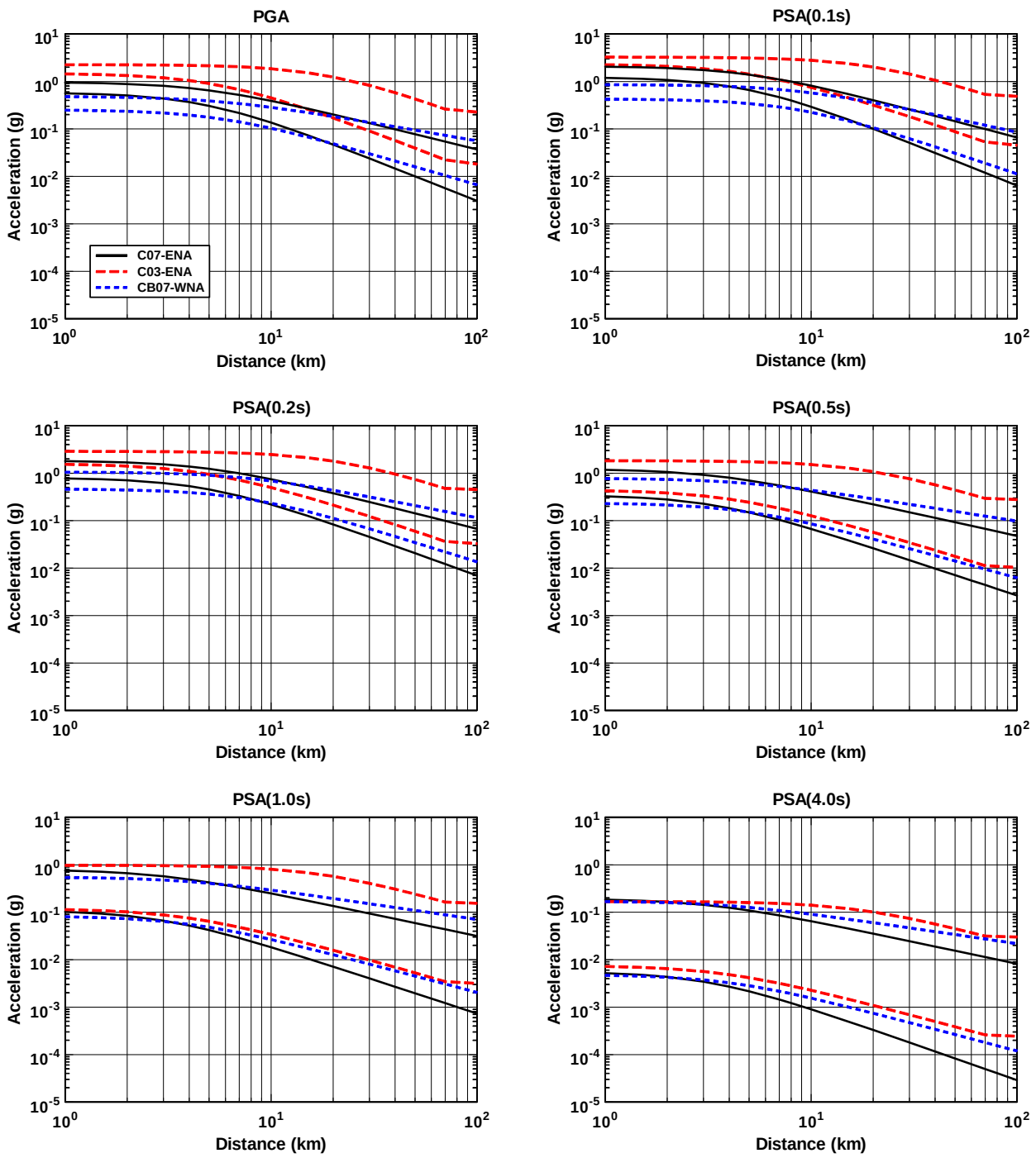

Figure 14. Attenuation characteristics predicted by (1) WNA and ENA ground motion models that use the same functional form (CB07-WNA and C07-ENA) and (2) ENA ground motion models that were derived from the same methodology using different stochastic model parameters (C03-ENA and C07-ENA): (lower curve) magnitude 5.0; (upper curve) magnitude 7.0. C07-ENA, revised hybrid empirical model (this study); C03-ENA, previous hybrid empirical model (Campbell, 2003a, 2004); CB07-WNA, empirical model used to represent the host region (Campbell and Bozorgnia, 2007a, 2008).

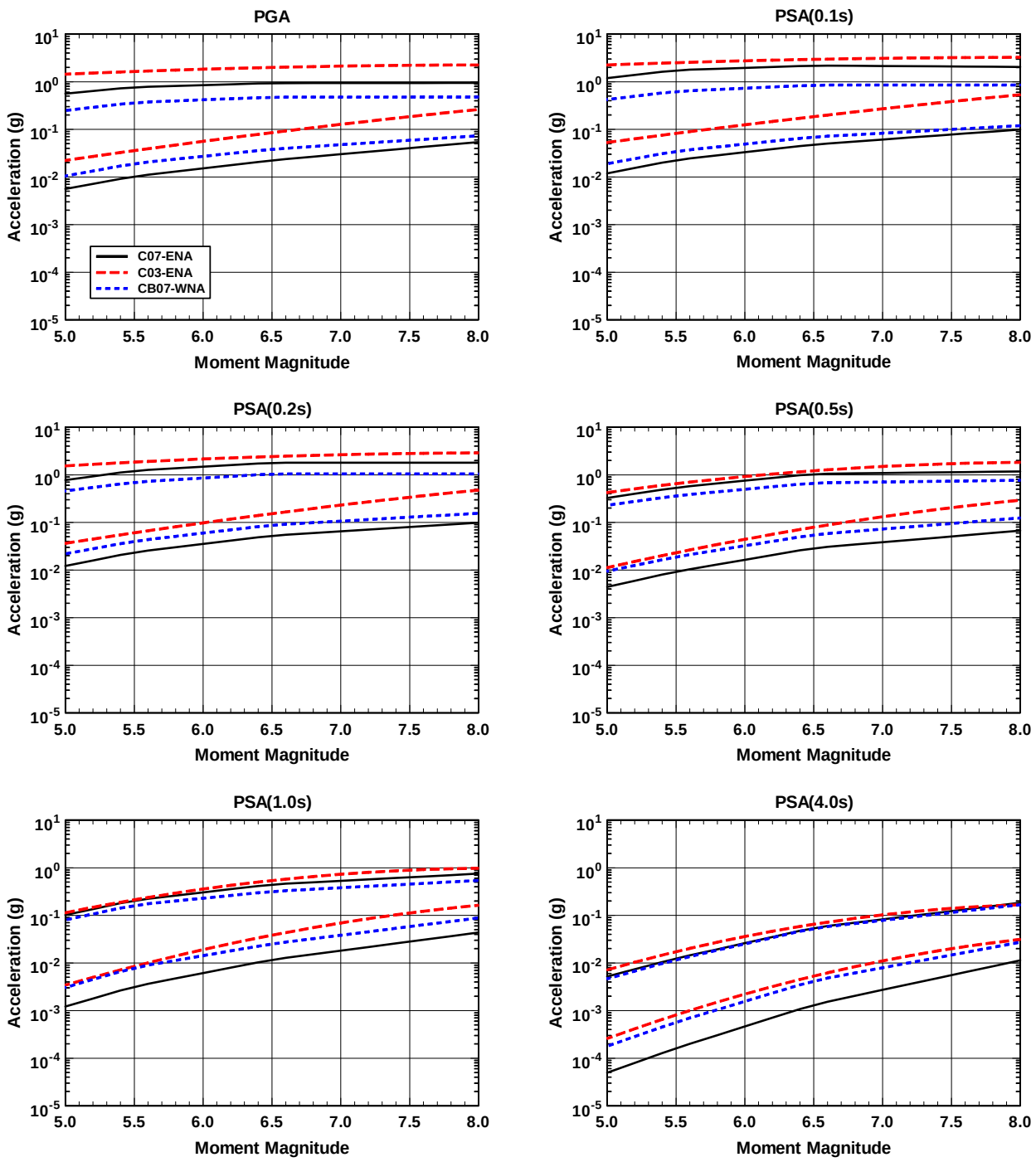

Figure 15. Magnitude scaling characteristics predicted by (1) WNA and ENA ground motion models that use the same functional form (CB07-WNA and C07-ENA) and (2) ENA ground motion models that were derived from the same methodology using different stochastic model parameters (C03-ENA and C07-ENA): (lower curve) 70 km distance; (upper curve) 1 km distance. C07-ENA, revised hybrid empirical model (this study); C03-ENA, previous hybrid empirical model (Campbell, 2003a, 2004); CB07-WNA, empirical model used to represent the host region (Campbell and Bozorgnia, 2007a, 2008).

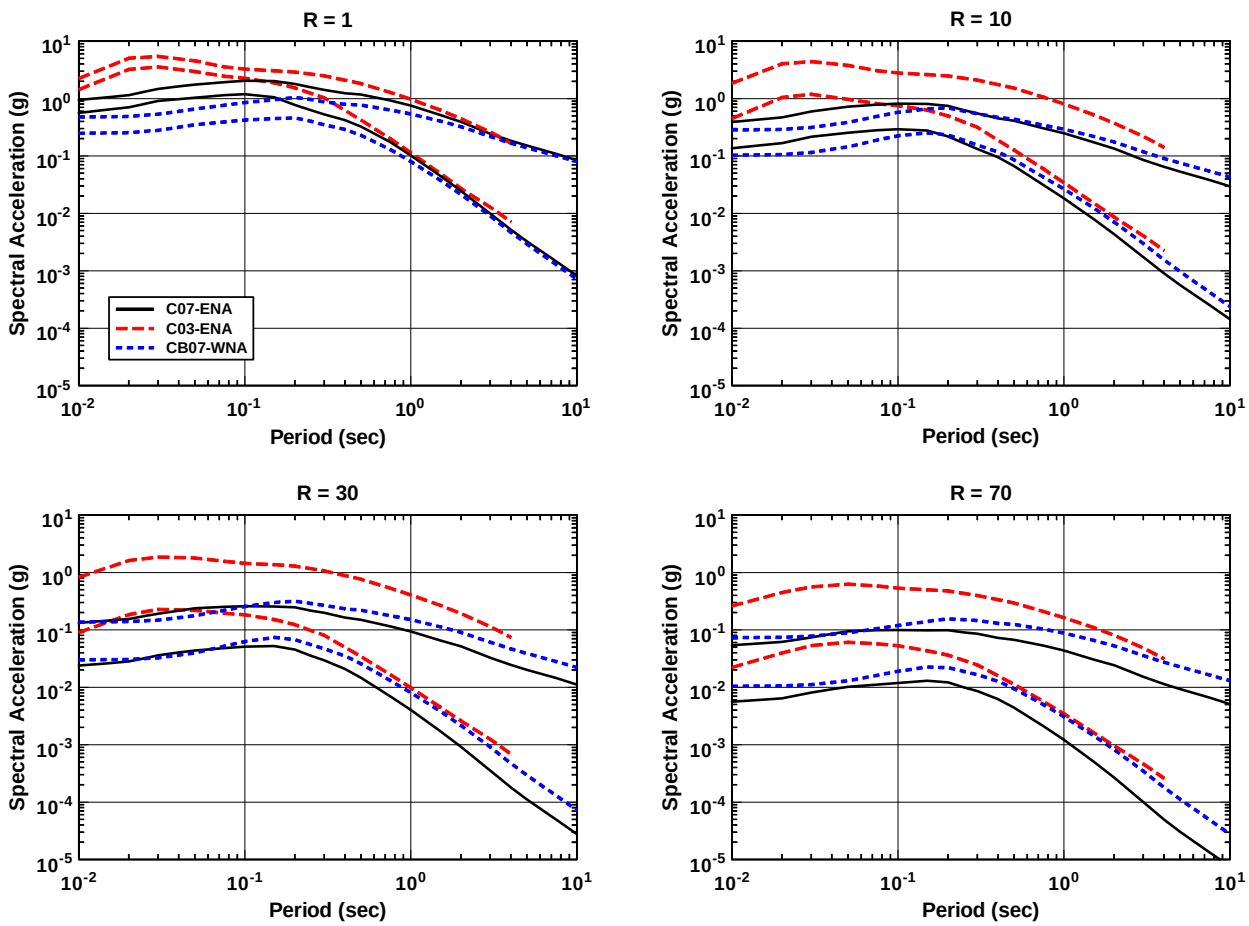

Figure 16. Response spectra predicted by (1) WNA and ENA ground motion models that use the same functional form (CB07-WNA and C07-ENA) and (2) ENA ground motion models derived from the same methodology using different stochastic model parameters (C03-ENA and C07-ENA): (lower curve) magnitude 5.0; (upper curve) magnitude 7.0. C07-ENA, revised hybrid empirical model (this study); C03-ENA, previous hybrid empirical model (Campbell, 2003a, 2004); CB07-WNA, empirical model used to represent the host region (Campbell and Bozorgnia, 2007a, 2008).

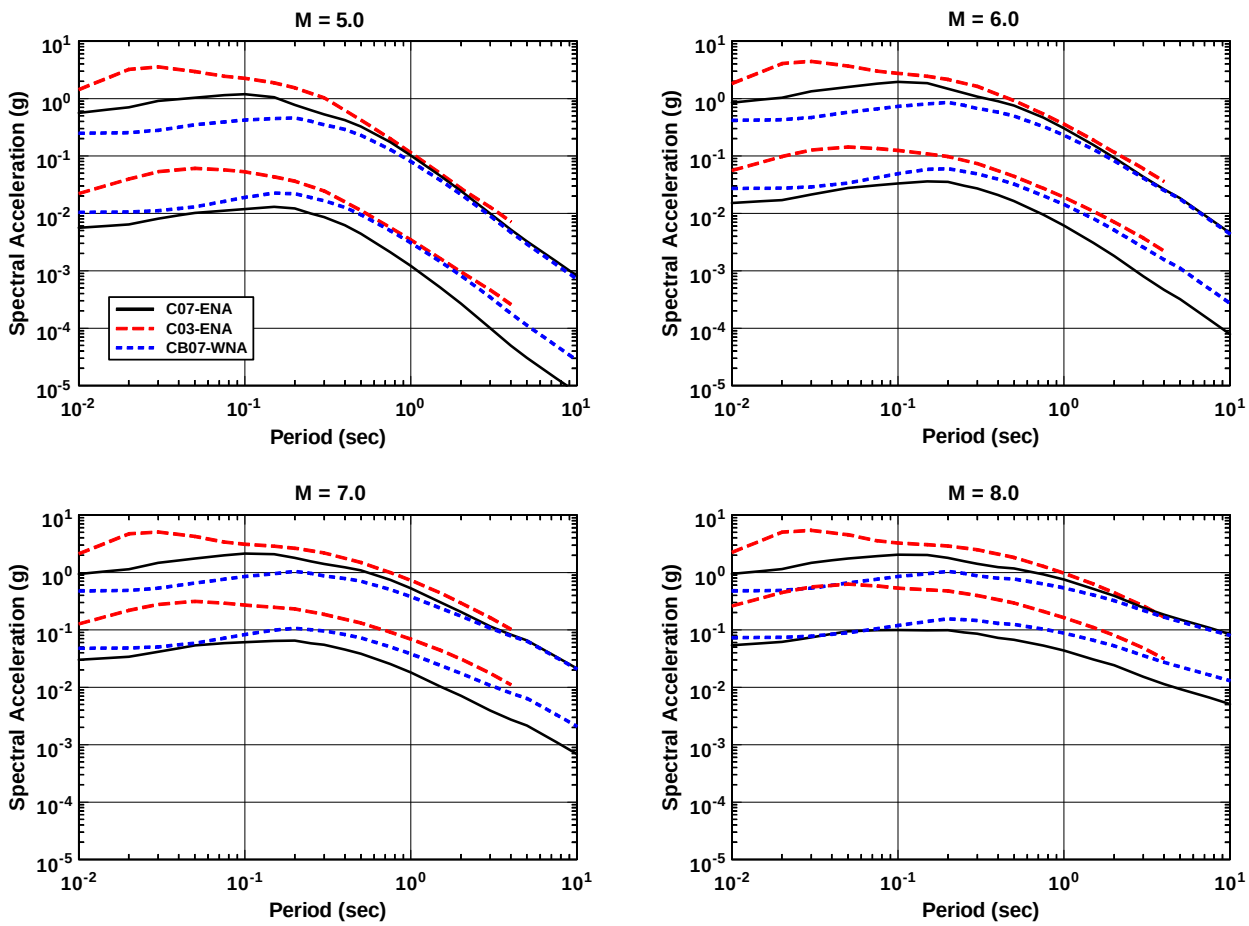

Figure 17. Response spectra predicted by (1) WNA and ENA ground motion models that use the same functional form (CB07-WNA and C07-ENA) and (2) ENA ground motion models derived from the same methodology using different stochastic model parameters (C03-ENA and C07-ENA): (lower curve) 70 km distance; (upper curve) 1 km distance. C07-ENA, revised hybrid empirical model (this study); C03-ENA, previous hybrid empirical model (Campbell, 2003a, 2004); CB07-WNA, empirical model used to represent the host region (Campbell and Bozorgnia, 2007a, 2008).

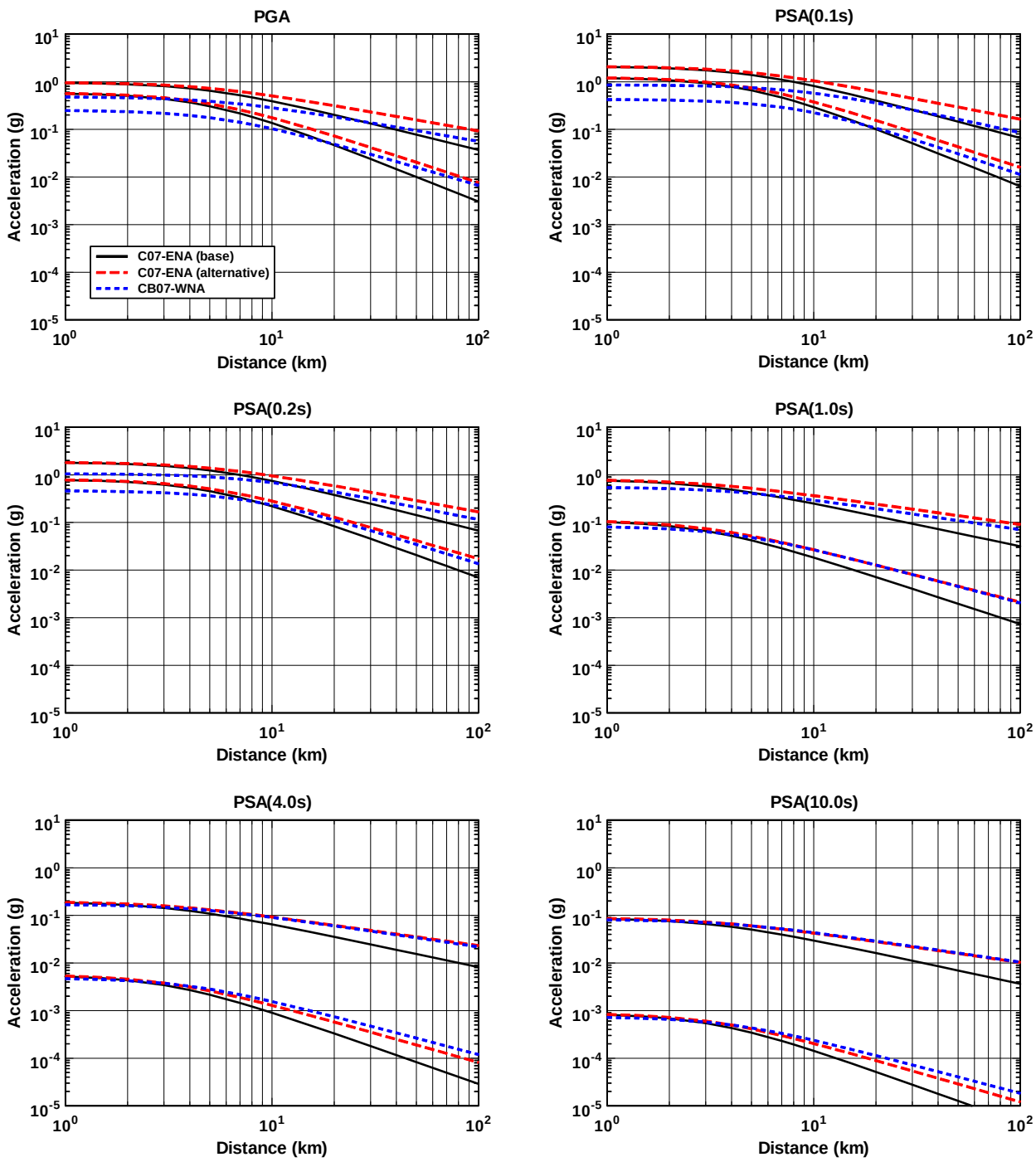

Figure 18. Comparison of predicted attenuation characteristics in WNA with those in ENA assuming different near-source geometric attenuation spreading coefficients in WNA: (lower curve) magnitude 5.0; (upper curve) magnitude 7.0. C07-ENA (base), base hybrid empirical model (this study) based on a spreading coefficient of -1.0 in WNA; C07-ENA (alternative), alternative hybrid empirical model (this study) based on a spreading coefficient of -1.3 in WNA; CB07-WNA, empirical model used to represent the host region (Campbell and Bozorgnia, 2007a, 2008).

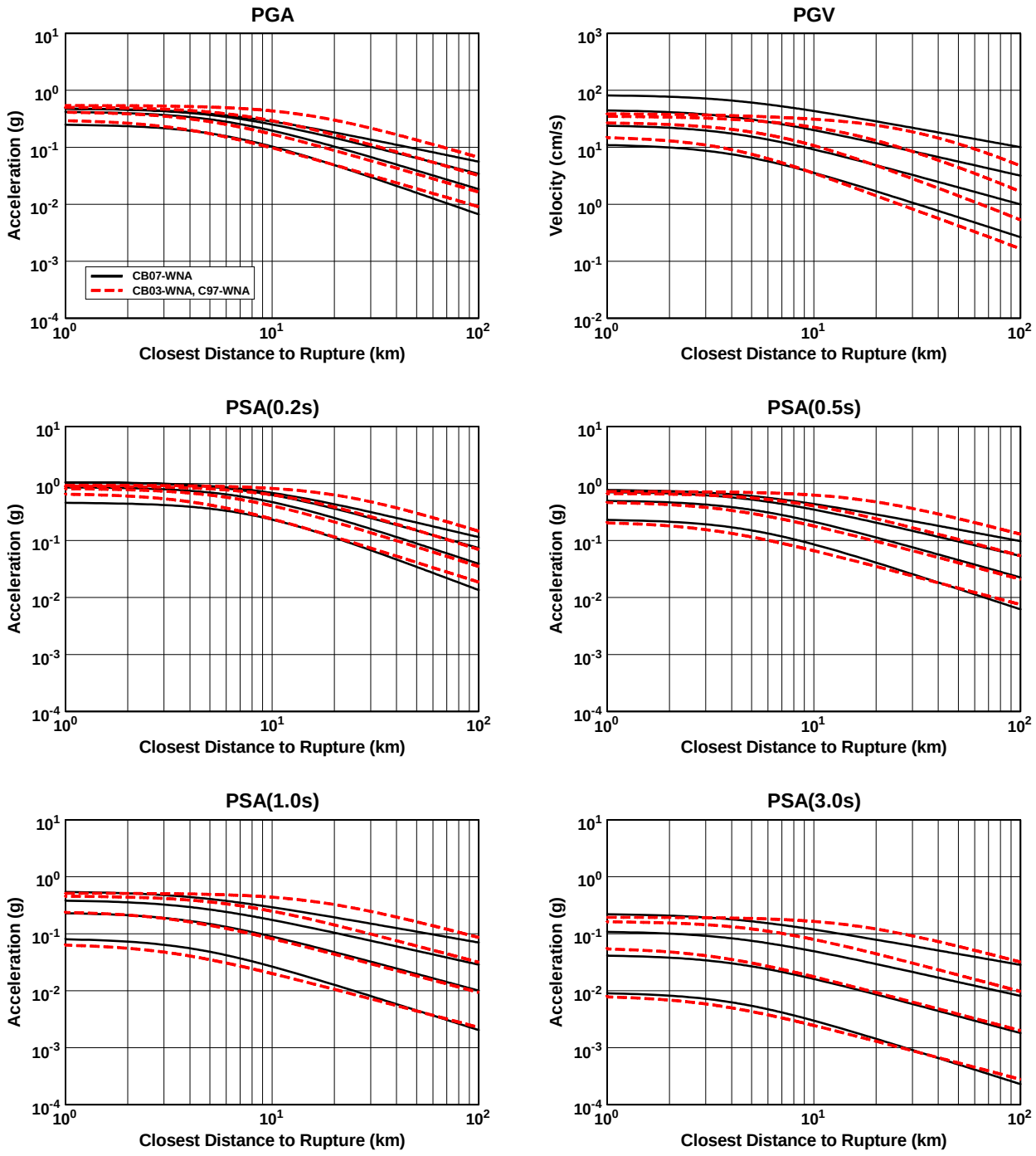

Figure 19. The difference in predicted ground motion in WNA resulting from the relaxation of constraints imposed on the functional form. CB07-WNA, revised empirical model for PGA, PSA and PGV (Campbell and Bozorgnia, 2007a, 2008); CB03-WNA, previous empirical model for PGA and PSA (Campbell and Bozorgnia, 2003a, 2003b, 2003c, 2004); C97-WNA, previous empirical model for PGV (Campbell, 1997, 2000b).